Hossam Aboelsoud
Takao Tsuji
September 2022

Hierarchical Operation and Control of DC Microgrids Using PSO

（PSOを用いたDCマイクログリッドの階層型運用制御手法）

By: ***Hossam Aboelsoud Eid Elhassaneen***
(ホサム アボエルサウード エード エルハサネーン)

Dissertation Submitted to Graduate School of Engineering Science
of Yokohama National University

In fulfilment of the requirement for the degree of
Doctoral of Engineering (PhD) in Electrical Engineering and Computer Science

Supervisor: ***Associate Professor Takao Tsuji***

Department of Physics, Electrical Engineering and Computer Science
Graduate School of Engineering Science
Yokohama National University

Yokohama, Japan
September, 2022

ACKNOWLEDGEMENT

All praise, glory and gratitude to God who said in the holy Qur'an that "He who taught the use of the pen and taught the man that which he didn't know". Peace be upon the Prophet Muhammad SAW, his family, companions and all those who followed him until the day of judgement.

I would like to show my gratitude and appreciation to my professor Takao Tsuji for the inclusive and over whelming support towards my study and research, for his continuous motivation, patience and knowledge. He guided and helped me in hard and needed times, and I was so glad to be under his supervision. Without his indispensable help and enthusiasm, my work discussed in this thesis couldn't be accomplished. It is such an honor to learn from him and be one of his students through my master's and PhD degrees.

Besides, I would like to appreciate the guidance and honor the prominent committee: Prof. Fujimoto, Prof. Akatsu, Prof. Shimono Prof. Nakata and Prof. Obara for their various perspectives.

My gratitude also extend goes to all my lab colleagues who have showed a greet support at various occasions. Finally, I would like to express my sincere thanks to my wonderful family especially my parents, wife, my beloved baby and my brothers for believing in me and my efforts.

ABSTRACT

This work presents a contemplate study on a hierarchical based online voltage control strategy with different loading conditions in a DC microgrid using particle swarm optimization (PSO). As a result of complexities and nonlinear network constraints in microgrids, sometimes it is difficult to solve optimization problems using conventional methods. In that context, this study introduces online voltage control using an advanced PSO technique to frequently update control gains based on sudden and unexpected changes in loads. A parallel operation of local and global searches is conducted to search optimum control gains by allocating a part of the particles to flow in a random pattern. Network fitness function is set and updated with every load change to meet the control target.

Simultaneously, eigenvalue analysis is performed to precisely describe grid characteristics and to easily update eigenvalues based on load changes or network configurations. With this proposed strategy, the expectancy of network stability was raised even with those uncertainties. However, the afore-mentioned primary controller is not sufficient to restore voltage within an allowable range and an offset might occur. Consequently, an inclusive hierarchical control was proposed in this thesis. Voltage is restored to the allowable range using secondary controller when any voltage violation still remains after the primary control. Moreover, a tertiary controller would be implemented for optimizing generation dispatch by reducing the generation cost. In that context, whenever there is any load change, a full PID control is utilized. Firstly, primary control works to stabilize the voltage based on PD logic. Then secondary and tertiary controls are implemented with Integral logic to eliminate voltage deviation and maintain lower generation cost. The primary control is always working, and its control parameters could be updated every short time interval for optimization with the proposed method, while secondary and tertiary controls are with longer time intervals.

The validation of the suggested method was performed firstly using a 3-bus DC microgrid model for simplicity then an 8-bus model is applied. The effectiveness of the proposed method was verified through numerical simulations using MATLAB/Simulink 2016b.

TABLE OF CONTENTS

CHAPTER **TITLE** **PAGE**

LIST OF FIGURES

LIST OF TABLES

LIST OF ABBREVIATIONS

- PSO: Particle Swarm Optimization
- RES: Renewable Energy Sources
- VRES: Variable Renewable Energy Sources
- ESS: Energy Storage Systems
- DG: Distributed Generation
- AI: Artificial Intelligence
- MI: Machine intelligence
- HI: Human Intelligence
- CPL: Constant Power Load
- LRC: Line Regulating Converter
- SDC: Step down Chopper
- POL: Point of Load Converter
- RNW: Random Number Weight
- CO_2: Carbon dioxide gas
- FIT: Feed in Tariff
- NEC: National Electrotechnical Commission
- NEM: Net Energy metering
- GW: Giga Watt
- PV: Solar Photovoltaic
- GA: Genetic Algorithm
- DE: Differential Evolution
- TSO: Transmission System Operator
- DSO: Distribution System Operator
- EDC: Economic Dispatch Control
- rp: Random Particles

LIST OF VARIABLES

- $V_{Bi.\ ref}$: New local voltage setpoint of converter *i*.
- $V_{Bi.\ ref_0}$: Global voltage setpoint all over the microgrid of converter *i*.
- V_{Bi}: Actual measured local voltage of converter *i*.
- V_{Bj}: Average measured voltage of neighbouring converter.
- ΔV_{Bi}: Voltage offset for converter *i*.
- E_i: Internal voltage of generator *i*.
- D_i: Duty ratio of generator *i*.
- d_i: Instantaneous value of duty ratio of generator *i*.
- Δd_i: adjusted part of duty ratio with PD control logic of generator *i*.
- i_i: Local converter output current of converter *i*.
- i_j: Neighbouring converter output current.
- i_{total}: Sum of converters' output currents.
- P_{Gi}: Local output power of generator *i*.
- $P_{G.total}$: Sum of all generators output power.
- C_{VBi}: Local terminal voltage coefficient of generator *i*.
- C_{VBj}: Neighbouring generator terminal voltage coefficient.
- C_{Ii}: Local converter output current coefficient of generator *i*.
- δ^1_{VBi}: Voltage regulator correction term of generator *i*.
- δ^2_{VBi}: Current regulator correction term of generator *i.*
- r_i: Loading ratio based on tertiary controller of generator *i*.
- I_{Si}: Source current of generator *i*.
- I_{Di}: Distribution line *i* current.
- I_{Dj}: Distribution line *j* current.
- I_{Li}: Load current connected to bus *i*.
- R_s: The resistance when MOSFET is on.
- R_d: The resistance when current flows through the diode.
- R_L: SDC Inductor resistance.
- L_S: SDC Internal inductance.
- V_D: Diode voltage drop.
- L_{Di}: Inductance of distribution line *i*.
- R_{Di}: Resistance of distribution line *i*.
- P_L: Load power.
- C_{Bi}: Capacitance at terminal *i*.

- C_{SDC}: Internal capacitance of SDC.
- $I.C_i$: Incremental cost at local terminal i.
- $I.C_j$: Incremental cost at neighbouring terminal j.
- $I_{Di.rated}$: Rated value of distribution line i current.
- $I_{Dj.rated}$: Rated value of distribution line j current.
- $I_{Di.normal}$: Normal case of distribution line i current (not overloaded).
- $I_{Dj.normal}$: Normal case of distribution line j current (not overloaded).
- $I_{Di.diff.}$: Difference between rated and measured values of distribution line i currents.
- $I_{Dj.diff.}$: Difference between rated and measured values of distribution line j currents.

CHAPTER 1

INTRODUCTION

1.1 Research Background

Many countries all throughout the world have focused their effort on finding alternatives to their conventional power sources. Renewable energy sources (RES) such as solar, wind, hydro and geothermal powers have grabbed the most attention as a countermeasure against environmental problems such as fossil fuel depletion and global warming. Supported with governmental policies and incentives, the environmental awareness by customers increased to use variable renewable energy sources (VRES) as solar and wind energies in their electricity production. Backed by advanced technologies, integration of VRES in the last decade showed a huge and overwhelming rise all over the world. However, the intermittent and fluctuating nature of VRES caused many stability issues, especially when their share increases, which consequently means less inertia and high vulnerability to blackouts [1], [2]. Modern technologies tried to reduce that impact on the network by inserting energy storage systems (ESS) as a backup for voltage support [3]-[5]. However, complexities and number of nonlinear network constraints increase, that is difficult to cope with conventional control methods.

DC microgrids played one of the biggest roles in easing renewables integration. DC microgrids have high reliability of power supply and is desirable for loads such as factories and computer systems that cannot tolerate a short power outage [6]-[8]. Rather than its higher efficiency, lower cost and system size, simplicity of interconnection of renewables and distributed generation (DG) is one of the key factors in modern smart grids. However, a DC microgrid exposes the issue that the voltage fluctuates due to mutual interference between several installed converters. Therefore, it is required to have a control method that eliminates voltage instability and though it can be operated with higher efficiency. Yet, to deal with these problems and stabilize the network, a hierarchical control method is one of the candidates. The hierarchical control as

imagined in our research is mainly comprised of primary, secondary, and tertiary controllers, each of which has its specific features as shown in Fig. 1.1 [7], [8].

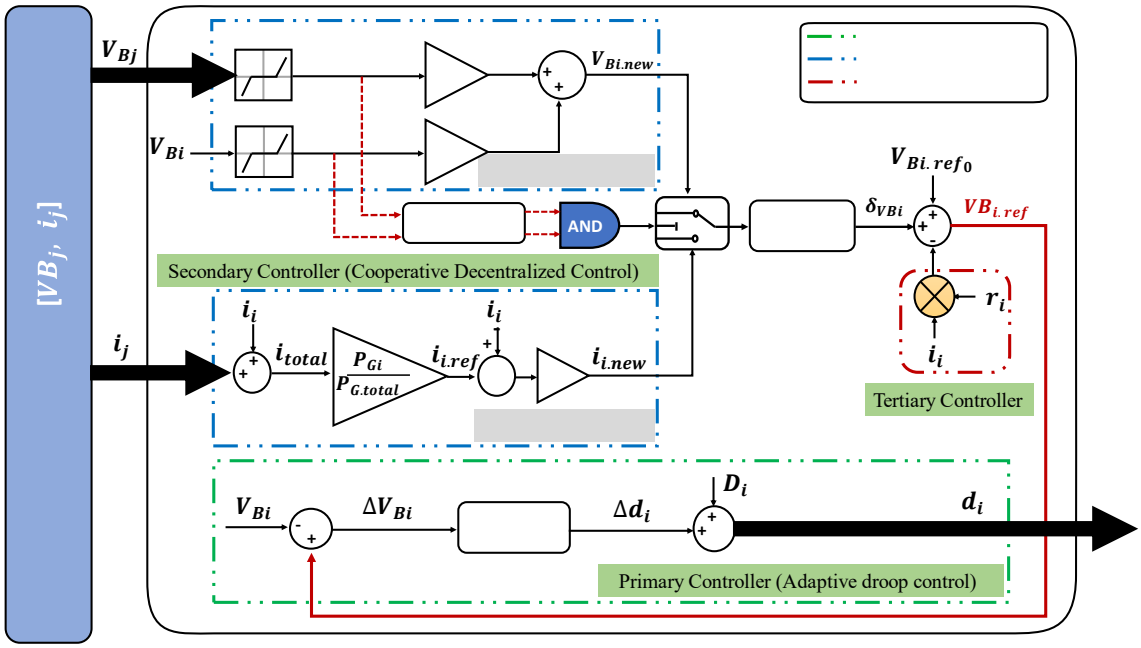

(a)

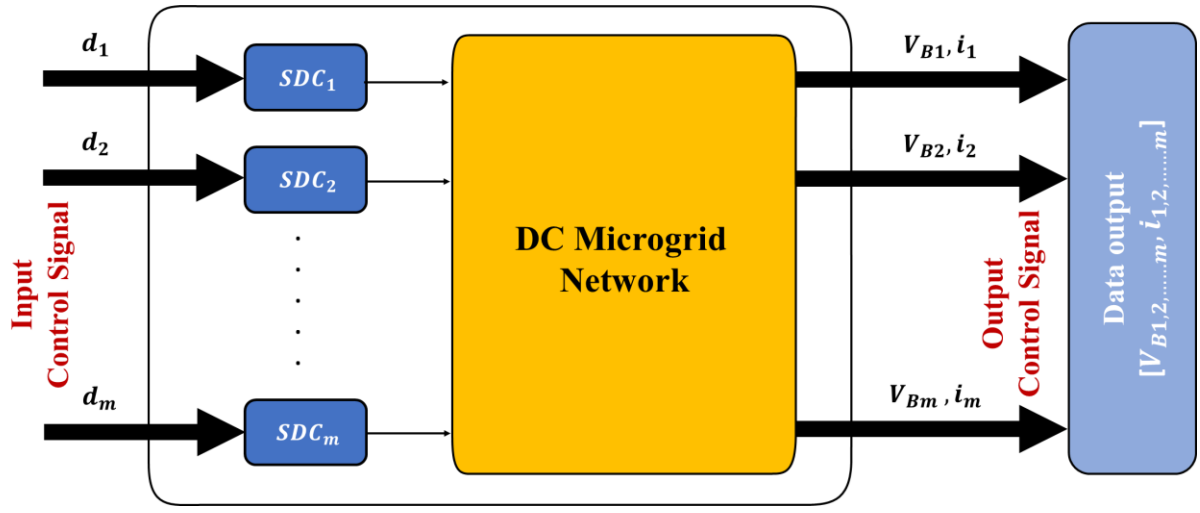

(b)

Fig. 1.1 (a) Hierarchical control structure for local converter *i* [7], [8] and (b) Input/Output control signals for whole DC microgrid network

Firstly, in primary control, the converter responds quickly to voltage changes due to load fluctuations by adjusting the duty ratio of generation sets through updating the control gains of the PD controller [9], [10]. This alleviates voltage fluctuations a little on a primary level. However, due to utilization of PD controller, voltage offset might occur which requires a secondary controller with

an integral part to eliminate it. Secondary control method is implemented to adjust the target voltage control value to keep it within the appropriate range [11], [12]. Secondary control is divided into two main parts, voltage and current regulators, each of which update the converter reference voltage based on its perspective. Voltage regulator cuts voltage fluctuations exceeding the stability limit and regulates terminal voltage reference value. On the other hand, current regulator maintains terminal voltage by adjusting converter output current based on generator capacity connected to it. Finally, under constraints such as upper and lower limits of distribution line power flow, tertiary controller is applied to control voltage, minimize the total power generation cost, and adjust transmission line currents below thermal limits [13]-[19]. The new voltage reference value is given as a control signal to the converter to maintain its output voltage and reduce the voltage offset. In this study, we will focus on primary controller in the first section, as secondary, and tertiary controllers will be focused on in later sections. The optimum PD control gains for primary controller are changing depending on load changes. It is desired that the control gains are automatically updated to keep the best control performance. To this end we have developed a meta-heuristic approach to repeatedly update the control gains.

PSO is a meta-heuristic artificial intelligence (AI) method suggested by Dr. Eberhart and Dr. Kennedy in 1995 [20]. It is an optimization technique expressing Swarm Intelligence mechanism and inspired by fish, birds or ant swarms' behavior. There are various types of PSO depending on the application, the problem to be solved and computational speed. For instance, PSO could be implemented to identify the parameters of photovoltaic modules [21]. PSO might help to configure the best accuracy when searching for the area near the global maximum power point under partial shading conditions [22]-[25]. In [26], a basic algorithm of PSO is developed to search for the optimal set of droop parameters for effective DC microgrid operation. Moreover, PSO is utilized for determining the optimal location to place constant power loads (CPL) of DC microgrid [27]. In [28], PSO is implemented to optimally schedule DG units under certain scenarios. PSO is also used for optimal sizing of DGs and ESS to reduce annual capital and operation costs [29], [30]. In [31], the paper presents how PSO is utilized to update PI control parameters during photovoltaic power plants modelling for voltage control. In [32], PSO is applied to find the optimum economic dispatch for solar integrated power systems. However, in this work, a new PSO strategy was suggested for the primary control as follows:

- It is supposed that PD control gains must be updated in a short cycle, such as to keep the appropriate control performance even under frequent load changes. Hence, the computation time for the optimization should be as short as possible.

- The initial positions of particles in PSO should be around the optimal solution obtained at the previous steps if the state space did not change largely. However, if the state space was largely changed, there is a possibility that the optimal solution appears at any distant location. To keep both; the good exploration and exploitation abilities in the continuous optimization, even under uncertain changes in the state space, the particles are divided into random particles that realize exploration and normal particles which have converged for the exploitation. The fast and flexible search against the time-depending state space can be realized throughout the information exchange between all the particles.

- Here, the objective function was defined based on eigenvalue analysis. As the PSO was used, the proposed method could successfully find the optimal solution, although the state space was non-convex with multiple extreme values.

1.2 Problems to be Stated

In various former studies, PSO has been used to search for optimum control gains in a search space using normal search schemes. Exploration or global search takes part primarily where particles start to search seeking the optimum gains in a wide area followed by exploitation or local search where the optimum control gains reside in a narrower area called local minima. In that context, global search is performed when the inertia weight of particles is high and local search is carried out when inertia weight is small. This pattern of search technique has many demerits. For instance, this case might lead the inertia weight to exit some unclear mechanism and to tap the algorithm in local optima.

Hence, in this study, we focus more on implementing a random number weight (RNW) PSO. In such type, inertia weight of particles is set to a random number between 0 and 1 to decrease the dependence of inertial weight on the maximum number of iterations that is difficult to be initially predicted. Moreover, we created the idea of allocating part of the particles to search for optimum gains simultaneously with the normal search. This strategy avoids the lack of local

search ability at the beginning of the process and global search at the end of the process. This technique improves the control performance compared to other methods discussed in literature.

1.3 Objectives and Study Scope

The principal objective of this study is the assessment of DC microgrids' voltage stability and validate the impact of the suggested online voltage control strategy with random search techniques to optimize control gains and reduce voltage fluctuations in case of sudden and unexpected load changes. In addition, validate the application of secondary and tertiary controllers in mitigating voltage withing the allowable range simultaneously with optimal dispatch of generators.

At the early stage of this research study, eigenvalue analysis is conducted on a 3-bus DC microgrid model to precisely describe the grid characteristics based on the known state space parameters. In addition, a fitness function is developed to maintain voltage stability by focusing on the dominant eigenvalues that has the worst impact on model stability. Online voltage control gives the optimized gains based on loading configuration in every step of the time series simulation. These gains should have a better influence on voltage stability when compared with no random search pattern.

Finally, in the second part of this study, a hierarchical control scheme based on primary, secondary and tertiary controllers is applied to enhance voltage stability inclusively with optimal dispatch of generators to reduce generation cost.

1.4 Thesis Organization

This work is divided into six chapters. In addition to the first chapter which presented the Abstract and thesis introduction, the next five chapters will illustrate the following:

Generally, in Chapter 2, Distributed generation, its impact on grid stability and RES potential in Japan is discussed.

Consequently, in Chapter 3, Modelling of a generalized m-power supplies n-loads dc microgrid and eigenvalue analysis for the suggested DC microgrid model is presented.

Chapter 4 presents the proposed online control method using particle swarm optimization of combined random and normal search particles.

Chapter 5 presents Simulation results of primary controller and comparison between conventional and proposed methods in online voltage control using PSO.

Chapter 6 The hierarchical structure of proposed control method is introduced to enhance voltage stability with optimal dispatch of generators and simulation results when comparing all levels of control in terms of voltage stability.

Finally, conclusion and future work is being presented in Chapter 7 and further suggestions to enhance and improve the outcomes.

CHAPTER 2

DISTRIBUTED GENERATION

2.1 Introduction to DG

Recently, the drastic rise in fossil fuel production compared to market prices and competency between energy sources to be integrated in the electric grid for power generation, has motivated both economists and engineers to search for alternatives. In addition to greenhouse gas emissions and pollution caused by CO_2 outcomes of factories and industrial compounds that used to drain their wastes in water resources leading to a negative impact on ecological life and fish wealth.

Considerably, DG currently receives decent attention for power industry stakeholders who began to invest enormous money to meet with electric energy business trends. DG is considered a perfect solution to many technical and economic problems. Wind and solar energy resources form the great share of investment in that field, and they form the largest portion of prospective penetration in the electric market. However, despite the affordability of renewables and reliable solution offered by distributed generation, stability issues have been taken into consideration and raised concerns related to the intermittent nature and availability of renewables all over the time.

Furthermore, promoting renewables integration is not only a technical issue, however, an economic perspective must be taken into consideration. For that reason, highly advanced research is substantially taking place in a very rapid pace. Moreover, governments started to implement feed in tariff (FIT) mechanism to motivate users to contribute to decisions being taken and own shares in electric markets as it introduces the concept of two-way power and payment.

DG as a concept has a very positive impact on grid stability - especially voltage stability - in power transmission and distribution networks, whether in isolated islands or highly crowded big cities. In highly crowded countries as

Asian ones which has a high rate of birth every year as China and India, distributed generation showed its effectiveness for supplying loads in locations and destinations that it's hard to reach. Converters are always connected to DG units to convert power from one way of power to another. In addition to that, converters could be used as a part of the control scheme. DG can be divided into two types. Firstly, inverter-based DG such as solar photovoltaic and Wind power sources. The second type is non-inverter-based DG like mini hydropower that is easily to be connected to the grid. Ultimately, very neat collaboration between all system devices and equipment to sustain system stability and ensures soft performance of the electric grid is a must.

2.2 Inverter and Non-Inverter Based DG

Typically, an inverter is a developed device that converts voltage and current from a DC image into AC ones electronically. The inverter can synchronize both voltage and frequency to the grid references and improve power factor compared to non-inverter-based DG. However, non-inverter-based DG depends on supplied fuel to control the generator speeds to force them to deliver recommended AC power frequency, which is not required by PV or Wind powers as no fuel is needed in their cases. Furthermore, ESS is not of proper use in larger power system with grid tie. In the blackout cases, the grid tie inverter should follow the standards to disconnect faulty areas to avoid any other potential harming occurrence on the grid.

2.3 Impact of DG on Stability

To ensure grid stability, all generation and load demand must match at all times. DGs in most cases are added nearby the load demand side. Conventional power generation in the transmission level is modeled in power flow calculation studies held in the design phases at the beginning of any project. However, DG has to undergo the same procedures related to stability issues. If the supply and demand balance is not met at any operating point, this might lead to voltage collapse or as technically known “blackouts”. Despite, some compensating ancillary devices could be used in such cases to support voltage as synchronous

compensators. However, in some cases, such devices are not sufficient enough. Hereby, electric network must be subjected to reinforcement and DG represents the most perfect solution for meeting the demand and voltage support in rush hours. For instance, renewable power resources as PV could be mounted on rooftops in residential areas to supply loads in rush hours, while in normal times could be a kind of reinforcement for the grid. Wind power can be also treated as an ancillary and backup power resource in rural areas where no crowded businesses and residential areas exist. Thus, in modern networks, substantial interaction and communication between conventional and DG plants is a must to guarantee a sufficient coordination between them to meet load demands in contingencies and for enhancing voltage profile under any transient perturbations.

2.4 Potentials and Prospects of Renewables in Japan

Electric power generated from RES should be delivered to the consumption areas. Therefore, a tie system must be implemented to allow the interaction between them and the utility. Moreover, battery storage system could be installed in smaller networks, however in large networks, it is hard enough to be installed, not only for technical impracticality but for money wise as well. Depending on each country, before integrating renewables in their national grids, it must be permissible to allow users to connect their devices to the network. Ideally, users could benefit from their renewables connected domestically, any surplus of power could be sold to the utility which is widely known as FIT. Net Energy metering (NEM) devices as shown in Fig. 2.1 and Fig. 2.2 are allocated to measure the flow of power on a two-way connected network as an open market, where every user could act as a separate electric company owner for resilient power share to decrease our reliability on fossil fuels in the future.

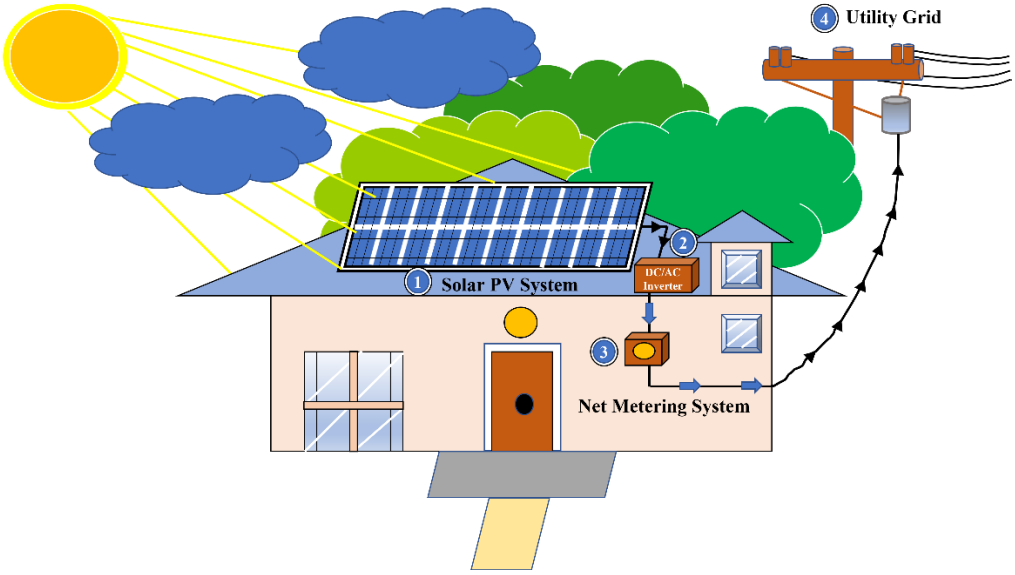

Fig. 2.1 Net Energy Metering (NEM) System W/O Battery Storage [33]

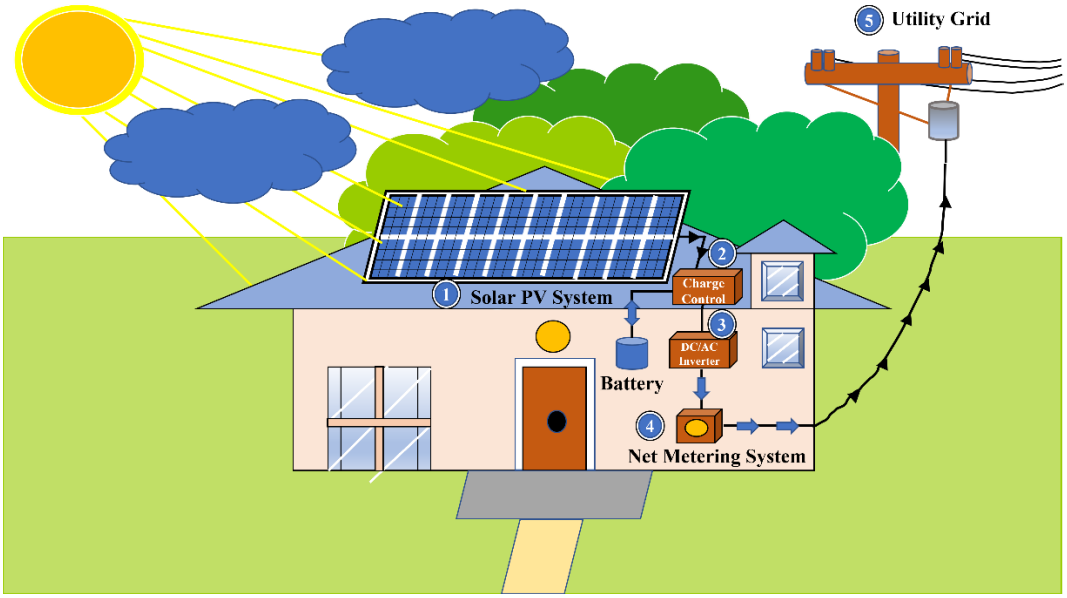

Fig. 2.2 Net Energy Metering (NEM) System with Battery Storage [34]

In this section, a core image of RES prospects in Japan are given to handle the potentials to support RES integration in the future. Japan is one in every of the foremost developed countries within the world, however it still behind the curve in terms of its energy policies. Japan is hierarchically ranked eighth on a world scale as one of the highest countries that produce carbon dioxide gas emissions per capita. Achieving net-zero is an imperative task for the Japanese government. That's why Japan began to amendment its policies targeting to cut back emissions by twenty sixth percent (26%) or more by 2030 and achieve carbon neutrality by

2050. Beyond these plans, Japan targets to raise its share of renewables to twenty four percent (24%) of its electricity needs by 2030. As of 2018, the share was seventeen percent (17%). Despite all this potential, Japan still has lower proportion of wind energy integrated in their grid which was recognized as 0.6% in 2017 as shown in Fig. 2.3.

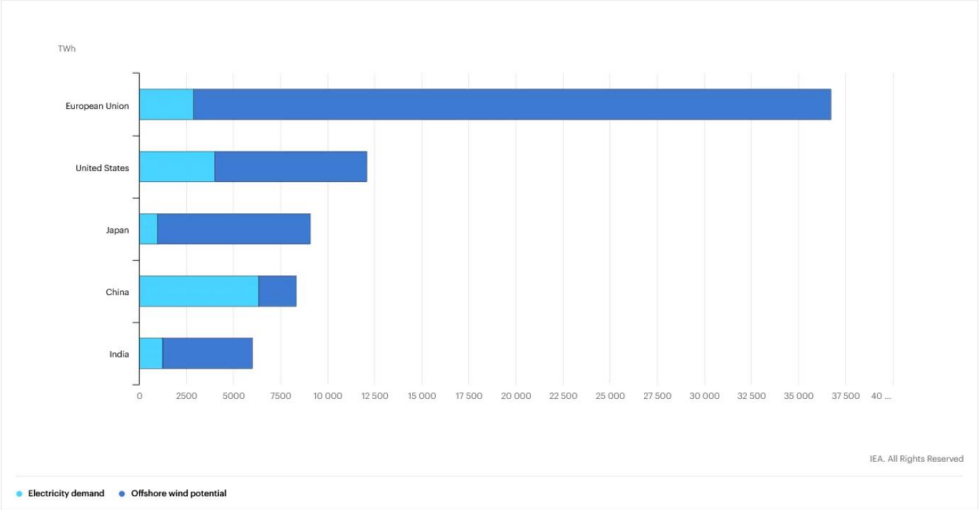

Fig. 2.3 Offshore Wind Power Potential in Japan 2017 [35]

The Japanese government is aiming to extend the grid capacity to ten gigawatts (GW) by 2030. In this plan, offshore wind power is set to reach between thirty and forty-five GW by 2040. This may raise the country's rank into the third-largest generator of such renewable energy in the world. In keeping with IRENA, Japan has the third-highest potential for geothermal energy in the world by twenty three GW. However, Japan only exploits about two percent (2%) of it. Likely with solar photovoltaic (PV), the case is considered similar to that of geothermal energy. Although it has the potential to account for over twelve percent (12%) of the country's energy mix by coming 2030. However, in 2018, it accounted only for four percent (4%).

The Japanese share of RES has been raised to be around eighteen and a half percent annually from almost seventeen and a half percent in the past year. On the other hand, the solar photovoltaic share gave a rise from six and a half percent in 2018 compared to 2019 where it reached almost seven and a half percent. On the other hand, VRE such as solar and wind power has increased its share from seven percent to eight percent. In 2019, the share of Biomass was almost three percent, Wind power was less than one percent and Geothermal power that has a great generating potential was about a quarter percent. However, hydro power

didn't change its share recording no increase in power generation. In terms of the annual quota of fossil fuel, its percentage has shown a slight decrease from seventy eight percent in the previous year to seventy-five, however, this shows that what is done is not enough, also the annual quota of nuclear power generation has recorded a rise with one and a half percent as it increased its share from almost five percent in the former year to about six and a half percent by 2019. Fig. 2.4, 2.5 and 2.6 show the Japanese power generation 2019, Share of renewables in Japanese power network and Renewable Energy Monthly Share in Japan 2019 respectively.

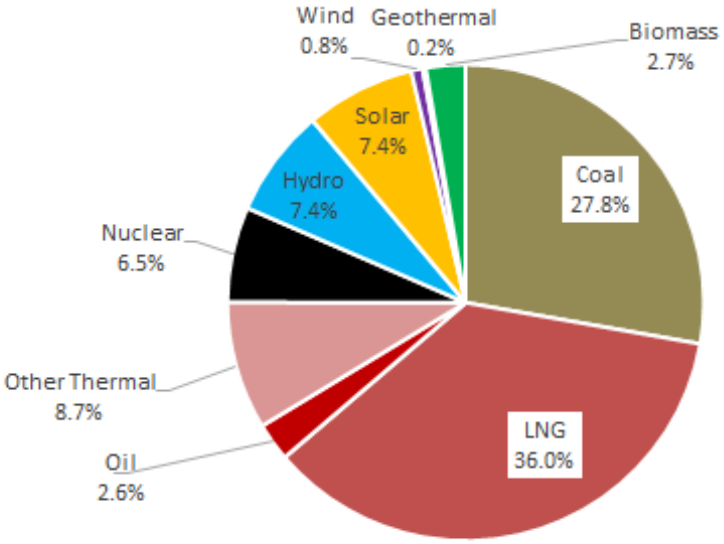

Fig. 2.4 Japanese power generation 2019 [36]

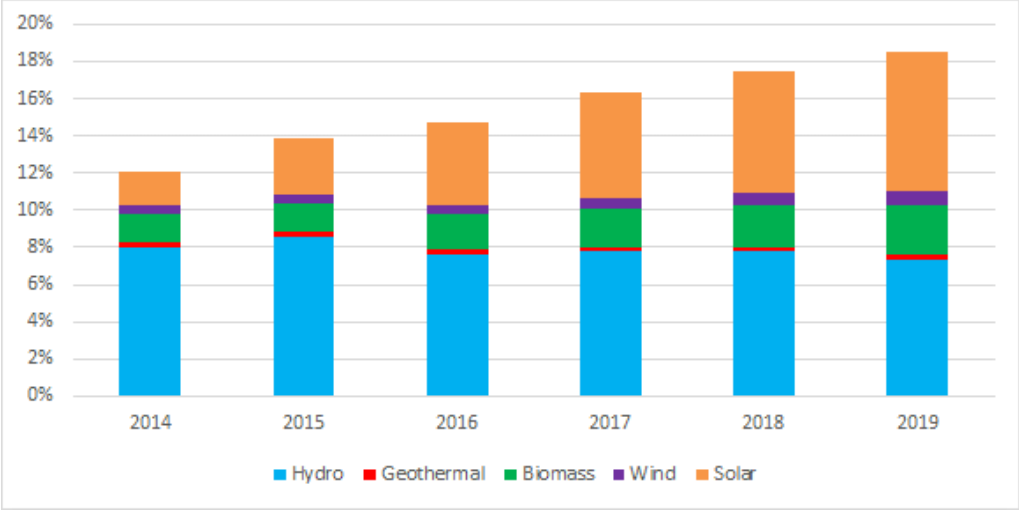

Fig. 2.5 Share of renewables in Japanese power network [36]

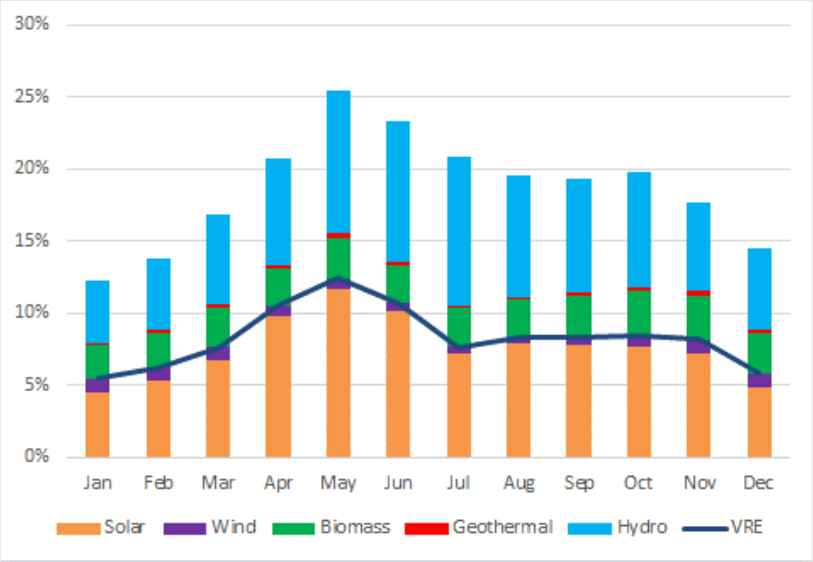

Fig. 2.6 Renewable Energy Monthly Share in Japan 2019 [36]

In Europe, many countries have raised their annual share of RES power generation over thirty percent (30%) as Denmark that enhanced its electric network extending the share of RES to eighty four percent. In many countries, the VRE quota has recorded over twenty percent, while it is fifty five percent in Scandinavian countries as Denmark. European countries have a long-term target for applying more integration of renewable energy, and a few of them aim to abandon fossil fuels by 2030. On the contrary, Japan is aiming at twenty four percent of its total generation to be of RES that is considered very low. In China, the share of renewables is about twenty-six and a half percent annually, including wind power records five and a half percent, solar power quota stands for about three percent and VRE share is almost eight and a half percent greatly exceeding the nuclear power share which is around five percent.

2.5 Summary

This chapter discussed Distributed Generation overview and highlighted the positive impacts of integrating DG in the grid from the perspective of voltage profiles and transient stability analysis. Moreover, this chapter mentioned the prospective envision and potentials of renewables in Japan, mentioning the strategy of the Japanese Government to integrate and invest more in renewables and increase its share to reach nearby by 2040 and reducing carbon dioxide gas emissions to reach zero neutrality by 2050.

CHAPTER 3

DC MICROGRID MODELLING

3.1 Background

To verify the DC microgrid voltage stability control in a latter section, the microgrid stability under constant power loads has to be taken into consideration [37]-[39]. In this section a model based on m number of power generators and n number of buses must be presented to verify our control method. This could be achieved through several steps. Firstly, one generator one load model is created and then develop it to a model of variable number of generators, buses and loads. Fig. 3.1 is a simplified one-power-one-load DC microgrid model that combines a single DG unit, line regulating converter (LRC), point of load (POL) converter and with a constant power load [37]. In this model, the rated output voltage "*E*" is given from the power supply, and power is transmitted through LRC — which is a simple chopper circuit — to the POL converter then to the load. In this research, we observe and control the current and voltage sent to the POL converter through LRC. In this work LRC could be sometimes be referred as step down chopper (SDC).

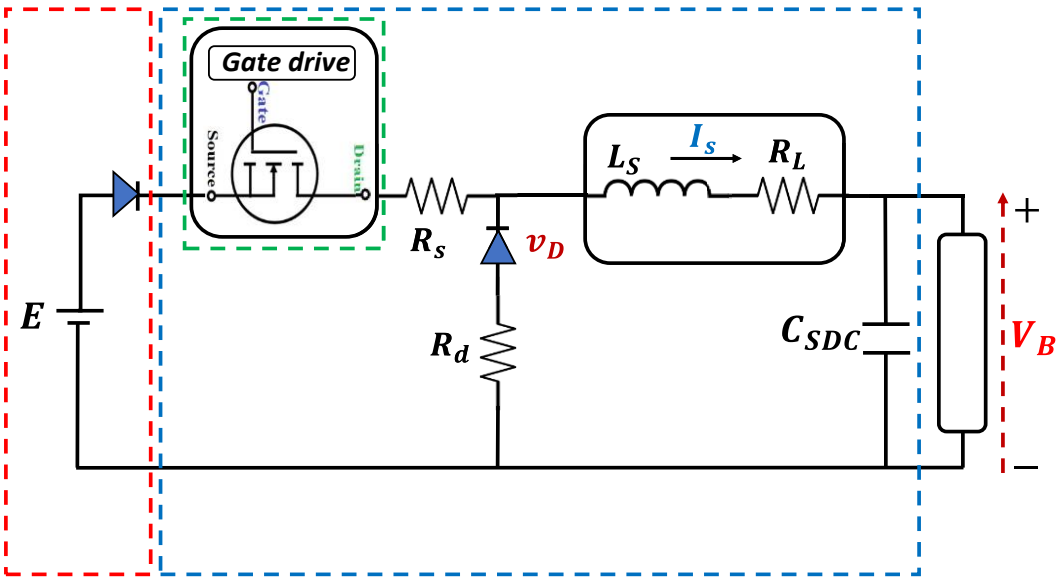

Fig. 3.1. One power supply-one load dc microgrid model

The internal circuit of SDC is detailed as shown to observe the current and voltage sent to the POL converter. In this circuit, the voltage output of power supply could be adjusted through gate switching, while the main purpose is to observe and control SDC output voltage "V_B" and current "i_B" to the POL. The illustration of each parameter in the circuit diagram of Fig. 3.1 is as shown below:

R_S: Resistance when MOSFET is on

R_d: Resistance when current flows through the diode

R_L: Inductor resistance

I_s: SDC internal current flowing though inductor

V_D: Diode voltage drop

V_B: Voltage output of SDC applied to POL

P_L: Load power

Where $d_i(t)$ represents the instantaneous value of duty ratio at time t in an average value linearized model, where MOSFET switching time delay was ignored and just the ratio of ON/OFF was taken into account.

To simplify the model, as SDC is very efficient with overall efficiency approaching 96% and its losses are very small compared to other types, we assume SDC as an ideal converter with no losses. Mathematically, that is interpreted as follows:

$$R_S = R_d = R_L = V_D = 0$$

Consequently, circuit equation of the one power supply-one load DC microgrid shown in Fig. 3.1 can be expressed as follows:

$$L_s C_{SDC} \frac{d^2 V_B(t)}{dt^2} - L_s P_L \frac{dV_B(t)}{dt} \frac{1}{{V_B}^2(t)} + V_B(t) = d(t)E \qquad (1)$$

$$I_s(t) = C_{SDC} \frac{dV_B(t)}{dt} + \frac{P_L}{V_B(t)} \geq 0 \qquad (2)$$

From both equations (1) and (2), the values of voltage "V_B" and current "I_s" applied to the POL could be obtained. In [37]-[39], it is obvious that CPL has a bad

impact on the stability of the network due to its negative impedance characteristic. Consequently, voltage and current outputs at CPL terminals oscillate and stable control cannot be performed only by controlling SDC.

3.2 Primary Control Method For Voltage Instability

In this section, the primary control strategy is introduced. Primary controller is based on adjusting duty ratio of all generators with every load change through adjusting PD controller gains to damp oscillations and avoid voltage instability. The duty ratio control for DG_i can be shown by the following formulation.

$$d_i(t) = k_{pi}e_i(t) + k_{di}\frac{de_i(t)}{dt} + D_i \qquad \left(0 \le d_i(t) \le 1\right) \tag{3}$$

$$e(t) = V_{ref,i}(t) - V_{Bi}(t) \tag{4}$$

k_{pi} and k_{di} represent proportional and differential control gains of PD controller for DG i respectively. D_i is the reference value of duty ratio of DG i, $V_{Bi}(t)$ and $V_{ref,i}(t)$ are the terminal voltage and its target value for DG i at time t, while $e_i(t)$ is the error between the terminal bus voltage and its target value at time t. In this study, $\pm 5\%$ is the considered upper and lower limits for voltage control.

3.3 m-Power Supply and n-Bus DC Microgrid Model

As referred to the previous section, where one power supply-one load DC microgrid model with connected CPL was introduced. Likely, a generalized form is created to observe and control voltage and current states. Fig. 3.2 shows the model with numerous DG units with their internal DC voltages "E_1, E_2, …. E_m", connected SDCs and several dispersed loads connected at the various locations in the grid "P_{L1}, P_{L2}, ….., P_{Ln}". Terminal voltages connected to DG units are expressed as "V_{B1}, V_{B2}, …, V_{Bm}", while voltages at other terminals are expressed as "$V_{B(m+1)}$, $V_{B(m+2)}$, ….., $V_{B(m+n)}$". CPLs can be connected to any buses including DG buses with point of load converters (POLs). L_S and R_L are transmission line inductances and resistances respectively. "I_{S1}, I_{S2}, ….., I_{Sm}" are the currents

flowing through SDC. CPLs are simply modelled as product of terminal bus voltage and load current without using SDC. Distribution lines are included in the DC microgrid which consists of l distribution lines. L_{Di} and R_{Di} are inductance and resistance of distribution line i, respectively, and "I_{D1}, I_{D2}, ….., I_{Dl}" are currents on the distribution lines.

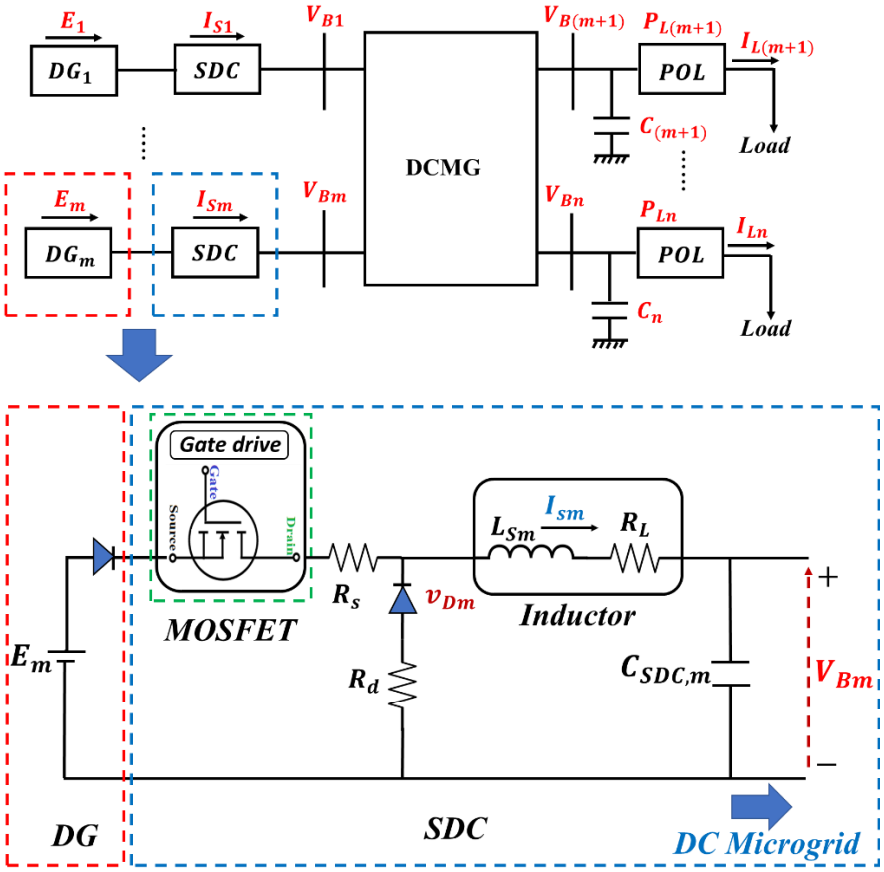

Fig. 3.2. m-power supply and n-bus DC microgrid model

The following equations (5) to (8) describe the m-power supply and n-bus DC microgrid model:

$$\frac{dI_{Si}(t)}{dt} = \frac{1}{L_{Si}}\left(d_i(t)E_i - V_{Bi}(t)\right) \quad \forall i \in M \tag{5}$$

$$\frac{dV_{Bi}(t)}{dt} = \frac{1}{C_{Bi}}\left(I_{Si}(t) - I_{Di}(t) - I_{Li}(t)\right) \quad \forall i \in B \tag{6}$$

$$\frac{dI_{Di}(t)}{dt} = \frac{1}{L_{Di}}\left(\sum_{k=1}^{n} A_{ik}V_{Bk}(t) - R_{Di}I_{Di}(t)\right) \quad \forall i \in D \tag{7}$$

POL is modeled as constant power loads as illustrated below:

$$P_{Li}(t) = V_{Bi}(t)I_{Li}(t) \quad \forall i \in B \tag{8}$$

Here, the direction of line current on distribution line i has to be defined so that A_{ik}=1 or -1 if the terminal bus k is start or end node of the line, and A_{ik}=0 if no connection between bus i and k. M, B, and D are set of DGs, buses, and distribution lines. By solving the above equations, voltage and current states could be observed and controlled easily.

3.4 Proposed Simulation Model

In this research a simplified 3-bus simulation model is used [37]. Two DG units and two loads are utilized as shown in Fig. 3.3. This model is derived from the model shown in Fig. 3.2. Consequently, same equations from (5) to (8) are implemented. In Fig. 3.3, two connected generators at terminals 1 and 2 with rated output voltage E_1 and E_2. On the other hand, Power loads are connected to terminals 1 and 3, with rated power P_{L1} and P_{L3}. However, Terminal voltages are expressed as V_{B1}, V_{B2} and V_{B3}. Directions of distribution line currents are defined as shown in the figure. The capacitance in SDC, C_{SDC} is combined with other capacitances and directly connected to buses such as C_{B1}, C_{B2} and C_{B3}.

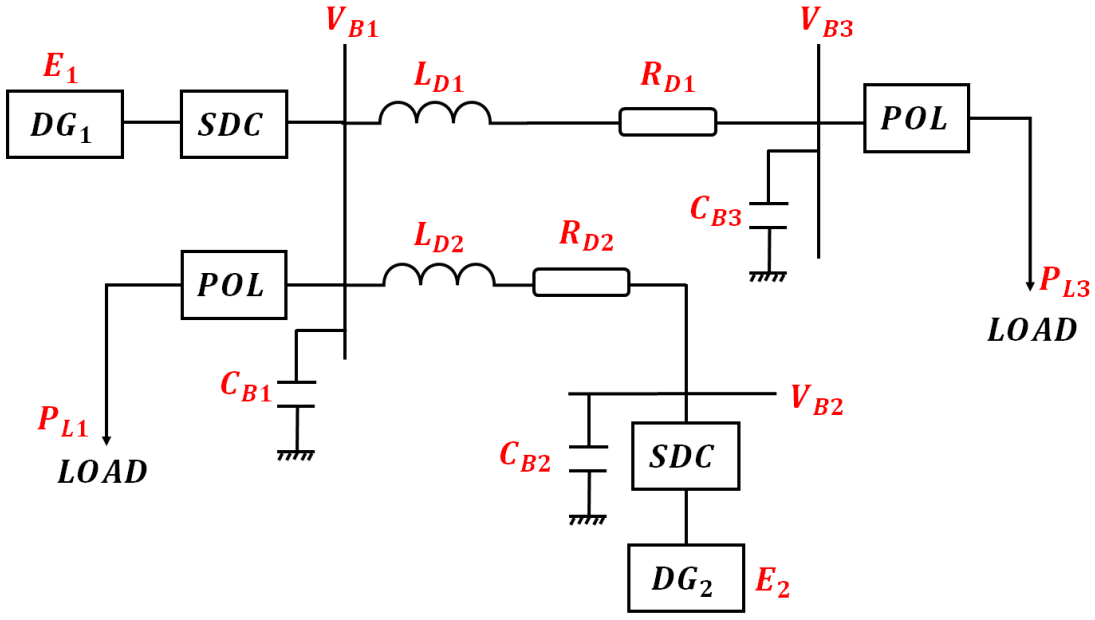

Fig. 3.3. Simplified 3 bus model of DC microgrid

We have been discussing so far, a method of adjusting terminal voltages and suppressing voltage fluctuations based on adjusting the duty ratio of power supplies through PD controller. However, optimum solution for gain search is subjective and dependent on many factors. For instance, in an actual system, there is a dispatch for optimal operation due to the differences in generation cost for each power supply, and the gain for efficient operation control differs in response to daily fluctuating load demand. For that reason, in this research, we propose a gain search method using eigenvalue analysis for constantly observing the system state online and performing efficient operation control for fluctuating load conditions.

3.5 Eigenvalue Analysis of Proposed DC Microgrid Model

Eigenvalue analysis is conducted in this research to arbitrarily determine the ability of the proposed control algorithm to achieve stability of the model based on the eigenvalues and how far dominant eigenvalues are from the stability boundary. Several steps are carried out to undergo this analysis. Firstly, determine all state variables and control gains through which voltage control could be achieved effectively. Then divide the circuit into sections and suppose electric currents' directions all over it as shown in Fig. 3.4. The following equations describe the circuit as follows:

$$\frac{d}{dt}I_{S1}(t) = \frac{1}{L_{S1}}(d_1(t)E_1 - V_{B1}(t)) \tag{9}$$

$$\frac{d}{dt}I_{S2}(t) = \frac{1}{L_{S2}}(d_2(t)E_1 - V_{B2}(t)) \tag{10}$$

$$\frac{d}{dt}V_{B1}(t) = \frac{1}{C_{B1}}(I_{S1}(t) - I_{D1}(t) - I_{L1}(t)) \tag{11}$$

$$\frac{d}{dt}V_{B2}(t) = \frac{1}{C_{B2}}(I_{S2}(t) - I_{D2}(t)) \tag{12}$$

$$\frac{d}{dt}V_{B3}(t) = \frac{1}{C_{B3}}(I_{D1}(t) - I_{L3}(t)) \tag{13}$$

$$\frac{dI_{D1}(t)}{dt} = \frac{1}{L_{D1}}(V_{B1}(t) - V_{B3}(t) - I_{D1}(t)R_{D1}) \tag{14}$$

$$\frac{dI_{D2}(t)}{dt} = \frac{1}{L_{D2}}(V_{B2}(t) - V_{B1}(t) - I_{D2}(t)R_{D2}) \tag{15}$$

$$P_{L1}(t) = V_{B1}(t)I_{L1}(t) \tag{16}$$

$$P_{L3}(t) = V_{B3}(t)I_{L3}(t) \tag{17}$$

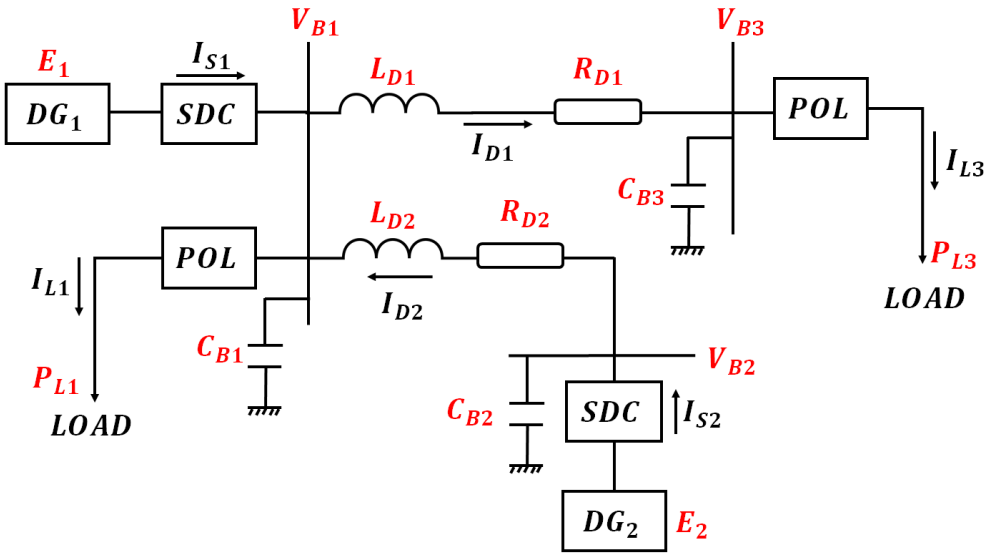

Fig. 3.4. Internal current of 3 bus model of DC microgrid

The three-bus DC microgrid is regarded as a linear system, and the S-matrix representing the characteristics of the three-bus DC microgrid system is obtained for the linear system model to assess the effectiveness of the proposed optimization method to stabilize the network. The method to obtain the S-matrix is shown as follows:

$$\Delta\dot{x} = A\Delta x + B\Delta y \tag{18}$$

$$0 = C\Delta x + D\Delta y \tag{19}$$

Equations (18) and (19) illustrate the state variables denoted as "x" , algebraic

variables denoted as "y" and the four matrices A, B, C and D of the escorting coefficients. By solving both equations S matrix could be obtained.

$$A = \frac{\partial f_n}{\partial x_n} \tag{20}$$

$$B = \frac{\partial f_n}{\partial y_n} \tag{21}$$

$$C = \frac{\partial g_n}{\partial x_n} \tag{22}$$

$$D = \frac{\partial g_n}{\partial y_n} \tag{23}$$

Where f_n is the equation including the differential term x_n and g_n is the equation including the differential term y_n. By solving both equations together we get:

$$\Delta\dot{x} = S\Delta x \tag{24}$$

Where $S = (A - BD^{-1}C)$

State variables are described by set of vector x, where $x = (V_{B1}, V_{B2}, V_{B3}, I_{S1}, I_{S2}, I_{D1}, I_{D2}, a_1, a_2)^T$ and algebraic variables are described by set of vector y, where $y = (I_{L1}, I_{L3})$. Here, a_1 and a_2 are variables related to partial differentiation. In PD control, simply differentiating the oscillatory control deviation ΔV_B may output a large value when the input changes suddenly. Here, partial differentiation is used as one of the methods for suppressing the large disturbance. Partial differentiation is a process in which a low-pass filter is added to the differentiation process as illustrated in the block diagram shown in Fig. 3.5.

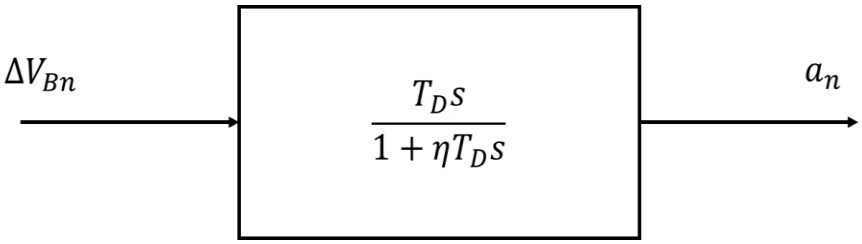

Fig. 3.5. Block diagram of partial differentiation

When the inexact differentiation is expressed by a mathematical formula, the term related to the differential gain k_d during PD control can be expressed by the following equation:

$$a_n = \frac{T_D s}{1 + \eta T_D s} \Delta V_{Bn} \tag{25}$$

Consequently, partial differential functions f_n and g_n are illustrated as described in the following equations:

$$f_1(\boldsymbol{x}, \boldsymbol{y}) = \frac{dV_{B1}(t)}{dt} = \frac{1}{C_{B1}} (x_4 - y_1) \tag{26}$$

$$f_2(\boldsymbol{x}, \boldsymbol{y}) = \frac{dV_{B2}(t)}{dt} = \frac{1}{C_{B2}} \left(x_5 - x_6 \right) \tag{27}$$

$$f_3(\boldsymbol{x}, \boldsymbol{y}) = \frac{dV_{B3}(t)}{dt} = \frac{y_4}{C_{B3}} \tag{28}$$

$$f_4(\boldsymbol{x}, \boldsymbol{y}) = \frac{dI_{S1}(t)}{dt} = \frac{1}{L} \left(-\left(k_{p1} E_1 + 1 \right) x_1 - k_{d1} E_1 x_8 + k_{p1} D_1 {E_1}^2 + D_1 E_1 \right) \tag{29}$$

$$f_5(\boldsymbol{x}, \boldsymbol{y}) = \frac{dI_{S2}(t)}{dt} = \frac{1}{L} \left(-\left(k_{p2} E_2 + 1 \right) x_2 - k_{d2} E_2 x_9 + k_{p2} D_2 {E_2}^2 + D_2 E_2 \right) \tag{30}$$

$$f_6(\boldsymbol{x}, \boldsymbol{y}) = \frac{dI_{D2}(t)}{dt} = \frac{1}{L_{D2}} \left(x_2 - x_1 - R_{D2} x_6 \right) \tag{31}$$

$$f_7(\boldsymbol{x}, \boldsymbol{y}) = \frac{dI_{D1}(t)}{dt} = \frac{1}{L_{D1}} \left(x_1 - x_3 - R_{D1} x_7 \right) \tag{32}$$

$$f_8(\boldsymbol{x}, \boldsymbol{y}) = \frac{da_1(t)}{dt} = -\frac{1}{\eta} \left(\frac{x_8}{T_d} + \frac{1}{C_{B1}} \left(x_4 - y_1 \right) \right) \tag{33}$$

$$f_9(\boldsymbol{x},\boldsymbol{y}) = \frac{da_2(t)}{dt} = -\frac{1}{\eta}\left(\frac{x_9}{T_d} + \frac{1}{C_{B2}}\left(x_5 - x_6\right)\right) \tag{34}$$

$$g_1(\boldsymbol{x},\boldsymbol{y}) = x_5 - x_6 + y_2 - y_1 \tag{35}$$

$$g_2(\boldsymbol{x},\boldsymbol{y}) = \frac{P_{L3}}{x_7} - y_3 \tag{36}$$

$$g_3(\boldsymbol{x},\boldsymbol{y}) = \frac{P_{L1}}{x_3} - y_2 \tag{37}$$

$$g_4(\boldsymbol{x},\boldsymbol{y}) = x_5 - y_3 - y_4 \tag{38}$$

By re-arranging the previous equations into a formula in terms of matrix *x* only, f_n would be as follows:

$$f_1(\boldsymbol{x}) = \frac{dV_{B1}(t)}{dt} = \frac{1}{C_{B1}}\left(-\frac{P_{L1}}{x_1} + x_4 + x_6 - x_7\right) \tag{39}$$

$$f_2(\boldsymbol{x}) = \frac{dV_{B2}(t)}{dt} = \frac{1}{C_{B2}}\left(x_5 - x_6\right) \tag{40}$$

$$f_3(\boldsymbol{x}) = \frac{dV_{B3}(t)}{dt} = \frac{1}{C_{B3}}\left(-\frac{P_{L3}}{x_3} + x_7\right) \tag{41}$$

$$f_4(\boldsymbol{x}) = \frac{dI_{S1}(t)}{dt} = \frac{1}{L}\left(-\left(k_{p1}E_1 + 1\right)x_1 - k_{d1}E_1x_8 + k_{p1}D_1{E_1}^2 + E_1D_1\right) \tag{42}$$

$$f_5(\boldsymbol{x}) = \frac{dI_{S2}(t)}{dt} = \frac{1}{L}\left(-\left(k_{p2}E_2 + 1\right)x_2 + k_{d2}E_2x_9 + k_{p2}D_2{E_2}^2 + E_2D_2\right) \tag{43}$$

$$f_6(\boldsymbol{x}) = \frac{dI_{D2}(t)}{dt} = \frac{1}{L_{D2}}\left(x_2 - x_1 - R_{D2}x_6\right) \tag{44}$$

$$f_7(\boldsymbol{x}) = \frac{dI_{D1}(t)}{dt} = \frac{1}{L_{D1}}\left(x_1 - x_3 - R_{D1}x_7\right) \tag{45}$$

$$f_8(\boldsymbol{x}) = \frac{da_1(t)}{dt} = \frac{1}{\eta}\left(\frac{1}{C_{B1}}\left(-\frac{P_{L1}}{x_1} + x_4 + x_6 - x_7\right) - \frac{x_8}{T_d}\right) \tag{46}$$

$$f_9(\boldsymbol{x}) = \frac{da_2(t)}{dt} = \frac{1}{\eta}\left(\frac{1}{C_{B2}}\left(x_5 - x_6\right) - \frac{x_9}{T_d}\right) \tag{47}$$

Since from definition $$B = \frac{\partial f}{\partial y} = 0 \tag{48}$$

Accordingly, and from equation (30), S matrix would be as follows:

$$S = A = \begin{bmatrix} \frac{\partial f_1}{\partial x_1} & \cdots & \frac{\partial f_1}{\partial x_9} \\ \vdots & \ddots & \vdots \\ \frac{\partial f_9}{\partial x_1} & \cdots & \frac{\partial f_9}{\partial x_9} \end{bmatrix} \tag{49}$$

By solving equations (39) to (47), we can obtain S matrix. S matrix represents the matrix that describes network configuration and includes the whole network parameters from loading powers and control gains. By getting the S matrix we can easily obtain its eigenvalues to assess network stability based on the eigenvalue analysis perspective. The eigenvalues are considered time variants, whenever any load change occurs, the proposed algorithm will try to find a new solution to the problem. Accordingly, the components of the S matrix will change and leading to a different combination of poles. The resulted eigenvalues are arranged in a descending order in terms of their real values, taken the sign into consideration. Ultimately, the objective function is updated based on the new eigenvalues and the stability of the network will be determined accordingly.

S matrix can be shown as follows:

$$
\begin{bmatrix}
S_{11} = \frac{P_{L1}^*}{C_B V_{B1}(t)^2}, S_{14} = S_{16} = -S_{17} = \frac{1}{C_B} \\
S_{25} = -S_{26} = \frac{1}{C_B} \\
S_{33} = \frac{P_{L3}^*}{C_B V_{B3}(t)^2}, S_{37} = \frac{1}{C_B} \\
S_{41} = -\frac{k_{p1}E_1 + 1}{L_S}, S_{48} = -\frac{k_{d1}E_1}{L_S} \\
S_{52} = -\frac{k_{p2}E_2 + 1}{L_S}, S_{59} = -\frac{k_{d2}E_2}{L_S} \\
S_{61} = -S_{62} = -\frac{1}{L_D}, S_{66} = -\frac{R_D}{L_D} \\
S_{71} = -S_{73} = \frac{1}{L_D}, S_{77} = -\frac{R_D}{L_D} \\
S_{81} = \frac{P_{L1}^*}{\eta C_B V_{B3}(t)^2}, S_{84} = S_{86} = -S_{87} = \frac{1}{\eta C_B}, S_{88} = -\frac{1}{\eta T_D} \\
S_{95} = -S_{96} = \frac{1}{\eta C_B}, S_{99} = -\frac{1}{\eta T_D} \\
\text{Other than that, } S_{ij} = 0
\end{bmatrix}
$$

Here, * denotes a value on an equilibrium point, and network parameters are assumed to be the same for all buses and distribution lines. S matrix here describes the characteristics of the 3-bus DC microgrid. To investigate stability analysis, it must be through the S matrix of eigenvalue analysis to check the optimum control gains to maintain voltage stability. In this study $\eta = 0.1$, while $T_D = 0.0001$.

3.6 Summary

This chapter gave an overview about modelling a general form of DC microgrid using an *m*-power supplies and *n*-loads to model terminal voltages, generation and transmission currents while POL is modelled as a constant power load. The next section includes conducting eigenvalue analysis on a simplified 3-bus model. Based on determining all state and dynamic variables, the model is sectionized, currents are given expected directions and eigenvalue analysis is conducted to perform an efficient operation control for fluctuating load conditions. Finally, S matrix that is inclusive to all grid characteristics is calculated and through which eigenvalues are updated after receiving optimized control gains from the online voltage control using PSO.

CHAPTER 4

PARTICLE SWARM OPTIMIZATION TECHNIQUE AND PROPOSED ONLINE CONTROL STRATEGY

4.1 Introduction to Artificial Intelligence

AI or as generally been known as Machine Intelligence (MI) is performed by machines, in contrary with human intelligence (HI) that is performed with humans. AI research tries to solve the problems and expect the future by conducting research and trying to mimic the human mind in learning and taking actions. Nowadays, there are many classifications for AI. As an example, successfully understanding human speech, automatic face recognition, competing in chess, military simulations, and image processing. However, AI raises the philosophical arguments concerning the ethics as machines have no moralities or preferences to return back to. Some other people consider that it is primarily a huge risk to employment: as researchers found that almost many jobs in the US are at risk due to AI. Nowadays, AI technologies have been through several progresses and due to overwhelming advances in computer programing, data collection and processing, AI plays an important role in modern trade, engineering science and many other fields.

4.1.1 History of AI

AI research was created at a workshop at Dartmouth College in 1956. Several attendees at this workshop have taken the lead and played a pivotal role in the AI research. They and their students created programs that the press considered as the stepping-stones in the AI field. In the early eighties, AI research continued its progress by the introducing expert systems, a form of AI program that mimicked the skills of human experts. Nowadays, AI started to be used for many alternative areas. For instance, AI can be used for face and speech recognition, medical diagnosis and other areas. Deep learning system, faster computers and easy access to big data enabled progressive machine learning performances.

Year 2015 witnessed the re-birth of AI in industry, as Google increased its AI implementations in its fields to more than 2,700 projects. Moreover, the various applications of AI techniques including image processing have shown a prompt rise with less significant errors. Not to mention, other examples including the development of a Skype system by Microsoft that can translate from one language to another [40].

4.1.2 Phases of AI techniques

The overall target of AI techniques is to invent a technology that drives machines and devices to act as human intelligence. There are several characteristics and attributes that researcher think that any AI system has to be described with. The attributes are illustrated below as follows:

1. **Reasoning, problem solving**

In the eighties and nineties, researchers in the field of AI had created strategies for acting with uncertainties and mis-leading information. These strategies comprise of implementing probability concepts like those applied for economics. However, for difficult issues, algorithms may need different computational resources. For instance, computer memory size or time required becomes unlimited for bigger problems. The highest priority now is to look for more efficient algorithms in solving problems.

2. **Knowledge Representation**

Many of the issues that machines confront and are expected to solve requires a huge bulk of information. AI can inclusively represent, objects, shapes, colors situations, states, events, time, causes and effects.

3. **Planning**

Intelligent systems have to predict the future and try to figure out how their actions will change by time. In classical single agent planning problems, the agent is assumed to be acting solely in the world and has the only impact on it. Though, it has to plan for its actions and the consequences of them. However, in multiagent planning systems, each agent has to assess its environment, predict, plan, take actions, evaluate the consequences, and adapt to it.

4. Learning

There are three types of learning patterns. Firstly, unsupervised learning which is being able to find models among a huge bulk of inputs and information. Secondly, supervised learning which comprises of both classification and numerical regression. The ability to refer objects, colors or properties to categories and divisions is called classification. However, regression is the ability to figure out the relationship between inputs and outputs based on the available information. In addition to that, try to figure out how the output changes if the input does. Moreover, in reinforcement learning the agent uses a set of rewards with positive values for good actions and negative values for bad performances to form a strategy for operating in the search space.

5. Perception

Machine perception is the ability to express its perception of the surroundings by using inputs such as cameras, microphones, sensors, and others.

4.2 AI Approaches

Since the born of AI and throughout 6 decades of research, AI has been developed progressively that created a set of tools to overcome the most intractable difficulties and problems in the field of computer science. Some of these methods and techniques are discussed below.

4.2.1 Artificial Neural Networks (ANN)

ANN are optimization techniques and computing systems based on neural networks forming human brains. These systems get trained and self-taught by examples without any former knowledge or prior information. For instance, face or image recognition, as they can analyze images identified by same or relevant names without knowing the content of that image or its characteristics. An ANN consists of artificial neurons that can transmit the signals and information from one to another using links between them. The neurons and the links between them actually have a weight that is pre-assumed then adjusted within the learning process. The output is calculated based on the sum of its inputs [41].

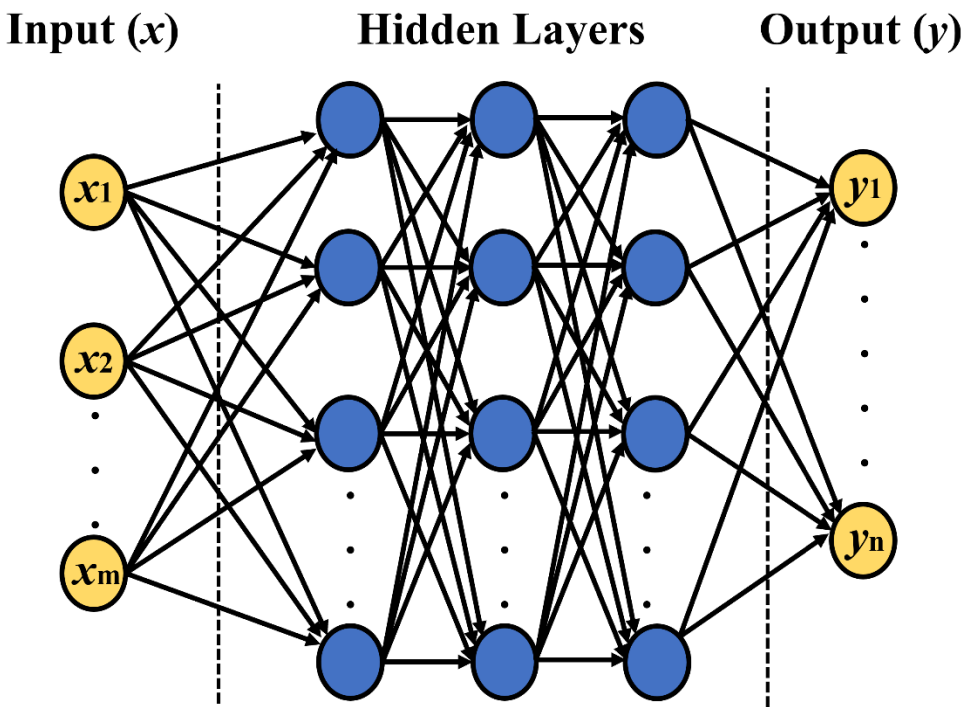

Fig. 4.1 Simple principle of Artificial Neural Network [42]

As shown in Fig. 4.1, artificial neurons are divided into layers. The left layer is the inputs' layer, while the right layer is the outputs' layer. The layers in between are hidden layers and used for the processing of AI techniques. The size of the hidden layers determines the accuracy of optimization and computation time. ANN technique mainly aims at solving problems and optimizing control performance in the same way that a human brain would. ANNs can be applied in various tasks, including image processing, video games and medical diagnosis.

4.2.2 Genetic Algorithm (GA)

A genetic algorithm (GA) is mainly used to solve optimization problems by relying on bio-inspired operators such as mutation, crossover and selection. There are several terms that describe the GA. Individuals are the population of candidate solutions. Generation is the population in each iteration, while chromosomes are the properties and characteristics of each individual. Originally, solutions are expressed as 0s and 1s. Fitness function is calculated and updated in every generation, after genomes of the candidate solutions are determined and modified. Finally, when either the maximum number of iterations is reached, or the control target has been met, the algorithm terminates [43].

4.2.3 Expert System

Expert system is mainly designed to solve very complicated problems relying on previous presented information. It is produced to mimic the ability of experts in decision-making. An expert system is divided into two sub-divisions: the knowledge base and the inference engine. The first one represents a set of facts and rules and the second one creates new facts based on the former knowledge base.

Expert system has many merits as ease of maintenance and rapid development. Expert systems avoided writing conventional codes that even with small changes can cause big problems. In addition, it is possible to make and develop a new prototype in days rather than months or years by entering a few rules. In that context, problems and computational issues are avoided. However, the performance was problematic because early expert systems were built using tools such as Lisp, which doesn't execute compiled codes but interpreted ones that has lower efficiency than languages like C. Expert system has been applied to fields like finance, marketing, sports psychology and defense [44].

4.2.4 Fuzzy Logics

Fuzzy systems use fuzzy and ambiguous sets to deal with incomplete data. In fuzzy set membership takes any value between 0 and 1. As shown in Fig. 4.2, Fuzzy logics' process is divided into three consecutive segments as follows:

a) Fuzzification: Fuzzify all input values into fuzzy membership functions.
b) Execution: Execute all rules to calculate the fuzzy output functions.
c) De-fuzzification: De-fuzzify the fuzzy output functions to get output values.

Fuzzy logic has many applications in Japan. For instance, the high-speed train in Sendai, handwritten symbols recognition in Sony pocket computers, enhanced fuel consumption for cars, automatic motor control for vacuum cleaners and early prediction systems of earthquakes [45].

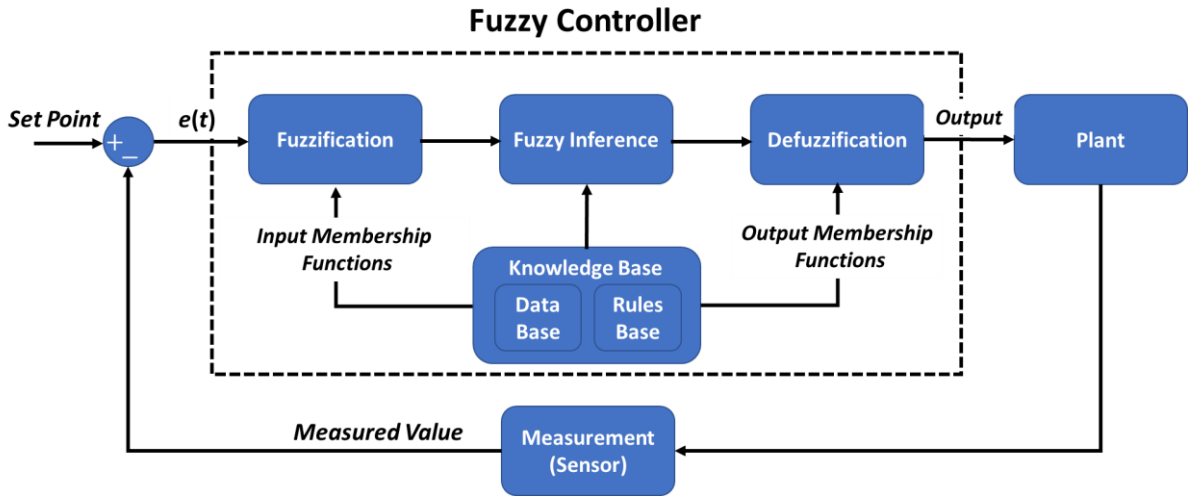

Fig. 4.2 Fuzzy Controllers in Closed Loop Structures [46]

4.2.5 Particle Swarm Optimization (PSO)

Swarm intelligence (SI) is a form of modeling and optimization technique inspired by colonies or swarms such as birds, ants or fish. The strategy of PSO is based on a collection of particles moving in the search space and trying to find the optimum solution. Each particle's movement is changing its position and velocity in every iteration based on both local and global best positions. Local and global best fitness functions are updated and calculated in every iteration as an indication to approaching the optimum solution. When the criteria are met or when the number of iterations reached to its max value, the optimization is terminated.

4.2.6 Hybrid Systems

Hybrid intelligent system is a computational system used for control system optimization which integrates more than one AI strategy and technique as follows:

- Neuro-fuzzy systems
- hybrid connectionist-symbolic models
- Fuzzy expert systems
- Connectionist expert systems

- Evolutionary neural networks
- Genetic fuzzy systems
- Rough fuzzy hybridization
- Reinforcement learning with fuzzy, neural, or evolutionary methods as well as symbolic reasoning methods [47].

4.3 PSO technique and proposed online voltage control strategy

In this research, an online control of DC microgrid terminal voltages using PSO is proposed. This proposed strategy is suggested for real time calculation of proper network control gains based on loading condition. PSO has been in comparison with other evolutionary optimization techniques as GA and Differential Evolution (DE) to determine which could be considered for this research. However, PSO when compared with the other techniques, we can observe that PSO has the fastest computational time amongst them. However, the dynamic performance of DE and PSO are close to each other [48]- [50]. On the hand, the tendency of PSO for pre-mature convergence is high compared to DE and GA which is a demerit.

The three evolutionary techniques are compared in [48]. According to Table 4.1, it is found that, GA requires ranking of solutions based on their fitness function values, while DE and PSO do not need that criterion. In addition, when the population size increases, GA requires longer time to find the optimum solution. Accordingly, GA is considered the slowest amongst the three techniques. However, the nature of how DE finds the best solutions might be a bit slower than PSO. DE tries to find the best solution through mutation by finding the mutant vector, then crossover to improve the diversity of the technique by obtaining a trial vector. Finally, comparing the fitness function value of the trial vector with the target vector to determine the new target vector for the next iteration. With this criterion, DE guarantees the improvement of the fitness function value in every iteration. However, PSO leads to a faster convergence which sometimes be considered a negative aspect if that leads to a stagnant solution.

A comparison between DE and PSO was conducted in [49] based on their dynamic responses. Eight benchmark functions are utilized as fitness functions and the dynamic performance is analyzed accordingly. Standard deviation and average values of the objective functions are set as assessment criteria for that conducted comparison. From the obtained results, the following was found:

- Best fitness values obtained from PSO algorithm do not change after a few iterations for most benchmark functions and approach to the optimum is found to be faster through the PSO method.

- Average and standard deviation values of best fitness fn. for 7 out of 8 are slightly better in case of DE compared to PSO, while they have almost similar values in one benchmark function only.

On the other hand, in [50], a PI controller is utilized to control voltage in a photovoltaic power plant. By comparing the dynamic performance in terms of voltage fluctuations in both cases, it was found that:

- It is obvious that the computational time in the DE case is higher compared to PSO.
- DE Shows better performance in terms of voltage control compared to PSO. However, by increasing the population size for PSO, the performance is enhanced.

Table 4.1. Comparison between the three evolutionary techniques

Comparison Aspect	GA	PSO	DE
Require ranking of solutions	Yes	No	No
Influence of population size on solution time	Exponential	Linear	Linear
Computational time	Slowest	Fastest	Medium
Influence of best solution on population	Medium	Most	Less
Average fitness cannot get worse	False	False	True
Tendency for premature convergence	Medium	High	Low

To conclude the above literatures, we can summarize that:

- Despite DE might be slightly slower than PSO in computational time, PSO and DE have a very close performance in terms of dynamic response.

- Even if normal PSO configuration is slightly inferior to DE, the proposed strategy is suggested to overcome this problem, improve the searching process for the optimum solution and reduce the gap between both techniques.

4.3.1 Overview of online PSO

In the previous section, system modelling of *m*-power supplies and *n*-loads DC microgrid was undertaken. Primarily, to determine optimum control gains for controlling network terminal voltages, eigenvalue analysis must be performed. However, the number of control gains is directly proportional with the complexity of the network. As when the network becomes bigger and complexity increases,

the needed number of gains to control grid stability increases in return. In that context, normal analysis and conventional control techniques would not work efficiently in that case. Therefore, this study introduces PSO as an optimization algorithm. PSO can correspond to a non-linear system and is privileged with its ability for flexible parallel processing, that it is a search that does not use gradient information. Each element shares its past information with the surrounding particles and searches for a solution.

The main goal of this work is to apply online voltage control for DC microgrid with a decentralized mode to emulate a factual case of frequent load changes as shown in Fig. 4.3. Unlike offline control that requires centralized voltage and load control from distribution system operator (DSO), online control would be faster in action with real time response. Therefore, this study implements a parallel operation of exploration and exploitation with allocating part of the particles to do random search in the search space. By that way, for any sudden load change, particles will continue searching for optimum control gains in local and global areas simultaneously depending on the past received data of surrounding particles to optimize their velocities and positions. Ultimately, local and global best fitness functions are updated to portray how close the solution is to achieving control targets.

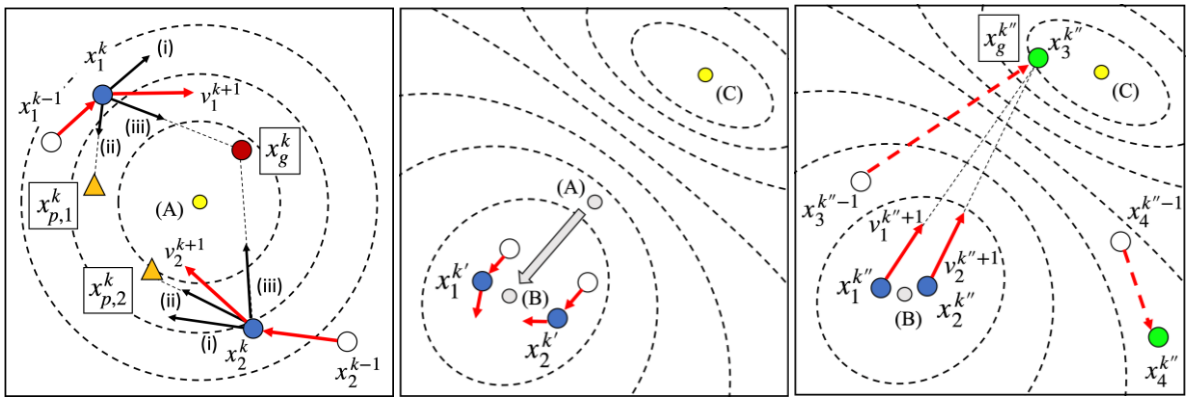

x_i^k, v_i^k : position and velocity of particle at iteration k (i=1,2 for normal particles, i=3, 4 for random particles). $x_{p,i}{}^k$: local best position of particle i at iteration k, $x_g{}^k$: global best position at iteration k

Fig. 4.3 Online voltage control strategy using PSO

Fig. 4.3 shows an overview of the proposed method. First, Fig. 4.3 (a) illustrates how the conventional PSO searches the optimal control gains on a two-dimensional frame with two particles. They are defined as normal particles following the conventional equations of PSO described later in subsection 4.3.3. Their new velocities and positions based on velocities at previous step (i), local

best positions (ii), and global best position (iii). These three factors from (i) to (iii) are corresponding to first, second, and third terms of velocity in Eq. (55) described in subsection 4.3.3. Normal particles mainly start explorations in a global area, and they start exploitations in a local area when they become closer to the optimal solution. It is expected that the positions of conventional particles gradually converge to the global best position as the iteration goes on throughout these processes. However, in the case of applications to dynamic problems in which the system condition is not fixed, the optimal solution might move during the search process. Namely, the global best position found by the conventional PSO might not be successfully updated if the search behavior has been already shifted to the exploitation phase. When the optimal solution moves continuously from (A) to (B) as shown in Fig. 4.3 (b), the conventional PSO algorithm can smoothly follow the trajectory with its high local searchability even if normal particles are in an exploitation phase. This is an important advantage of using PSO to dynamic problems. However, when the optimal solution discretely changes to a distant point, from (B) to (C), due to a multimodal characteristic of state space, normal particles which are in the exploitation phase cannot find the new optimal solution because they have no motivations to search distant positions.

On the other hand, in the proposed method, random particles are used in addition to normal particles. The random particles are searching the whole state space in a random pattern, and the normal and random particles share the information of their local best positions to successfully update the global best position when any random particle happens to find a better solution. Accordingly, as shown in Fig. 4.3 (c), normal particles are attracted by the updated global best position, and it is possible to avoid that the normal particles are being trapped in a local minimum. In other words, the random search can motivate the converging normal particles to move their positions in a wider area again, and it is expected that a parallel operation of exploration and exploitation can be always kept in order to contribute to the online optimization in dynamic problems.

4.3.2 Grid stability and fitness function

The stability of the network is investigated by adjusting control gains to various patterns. There are several techniques to assess grid stability through adjusting control gains. To understand that let us consider Fig. 4.4 that describes the eigenvalue and what factors are affecting its stability.

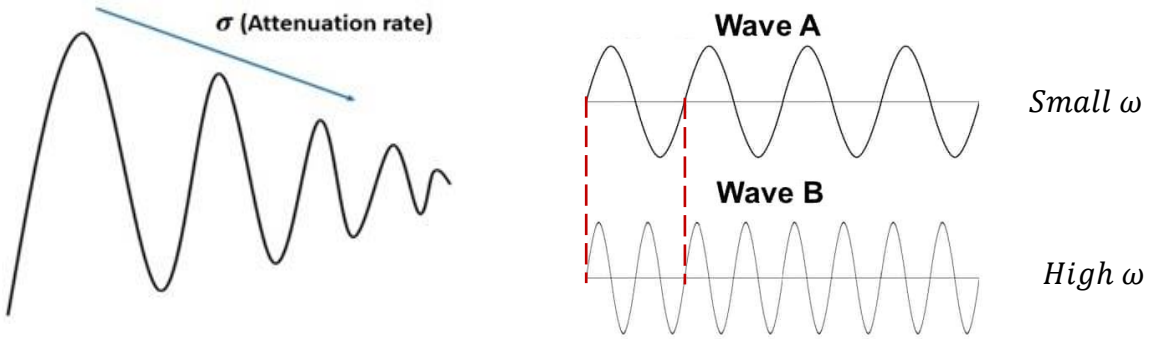

Fig. 4.4 Stability assessment for eigenvalues

As shown in Fig. 4.4, the main two factors affecting the stability of any eigenvalue λ are the attenuation rate σ and the angular frequency ω. The formulation is expressed as follow:

$$\lambda_n = \sigma_n \pm j\omega_n \tag{50}$$

A fundamental approach to stabilize a system using eigenvalue analysis is to put a dominant pair of conjugate eigenvalues whose real values are the biggest as far from the imaginary axis as possible, to obtain better damping effect as illustrated in Fig. 4.5.

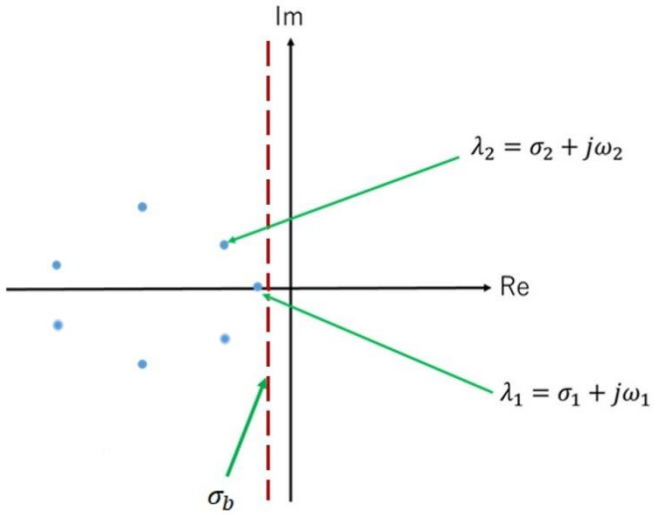

Fig. 4.5. Pole arrangement of dominant eigenvalues

Here, to improve the damping of eigenvalues whose angular frequencies are high is also important to eliminate high frequency noise from the control response. Based on the above ideas, the objective function in this study was defined as (51), so that the σ of the eigenvalues whose ω was high, can be placed as left as

possible. Namely, as ω gets bigger, σ should be smaller to achieve the same objective function. Moreover, not only the dominant eigenvalue but also the others are added with a weight coefficient;α. In that context, when an eigenvalue has a high value of ω, a high weight coefficient (A_i) will be added to it, so that it would have a smaller effect on stability as σ is smaller and placed away from imaginary axis, while α in that case would be very small. Here, eigenvalues are stated as $\lambda_1, \lambda_2, \ldots, \lambda_N$ in the order of the real part from the largest to the smallest, while the corresponding attenuation rates and angular frequencies are mentioned as $\sigma_1, \sigma_2, \ldots, \sigma_N$ and $\omega_1, \omega_2, \ldots, \omega_N$. It should be noted that the conjugate pair of eigenvalues is regarded as one eigenvalue and its corresponding angular frequency in the following equation is positive one. The ultimate objective is to obtain the lowest negative value of the objective fn. as an indication of stability.

$$f(\sigma, \omega) = \sum_{i}^{N} \alpha_i \sigma_i \left(\frac{A_i}{A_i + |\, \omega_i \,|} \right) + P(\alpha_d - \alpha_b) \longrightarrow min. \qquad (51)$$

Where σ_d is the attenuation rate of the dominant eigenvalue as $\sigma_d \in (\sigma_1, \sigma_2, \ldots, \sigma_N)$, σ_b is the attenuation rate at the boundary of the recommended control region, while α_i and A_i are the damping and vibration weight coefficients of each eigenvalue respectively where *i*=1, 2, 3, …*N*. *P* is a penalty term which excludes any eigenvalue that resides outside the recommended region by adding a high penalty factor, where $P = \begin{cases} +ve\ value\ , & \sigma_d - \sigma_b > 0 \\ 0, & \sigma_d - \sigma_b \leq 0 \end{cases}$.

To clarify the physical meaning of the objective function, consider the pole placement on the gaussian plane shown in Fig. 4.6. if we compare the blue eigenvalue with the red one in terms of horizontal position only, the blue one is more stable as it is further from the boundary than the red one. However, angular frequency is also affecting network stability. Accordingly, we took into consideration both damping ratio and angular frequency in the objective function. In that context, as simulation goes on, the algorithm will try to find the optimal placement of poles. Eigenvalues continue changing from the red to the blue to the yellow and so on and the best combination with the optimal pole placement (green color is somewhere between blue and yellow) is obtained that gives the best objective fn. Where α_i and A_i are adjusted to improve the value of the objective fn. Though, the physical meaning of the objective function is to obtain the best

combination of eigenvalues leading to the most perfect form of network stability. In that context, when ω_i is high, that would lead to a small absolute value of objective function and can be reflected on a worse performance of network voltage stability. On the contrary, when it is small, that gives a better indication of network stability as the value of the objective function is better. Likely, when the absolute value of the damping ratio is big taking its sign into consideration, it means that its location closer to the stability boundary and in terms of network stability it has a worse performance than when the damping ratio is small. On the other hand, the penalty factor is activated when the σ_d is exceeding the boundary of stability limit σ_b to exclude the eigenvalues with worse locations.

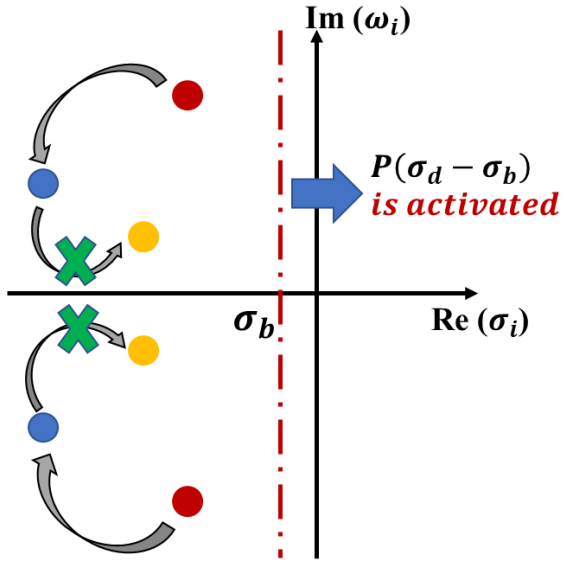

Fig. 4.6. Optimum pole placement of dominant eigenvalues

Fig. 4.7 illustrates deeply the physical meaning of the objective function by showing its contour figure. A full search frame of σ and ω is depicted vs the global best objective function value. From the figure it is shown that, if σ is fixed and absolute value of ω started to increase from 0 to a higher value, the value of the objective function gets worse. Consequently, if the absolute value of ω was not high enough, like at point (A), only σ could be reduced to a smaller value to improve the value of the objective function. On the other hand, when absolute value of ω was high enough to have the worse impact on the stability as point (B), both σ and absolute value of ω should be reduced to a smaller value to have better objective function value and maintain network stability.

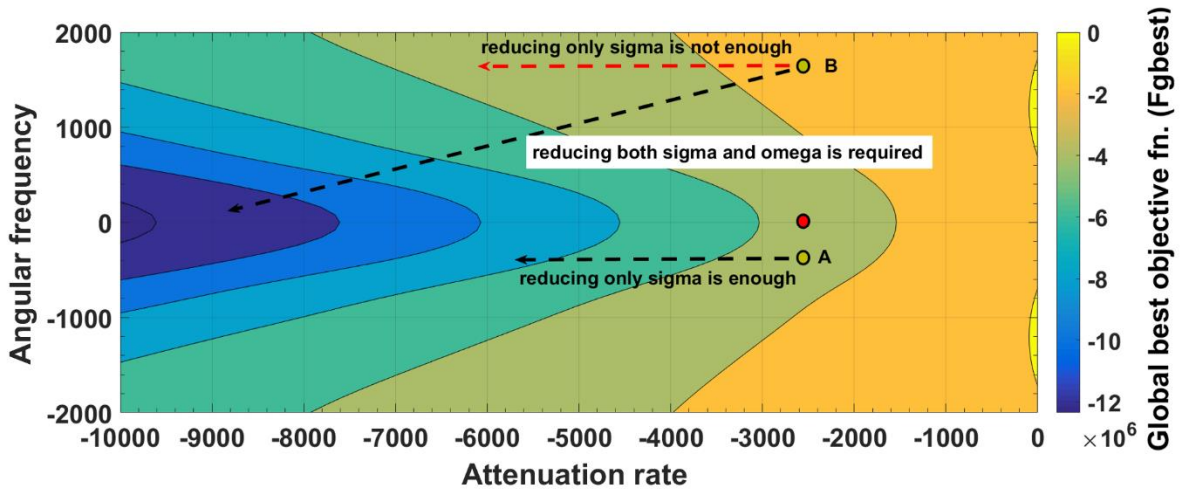

Fig. 4.7. Contour figure of the objective function

Similarly, Fig. 4.8 shows the plot of sigma and omega of one eigenvalue on a wide plane and trying to figure out which of them is more effective on voltage stability.

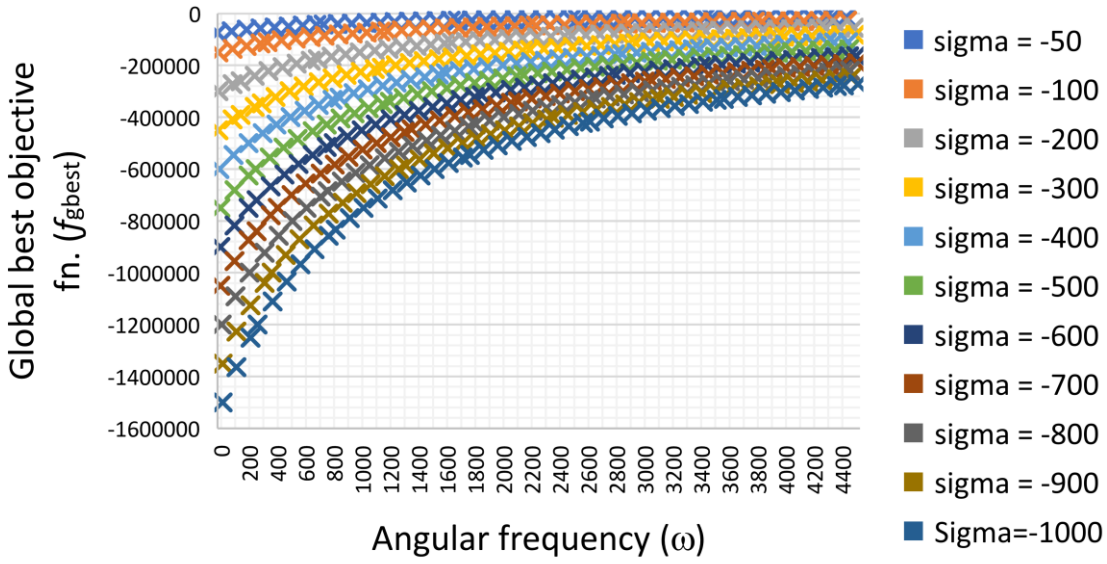

Fig. 4.8. Distribution of one eigenvalue on a full search frame

Fig. 4.8 illustrates that, whenever, sigma is reduced and going further from the origin, the objective function is improved. However, if we fixed sigma, the distribution shows that omega might have a bigger effect if its absolute value increases. In the figure, it is also shown that the best objective function is obtained when omega reaches zero at the lowest value of sigma by taking the sign of sigma into consideration.

On the other hand, Fig. 4.9(a) and (b) show the distribution of the dominant eigenvalues at high load condition. With fixing the load condition, two control gains out of four are fixed and a full search of the other two is applied. Accordingly, the distribution of the dominant eigenvalues all along the simulation was obtained. k_{p1} and k_{d1} are fixed, while k_{p2} and k_{d2} change on a full search space from 0 to the boundary of maximum position. From Fig. 4.9(a) we can observe that the optimal pole placement is at the light blue color where the best objective function is obtained (-6.90359*10^5). However, the dark red conjugates whose horizontal positions are better that the light blue one gave a worse objective function value (-6.65011*10^5).

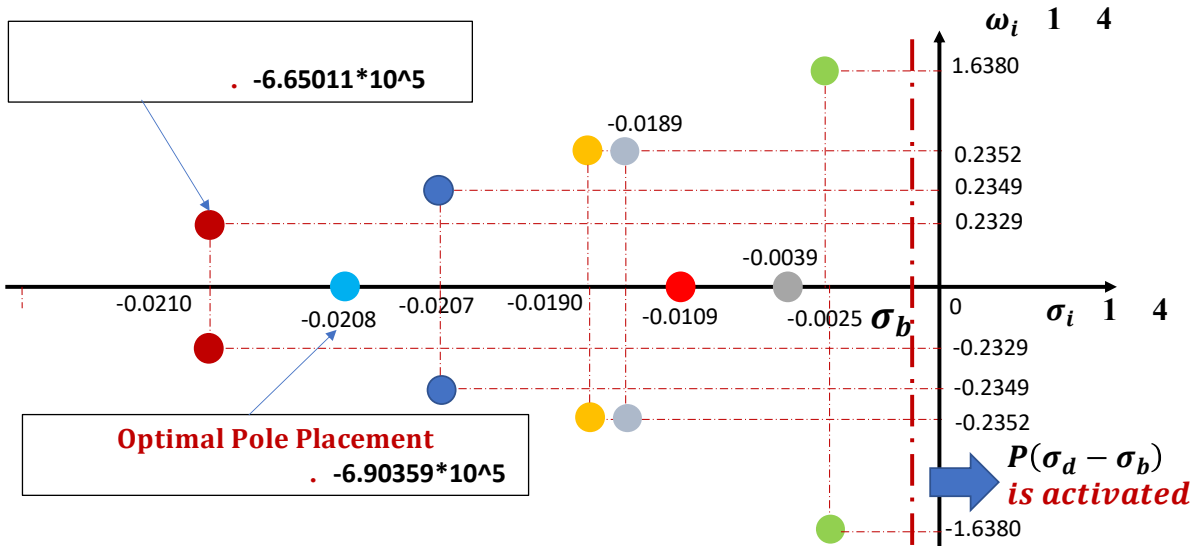

(a)

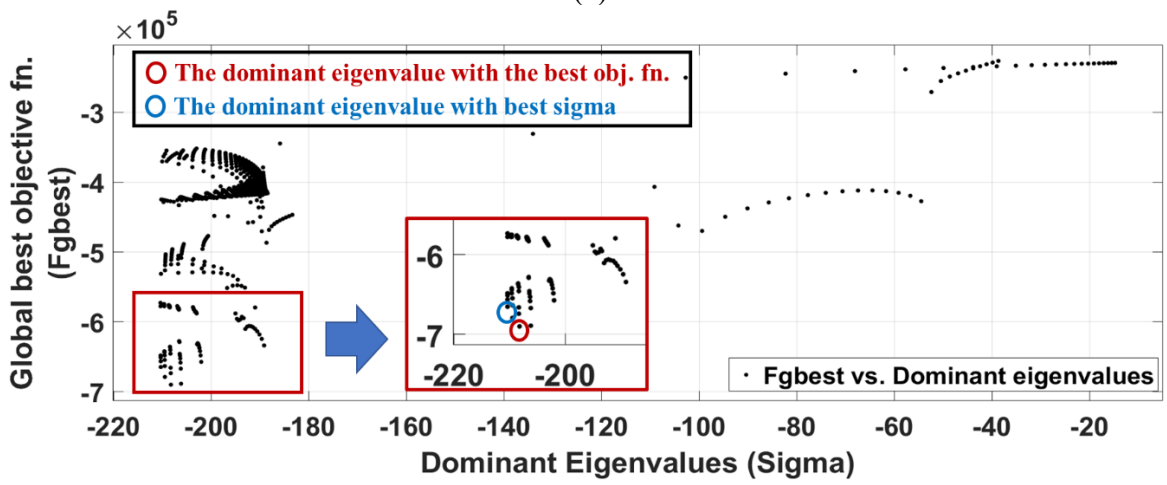

(b)

Fig. 4.9. Distribution of dominant eigenvalues at high load condition

Likely, Fig. 4.9(b) shows the same concept. The dominant eigenvalue with the best objective function (optimal pole placement) is portrayed in a red color, while the dominant eigenvalue with the best location away from the origin is depicted in a light blue color. We can conclude from that, the eigenvalue that can give the best objective function, isn't necessarily to have the smallest sigma. However, both sigma and omega are considered as arbitrary parameters. So, as much as omega decreases, is better. On the other hand, sigma cannot be reduced to -ve infinity for many reasons. Firstly, the model is non-linear because of the CPLs, so it has no meaning to reduce the value of sigma to -ve infinity. Secondly, the value of sigma mainly depends on the upper and lower limits of particles' positions. Thus, increasing the upper boundary of the position, leads to a lower value of sigma. In addition, sigma weight coefficient (α) is dependent on the location of sigma as the weight coefficient value reduces as sigma goes further from the origin because it will have lower impact on the stability of the model. Though, it has no meaning to reduce the value of the sigma to -ve infinity.

From all figures we can summarize the following:

- Even with better positions of dominant eigenvalue, the combination of eigenvalues might not result in a better objective fn. as ω_i is also taken into consideration.
- When ω_i increases, stability might decrease. That's why we add a smaller value of A_i for dominant eigenvalues to sustain a better value for objective function, while it is bigger for other eigenvalues.

4.3.3 Algorithm of online PSO

To clarify this research control idea of online voltage control, PSO will undergo several procedures as an imitation to a load changing situation to meet control goals.

▪ **Step 0 (preparation):** Set the number of particles $m \geq 2$, given that particle weight inertia $w \geq 0$, local and global inertia coefficients c_1 and $c_2 \geq 0$ respectively, and iteration number $k = 0$. The search space is defined in G dimension space where G represents the number of decision variables, namely, all control gains. The position of particle i at iteration k is denoted as $x_i^k = [x_{i1}^k, x_{i2}^k, \ldots, x_{iG}^k]^T$. Set the maximum value of x_{ij}^k as $x_{j,\max}$ supposing the minimum values are 0 in this paper.

▪ **1 z :** Set particles' initial positions x_i^0 (i = 1, 2,…, m) where x represents the state variable of all control gains, and initial velocities, v_i^0 (i = 1, 2,…, m). They are given using random numbers, $r_{x0,ij}$ and $r_{v0,ij}$, as follows:

$$\begin{cases} x_{ij}^0 = r_{x0,ij} x_{j,\max} \quad (0 \le r_{x0,ij} \le 1) \\ v_{ij}^0 = (r_{v0,ij} - 0.5) x_{j,\max} \quad (0 \le r_{v0,ij} \le 1) \end{cases} \tag{52}$$

Also, set initial values for local and global best positions as follows:

$$\begin{cases} x_{p,i}^0 = x_i^0 \quad (i = 1,2,...,m) \\ x_g^0 = x_{p,ig}^0 \quad (i = 1,2,...,m) \\ ig = \min\limits_i f(x_{p,i}^0) \end{cases} \tag{53}$$

Here, $x_{p,i}{}^0 = [x_{p,i1}{}^0,\ldots,x_{p,iG}{}^0]^T$ and $x_g{}^0 = [x_{g,1}{}^0,\ldots, x_{g,G}{}^0]^T$ are initial local and global best positions respectively.

▪ **Step 2 (update position and speed):** Update the position of random particles as follow:

$$x_{ij}^{k+1} = r_{ij}^k x_{j,\max} \tag{54}$$

Where, $r_{ij}{}^k$ is a random value between 0 and 1 generated by a uniform random sequence for dimension j of particle i at iteration k. Update both velocities and positions for normal particles as (55).

$$\begin{cases} v_{ij}^{k+1} = w\, v_{ij}^k + c_1 r_{1,ij}^k (x_{p,ij}^k - x_{ij}^k) + c_2 r_{2,ij}^k (x_{g,j}^k - x_{ij}^k) \\ x_{ij}^{k+1} = x_{ij}^k + v_{ij}^{k+1} \quad (0 \le x_{ij}^{k+1} \le x_{j,\max}) \\ \quad (i = 1,...,m, \quad j = 1,...,G) \end{cases} \tag{55}$$

Here, $x_{p,i}{}^k = [x_{p,i1}{}^k,\ldots,x_{p,iG}{}^k]^T$ and $x_g{}^k = [x_{g,1}{}^k,\ldots,x_{g,G}{}^k]^T$ are local and global best positions at iteration k respectively. $r_{1,ij}{}^k$ and $r_{2,ij}{}^k$ are random values between 0 and 1 generated by different uniform random sequences for dimension j of particle i at iteration k.

- **Step 3 (caluclation of objective function of each particle):** The position of particle *i* is converted into control gains as follows.

$$\begin{cases} k_{p1} = x_{i1} \\ k_{d1} = x_{i2} \\ k_{p2} = x_{i3} \\ k_{d2} = x_{i4} \\ \quad \vdots \\ k_{pm} = x_{i(2m-1)} \\ k_{dm} = x_{i(2m)} \end{cases} \tag{56}$$

S-matrix and eigenvalues are recalculated for all particles using the updated control gains and other system conditions such as loads. Obtained eigenvalues are sorted out in descending order of their real parts and the objective function for particle *i* is recalculated as follows.

$$f\left(x_i^{k+1}\right) = \sum_{i}^{N} \alpha_i \sigma_i \left(\frac{A_i}{A_i + |\,\omega_i\,|}\right) + P(\alpha_d - \alpha_b) \longrightarrow min. \tag{57}$$

The objective functions for $x_{p,i}^{\ k}$ and $x_g^{\ k}$ are also recalculated here because the eigenvalues change in accordance with changes of any system conditions such as loads.

- **4** **.:** Local and global best objective functions are updated based on the newly produced eigenvalues. Through every iteration, objective function of particle *i* , $f(x_i^{k+1})$, is calculated and compared with local best objective function, $f(x_{p,i}^{\ k})$, at the previous iteration. Local and global best positions are updated as follows:

$$\begin{cases} x_{p,i}^{k+1} = x_i^{k+1} \quad (\text{if} \quad f(x_i^{k+1}) < f(x_{p,i}^{k}), i = 1,...,m) \\ x_g^{k+1} = x_{p,ig}^{k+1} \quad (ig = \min_i f(x_{p,i}^{k+1})) \end{cases} \tag{58}$$

- **5** **:** Set $k = k + 1$ and return back to step 2. The process of above algorithm is shown as a flowchart in Fig. 4.10. Here, from "update of position at Step 2" to "update of local best position at Step 4" was processed for each particle to simplify the flowchart. The practical application of

the proposed online optimization technique consists of the following three steps. Firstly, collecting site data as load and generation information. Secondly, the optimization to determine control gains. Finally, distributing these control gains to generator sets. In order to follow frequent system condition changes successfully, the required amount of time for all those processes should be as short as possible. The proposed method contributes to reduce the calculation time for the second step by taking over the latest positions and velocities of the particles continuously.

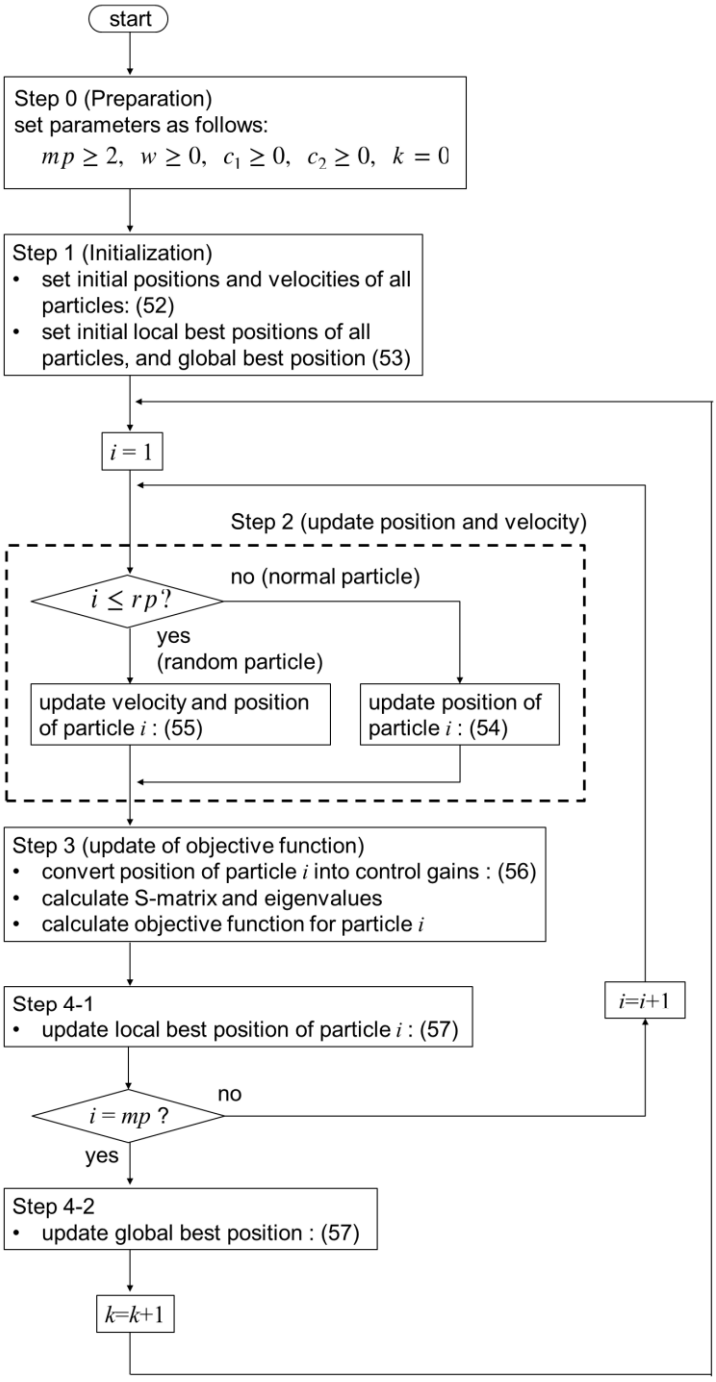

Fig. 4.10. A flowchart of the proposed online PSO

4.4 Summary

This chapter gave an overview of various types of Artificial Intelligence techniques and highlighted the applications of each in various fields of life. Moreover, this chapter mentioned the focused controller type in this study which is PSO based controller that is required for online voltage control in DC microgrid. Furthermore, a detailed algorithm of online PSO is illustrated to show the various steps being carried out during the online control.

CHAPTER 5

RESULTS AND DISCUSSIONS

5.1 Introduction to Simulation Model

Simulations were carried out using simplified 3-bus DC microgrid model. This model mainly comprises of two distributed generators and two load systems connected at different terminals as shown in Fig. 3.3. An Eigenvalue analysis is previously conducted in chapter 3 to precisely describe grid characteristics and to easily analyze the circuit in different loading conditions and contingency situations. Model parameters are presented as shown in Table 5.1.

Table 5.1. 3-bus DC microgrid model parameters

E_1 [V]	800	$R_{D1} = R_{D2}$ [mΩ]	9
E_2 [V]	800	$C_{B1} = C_{B2} = C_{B3}$ [mF]	1
P_{G1} [kW]	57.3	$L_{S1} = L_{S2}$ [mH]	0.5
P_{G2} [kW]	60	$D_1 = D_2$	0.4754
P_{L1} [kW]	30	T_D	0.0001
P_{L3} [kW]	80	η	0.1
$L_{D1} = L_{D2}$ [mH]	0.5		

Simultaneously, eigenvalues' weight parameters and coefficients are pre-set as shown in Table 5.2.

Table 5.2. Weight coefficients for each eigenvalue

α_1	1500	α_7	3
$\alpha_2 = \alpha_3$	500	$\alpha_8 = \alpha_9$	1
α_4	10	$A_1 \sim A_3$	1000
$\alpha_5 = \alpha_6$	5	$A_4 \sim A_9$	5000

The total load in this model was set to 110 kW, however, loads are normally fluctuating, and the optimal control gains will change depending on the load changes. Therefore, in this section, the robustness of the primary control was verified supposing the loads change stepwise between the following three conditions.

- High Load (H.L): P_{L1}=60 kW, P_{L3}=160 kW
- Medium Load (M.L): P_{L1}=30 kW, P_{L3}=80 kW
- Low Load (L.L): P_{L1}=15 kW, P_{L3}=40 kW

Although in Table 5.1, P_{G1} and P_{G2} were set to be 57.3 and 60 kW respectively based on M.L condition. However, in practical applications, load is changing in a continuous pattern, which requires frequent update of both reference generation output and terminal voltages. In this study, we suggested a step wise load change representing three time periods of the day. Practically, when load changes suddenly, primary control will try to maintain system stability by adjusting supply and demand balance based on PD logic right after the load change. Consequently, secondary and tertiary controllers will substantially try to adjust reference terminal voltages and generation dispatch based on the change in load condition.

Since we mainly focus on primary controller only in this chapter, P_{G2} is set to change in a step wise: 30, 60 and 90 kW for low, medium and high load conditions respectively. On the other hand, reference voltage at terminal 1 is set to 380 V. Consequently, reference P_{G1} and terminal voltages at terminals 2 and 3 are calculated based on that load change. Accordingly, it is found that P_{G1} equals 26.8, 57.3 and 158 kW respectively. On the other hand, reference voltage at terminal 2 changes from 387.7, 395.2 and 402.4 V, while terminal 3 voltage

changes from 369.2, 357.6 and 331.8 respectively.

5.2 Proposed Control Strategy

As previously mentioned in Chapter 3 that there is a proposed strategy based on online voltage control using PSO to control terminal voltages on real time after any sudden and unexpected load change. There are mainly two cases for implementing this control technique. One of which is to control terminal voltage in a conventional way through normal search by exploring wider area to conduct global search followed by local search in a narrower area seeking for optimal gains. The second case, which is the proposed methodology suggested in this work, that is to apply a parallel operation of global and local searches at the same time to avoid the lack of local search at the beginning of the search process and the lack of global search at the end. This is achieved through allocating part of the particles to fly in a random pattern to collaborate with normal particles to achieve the target and obtaining the optimum control gains. As follows, the fore-mentioned cases are exposed in detail.

5.2.1 Case 1, voltage control with conventional PSO

First, online voltage control without random particles ($rp = 0$) was applied as a conventional method with changing the loads every 200 iterations. All particles are seeking the optimum solution of control gains but without any parallel operation of local and global searches. In other words, when the particles finalize their exploration for optimum control gains in a wide search space, they start to concentrate their search in a smaller or local area, where the optimum gains are finally located.

5.2.2 Case 2, voltage control with the proposed PSO

Next, online voltage control is applied with the proposed method. One third of the particles ($rp = m/3$) is allocated for random search for optimum gains in the search space for simultaneous operations of exploration and exploitation, while the other two thirds are conducting normal search by firstly exploring in a global area then performing local search in a narrower search space consequently.

5.3 Simulation

To demonstrate the recommended results a sufficient simulation should be conducted regarding system parameters and configurations before and after sudden load change of 40 kW is applied at terminal 1. In addition, the simulation is conducted based on the comparison between the two previous cases mentioned in previous section of this chapter.

Fig. 5.1 shows f_{pbest} of all the particles, while Fig. 5.2 and 5.3 show f_{gbest} as the minimum f_{pbest} and corresponding control gains, respectively. Right after the simulation starts with L.L, PSO successfully reached the converged solution in around 50 iterations. Then, when the load changes from L.L to H.L at 200 iterations, the objective function got worse and gives a positive value right after the load change. That means the system was unstable, because the dominant eigenvalue was located in the positive side of the imaginary axis which activates the penalty factor term. Similarly, the search did not work well when load changed at iteration 400, 600, and 800 because most of the particles have reached the global best position. Namely, the search has been already converged and no motivation was given to the particles even if load changes. That is also reflected in Fig. 5.3 which depicts the control gains suggested by PSO in conventional case 1.

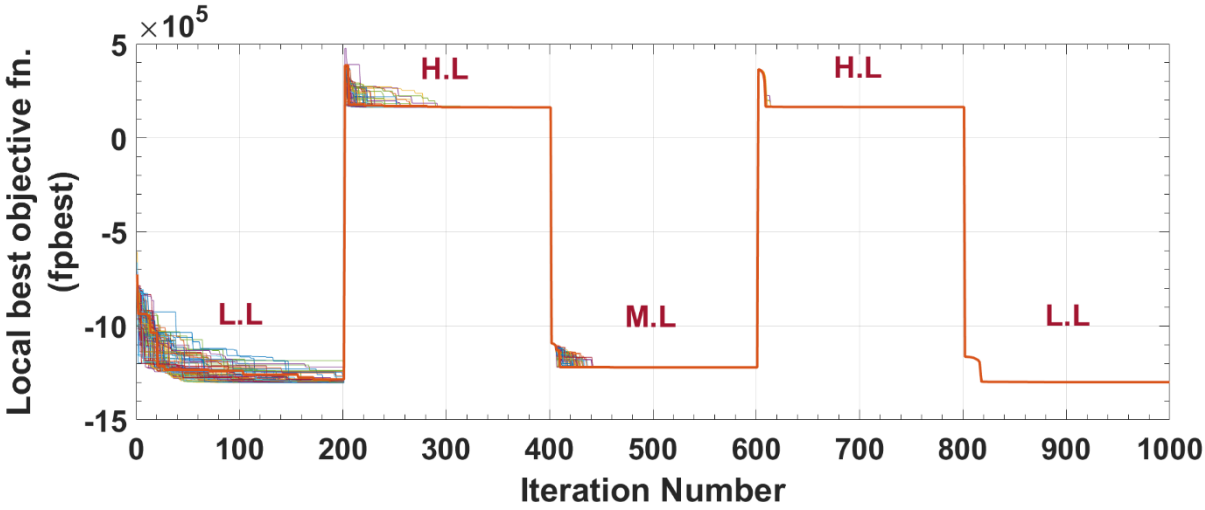

Fig. 5.1. Local best fitness function without any random particles search

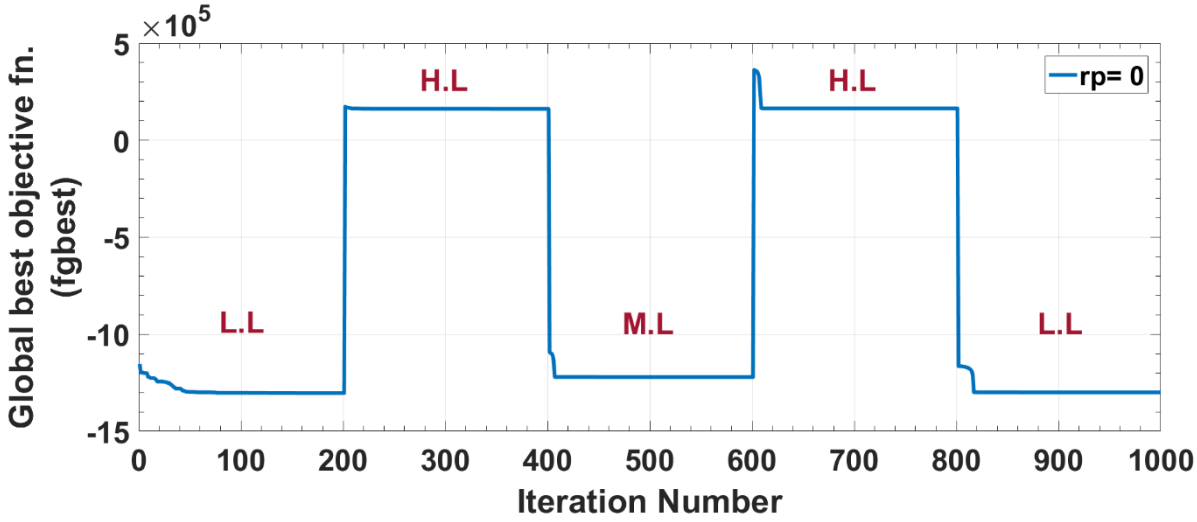

Fig. 5.2. Global best fitness function without any random particles search

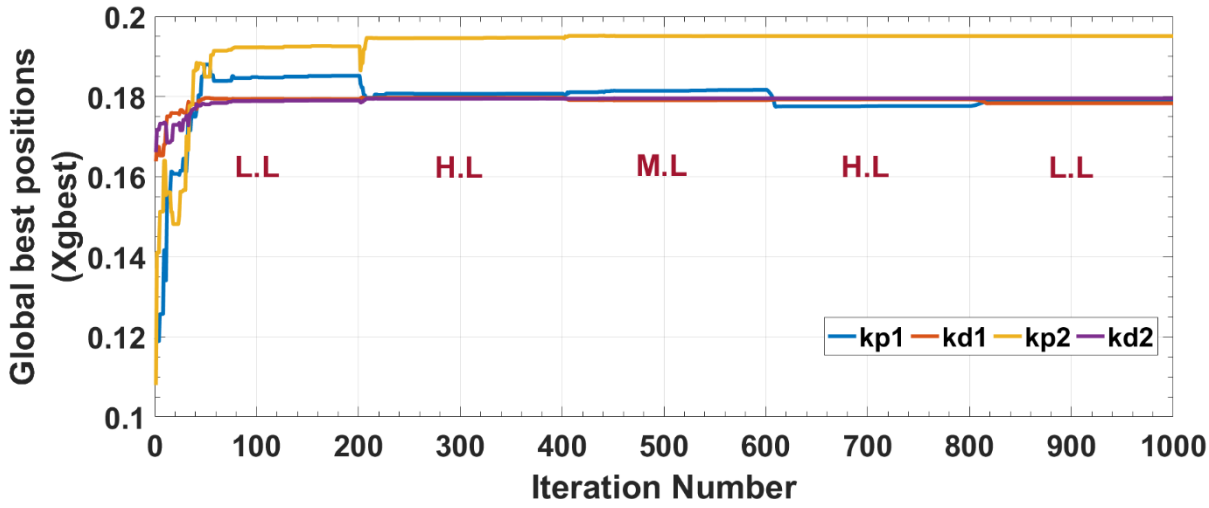

Fig. 5.3. Global best positions of control gains without any random particles

Consequently, Fig. 5.4 shows the position of all particles when all particles are following a normal pattern and there is no allocation of random particles.

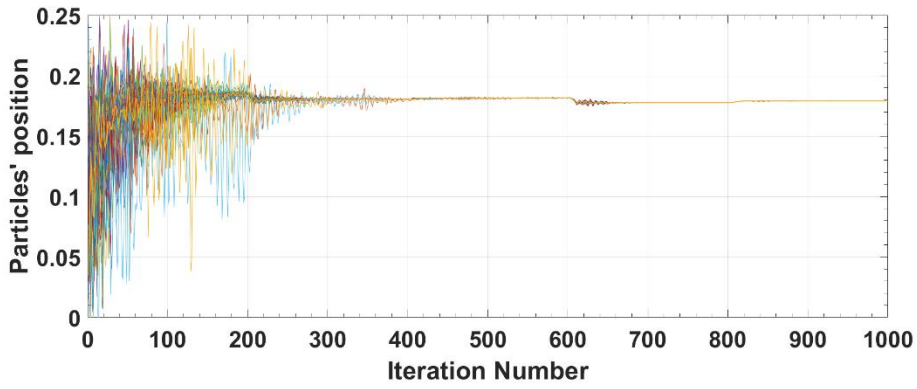

(a)

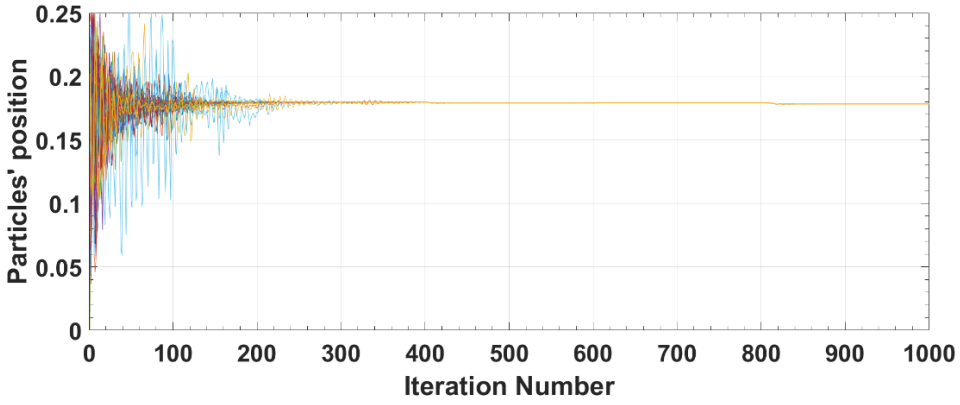

(b)

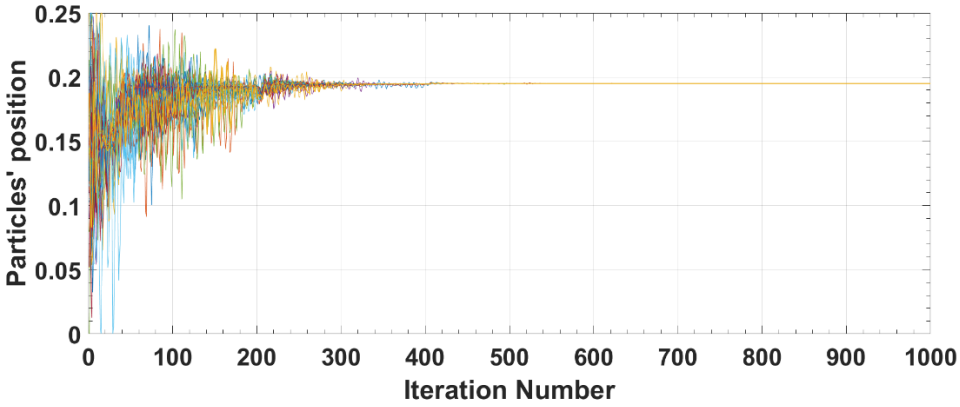

(c)

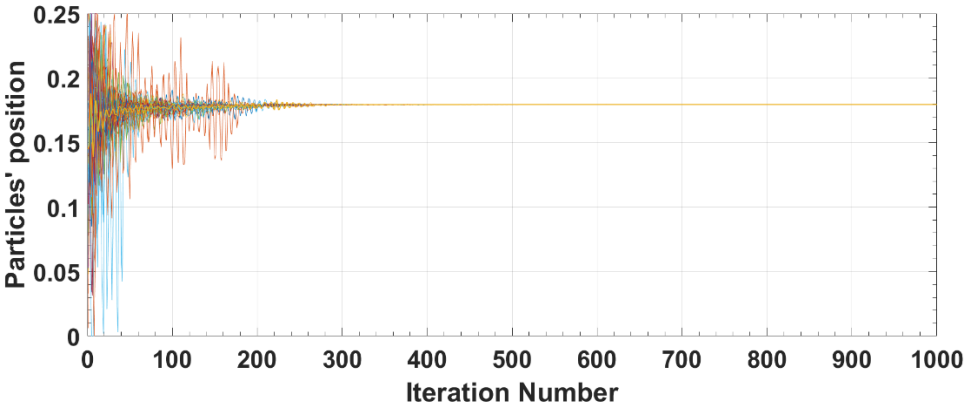

(d)

Fig. 5.4. Particle position without any random particles:
(a) x_{i1}, (b) x_{i2}, (c) x_{i3} and (d) x_{i4}

Here, the decision variable vector is defined as $x_i = [k_{p1i}, k_{d1i}, k_{p2i}, k_{d2i}]^T$ for all i from 1 to m.

On the other hand, in case 2, Fig. 5.5, 5.6 and 5.7 illustrate f_{pbest}, f_{gbest} and X_{gbest}, respectively. It is shown in Fig. 5.5 and 5.6 that many particles could successfully get rid of the local minimum and have improved their f_{pbest} and f_{gbest} accordingly

due to the enhanced exploration ability due to the random particles. As a result, control stability has been maintained even with H.L conditions with properly updating the control gains as shown in Fig. 5.7. Although the obtained control gains might have different combinations for the same load conditions, especially k_{d1} and k_{p2} are different between the first (from iteration 0 to 200) and the second (from iteration 800 to 1000) L.L conditions, the f_{gbest} are not drastically different in both periods.

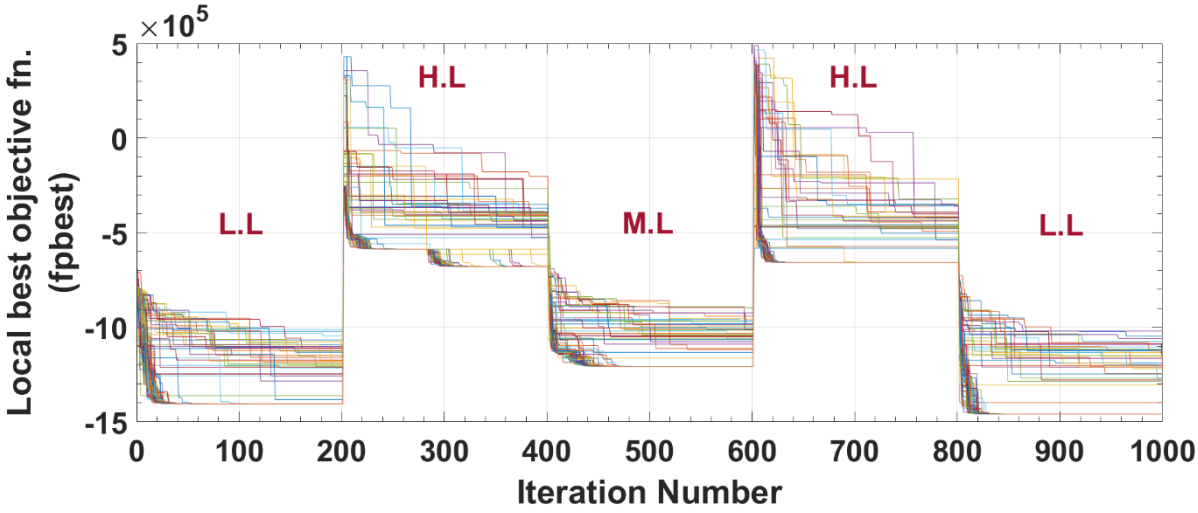

Fig. 5.5. Local best fitness function with 1/3 of whole particles doing random search

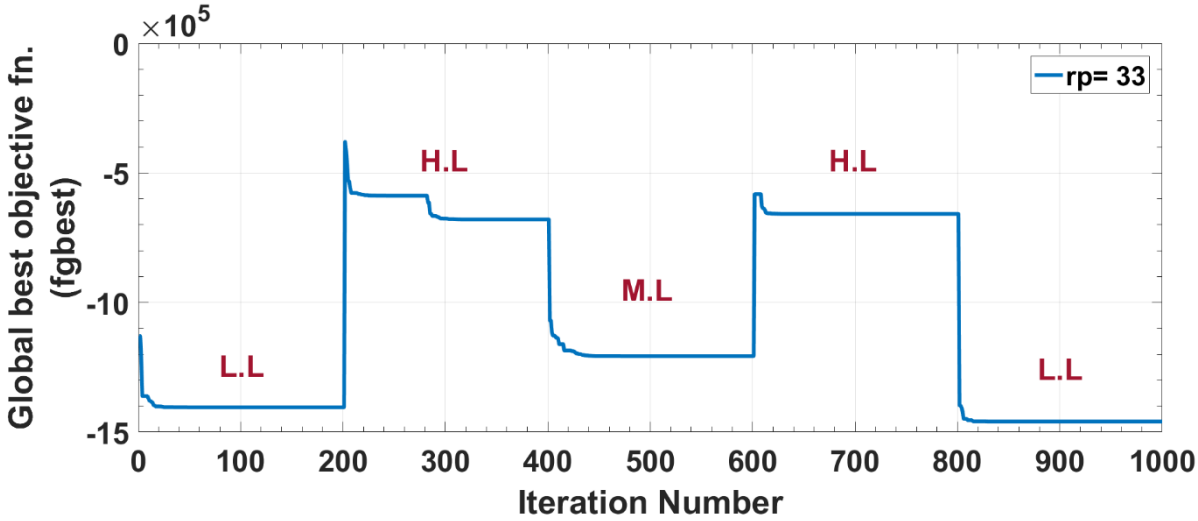

Fig. 5.6. Global best fitness function with 1/3 of whole particles doing random search

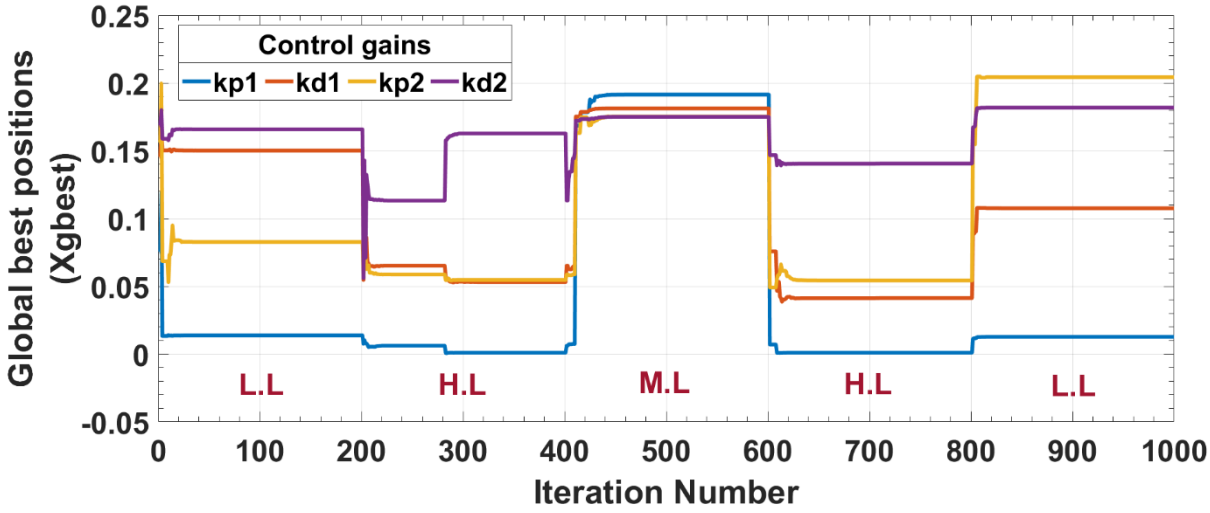

Fig. 5.7. Global best positions of control gains with 1/3 of particles doing random search

Fig. 5.8 shows the four-dimensional positions of conventional particles only in case 2 where 1/3 of the particles are allocated for random search (i= 1, 2, …, 2m/3). Unlike case 1, case 2 with the proposed random search technique managed to prevent particles to be trapped in local minima. With the privilege of the parallel operation of local and global searches, random particles continued to search for optimal solution in a global area where normal particles restart to search global area when the global best position was updated by any random particles. Hence, the normal particles move in a wider area every time when load changes.

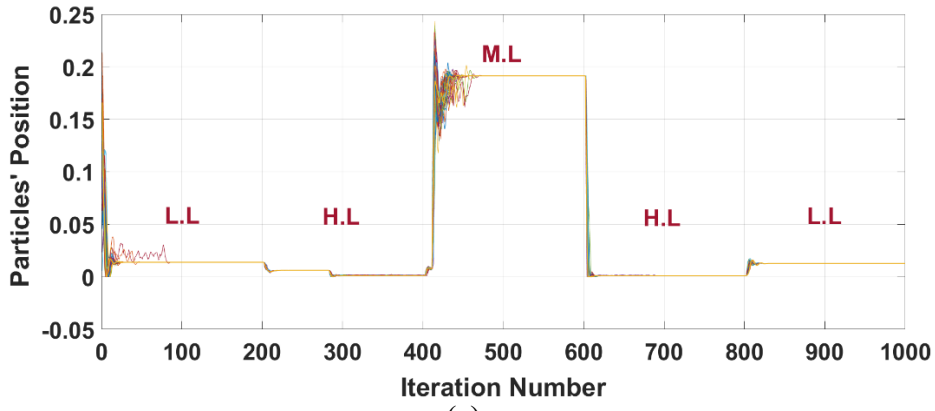

(a)

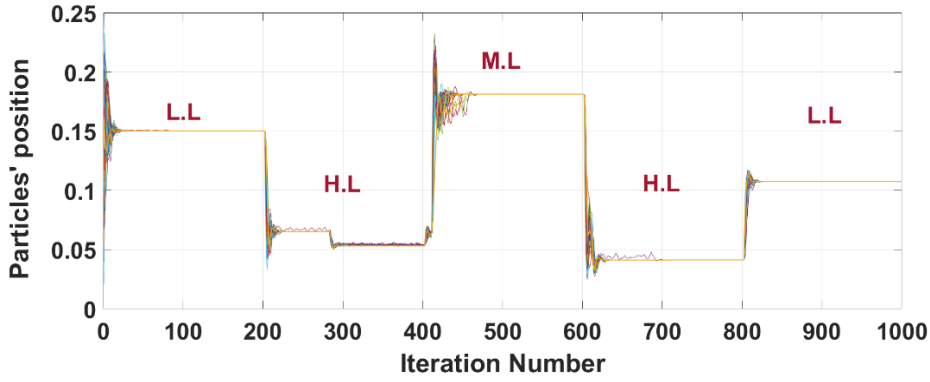

(b)

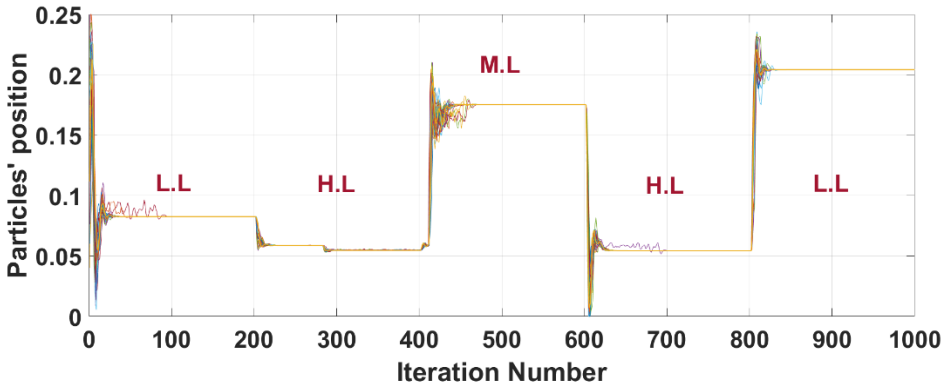

(c)

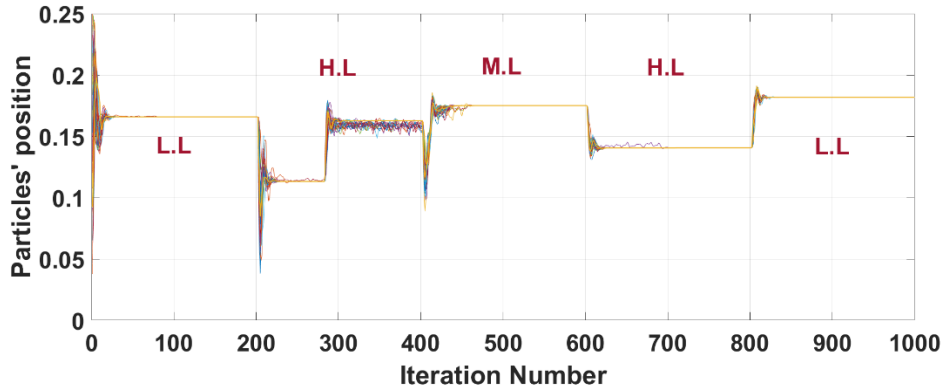

(d)

Fig. 5.8. Particle position with 1/3 of particles doing random search: (a) x_{i1}, (b) x_{i2}, (c) x_{i3} and (d) x_{i4}

Consequently, Fig. 5.9, 5.10 and 5.11 depict contour figures showing a comparison between objective functions in case of proposed method when compared with a full search strategy. These figures prove how effective the control technique is at different loading conditions. That was proved in three terms. Firstly, the values of objective functions are smaller with the proposed method than that of normal search only. Secondly, the values of objective functions based on online PSO with random search techniques are approaching the optimal objective functions resulted from full search technique. Finally, the values of k_{p2} and k_{d2} without random search scheme are not following the local minima as shown in the following figures.

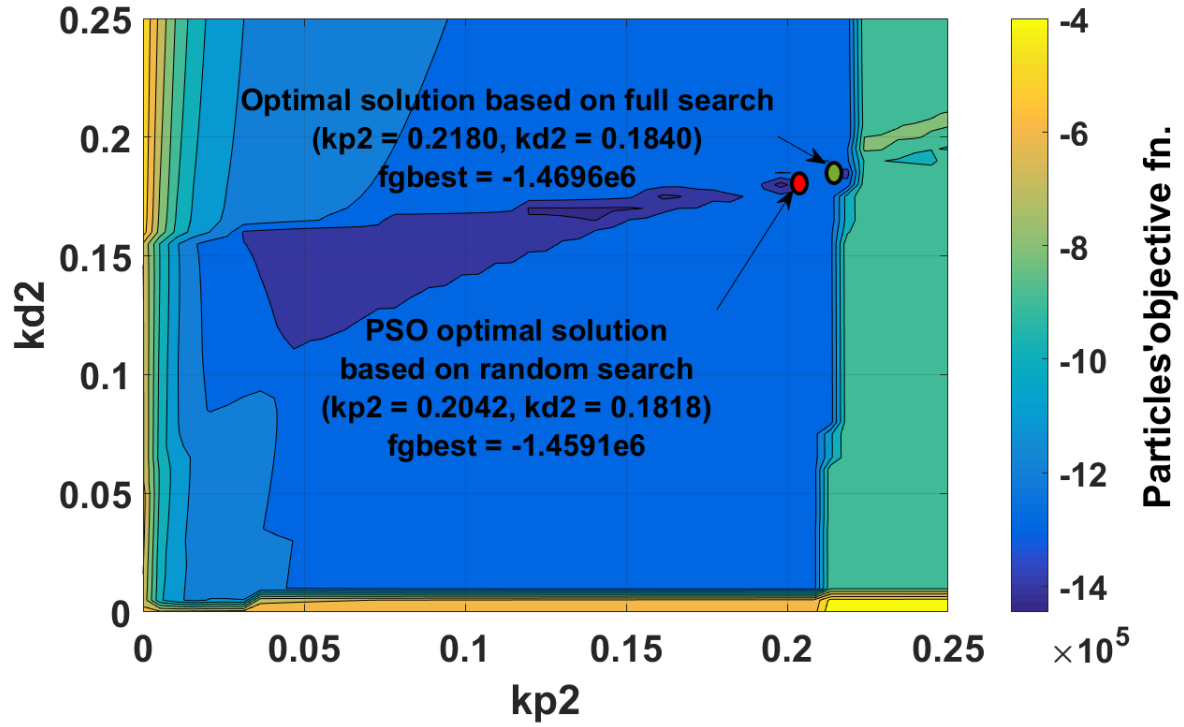

Fig. 5.9. Distribution of control gains and objective fn. at low load

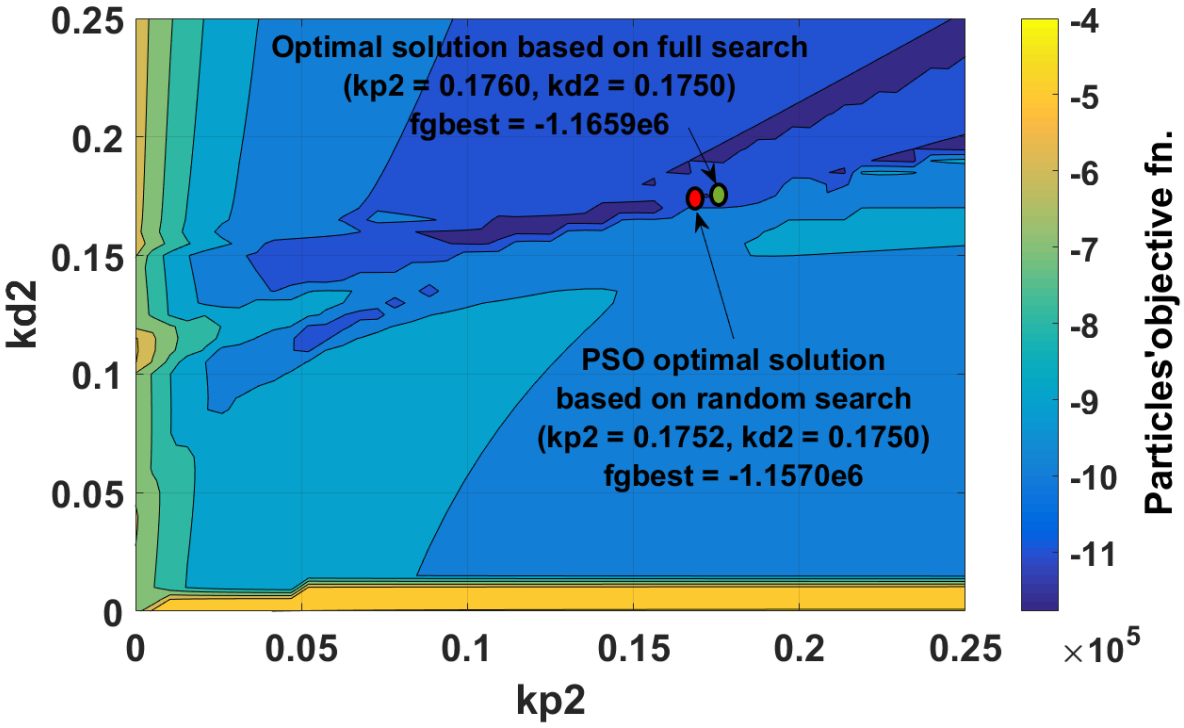

Fig. 5.10. Distribution of control gains and objective fn. at medium load

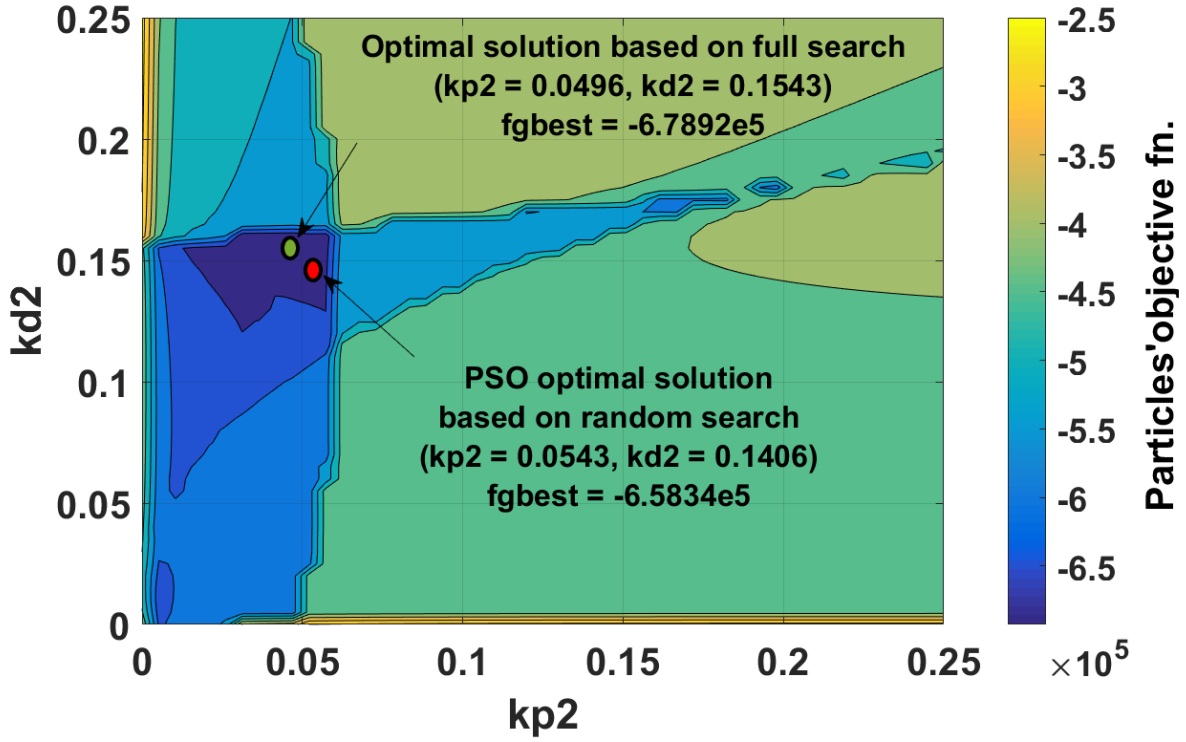

Fig. 5.11. Distribution of control gains and objective fn. at high load

A performance comparison has been also conducted to illustrate the relationship between the percentage of random particles and the obtained global best objective function that is reflected on the performance of the optimization.

Table 5.3. Comparison of f_{gbest} with and without random search without penalty factor constraints consideration

Loading Condition	f_{gbest} with random particles			f_{gbest} without random particles
	$rp = 50$	$rp = 15$	$rp = 1$	
H. L	-6.3160e^5	-6.6142e^5	-5.5483e^5	+1.6208e^5
M. L	-1.1743e^6	-1.2405e^6	-1.1820e^6	-1.2211e^6
L. L	-1.4136e^6	-1.3018e^6	-1.2651e^6	-1.3034e^6

Table 5.3 and Fig. 5.12 show that, even with just one random particle, the unstable result at L.L was avoided. However, the better results were obtained with 15 or

50 random particles compared to the case with just one particle. Regarding the difference between 15 and 50, the objective function was better with 50 random particles for low load although 15 random particles was slightly better for medium load. Moreover, the required number of iterations to achieve the converged solution was case by case as shown in Fig. 5.12. Generally speaking, it is expected that the ability for exploration should be enhanced, while the convergence characteristic for exploitation phase should deteriorate as the number of random particles increases. The optimization of the number of random particles has to be further examined in the future.

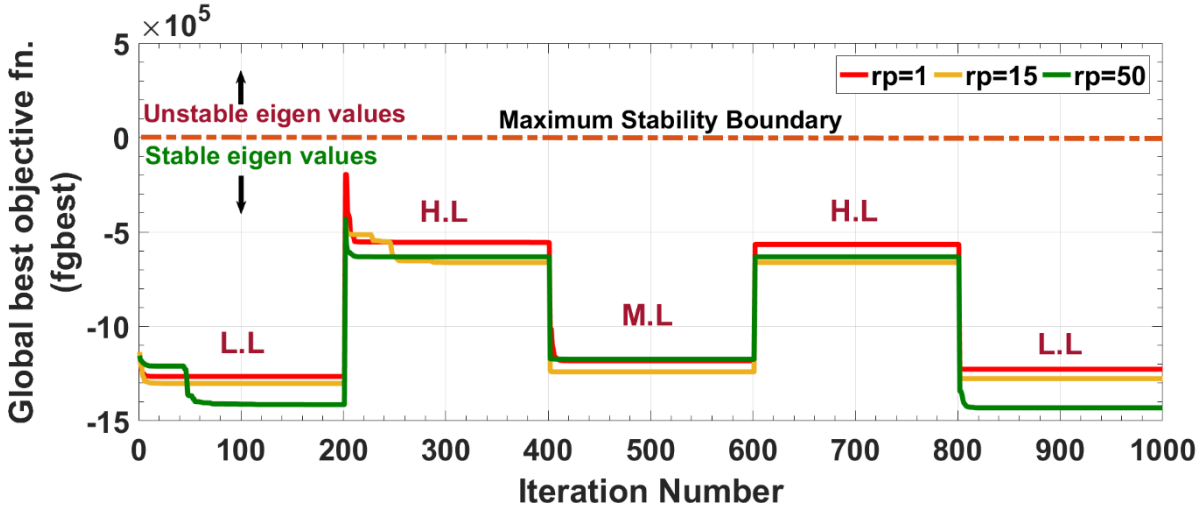

Fig. 5.12. Global best fitness function with one, 15 and 50 particles doing random search

Ultimately, Fig. 5.13 and 5.14 demonstrate the effectiveness of the control method through depicting network terminal voltages for low and high loading conditions respectively.

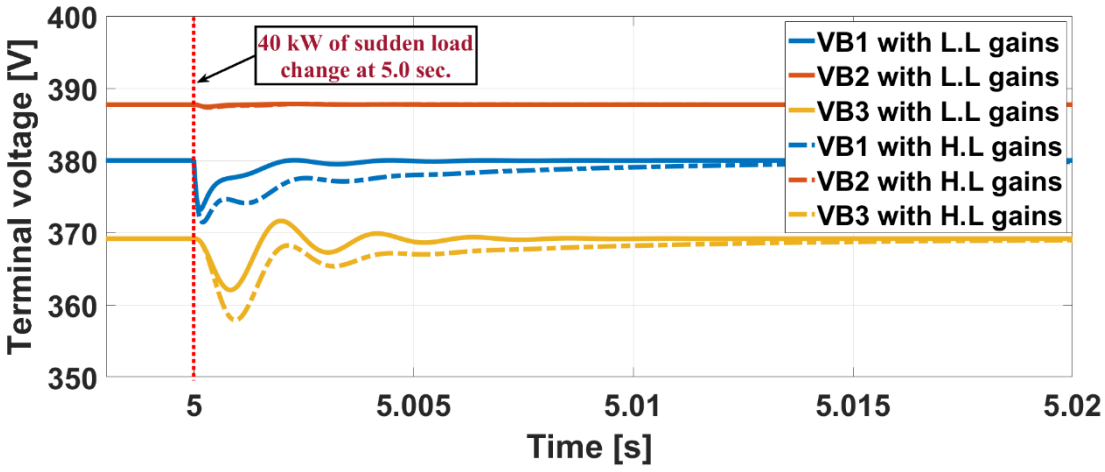

Fig. 5.13. Terminal voltages at low loading condition

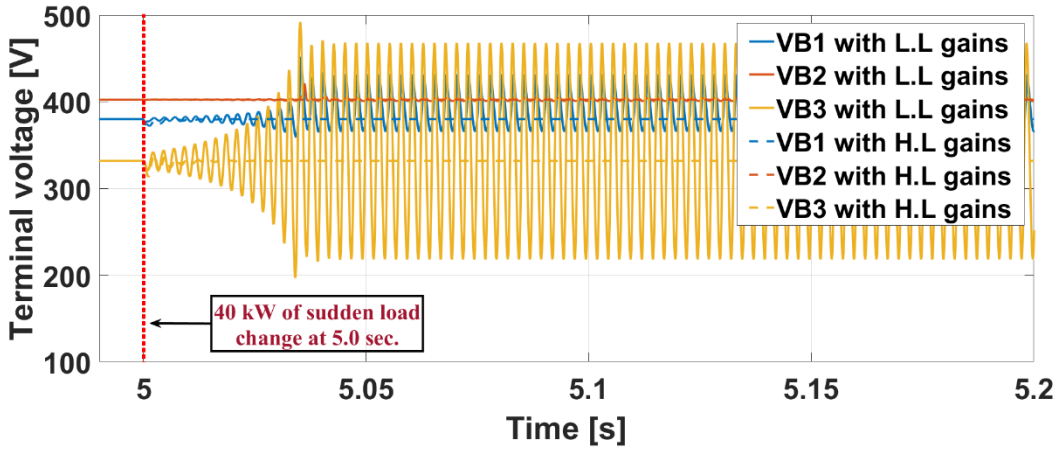

Fig. 5.14. Terminal voltages at high loading condition

Control response was observed by giving sudden load change stepwise at 5 seconds where the control gains obtained by the proposed method shown in Table 5.4 were used. These figures show that time varies from 10 to 15 ms at maximum to stabilize terminal voltages after any sudden load change. That proves the sufficiency of control gains suggested by PSO to reduce voltage fluctuations and to improve network performance. PD control gains needed to stabilize the network that resulted from the eigenvalue analysis are illustrated in Table 5.4.

Table 5.4. Online voltage control gains

Load gain	Control gains			
	k_{p1}	k_{p2}	k_{d1}	k_{d2}
H. L gains	0.0008	0.0899	0.0600	0.1430
M. L gains	0.0065	0.1304	0.0677	0.1662
L. L gains	0.0129	0.0842	0.0970	0.1506

These control gains can stabilize the grid at various loading conditions. However, the gains needed for stabilizing the network at low loading condition, could also stabilize it when medium loading is applied. However, they could not afford stability when high load is implemented due to the large difference in loading span as shown in Fig. 5.14.

Table 5.5. Comparison of eigenvalues in all cases

	Eigenvalues $*10^4$	
	High loading condition	Low loading condition
High load gains	-0.0172+0j	
	-0.0173 ± 0.2560j	-0.0330 ± 0.3005j
	-0.5101 + 0j	-0.0895 + 0j
	-0.5343 + 0j	-0.1636 ± 1.3719j
	-1.4053 + 0j	-0.9907 + 0j
	-3.3428 + 0j	-4.5060 ± 1.1098j
	-5.2398 + 0j	-9.6750 + 0j
	-8.9290 + 0j	
Low load gains		-0.0581 + 0j
	0.0228 ± 0.2905j	-0.0582 ± 0.2796j
	-0.0980 + 0j	-0.6873 + 0j
	-1.6773 ± 2.9824j	-0.6942 + 0j
	-1.9050 + 0j	-3.1756 + 0j
	-4.0271 ± 8.0113j	-3.4102 + 0j
	-6.6470 + 0j	-3.4102 + 0j
		-8.6082 + 0j

Likely, the same happened in medium loading gains. In that case, the gains needed to stabilize the grid at medium loading condition could be useful for low loading situation. However, when high load is applied, the medium loading gains could not stabilize it. Ultimately, the gains used for stabilization of network at high loading condition could stabilize it even for lower loading conditions as well

as illustrated in Fig. 5.13. In that case, the main aim in stabilizing the grid using Table 5.4 control gains is proved.

Fig. 5.13 illustrates that low load gains show a better impact in case of low loading condition than high load gains. Similarly, at high loading condition, high load gains stabilize voltage fluctuations compared with low load gains that were insufficient to support voltage stability after sudden change in load at bus 1 as shown in Fig. 5.14. Table 5.5 conforms those results by showing eigenvalues in all these cases. At high loading condition, by applying low load gains for voltage stability, the dominant eigenvalue shows a positive damping ratio which gives an indication of unstable pattern compared to the case of high load gains. On the other hand, at low loading condition, low load gains give a smaller damping ratio compared to the one in the case of high load gains.

There are several observations that could be discussed from the obtained results. However, one of the main points that need to be covered is the relationship between the optimization time calculation or what we can call the computation time of gains update with the whole-time interval through which the loading condition is applied. From Fig. 5.3 and 5.7 we can illustrate the following:

- For the proposed method, it is shown that, the control gains are updated in just 10 iterations that require only 2 sec. in an actual time frame.

- Since we don't have the actual data to determine the optimum time interval, in our simulation case, the time interval for every load condition was applied for 200 iterations like for 40 sec. In that context, around 5% of the time interval is used for calculation.

- Based on observations from the simulation results, the time interval could be shortened to reach about 20 iterations only so the load could be changed every 4 sec.

- In that case, especially for continuous load pattern, the time step for every load change shouldn't be less than the 10 iterations (2 sec.) to let the control algorithm be able to converge to optimum control gains.
- For the conventional method, and since the gains are trapped in a local minimum, it is quite difficult to focus on the optimization time or the time

interval. However, with the restarting technique, we can clarify that the algorithm takes nearly 80 iterations as of 16 sec. to calculate the optimum control gains.

- In that context, the time interval for load change should be around 100 iterations (20 sec).

- In that case, especially for continuous load pattern, the time step for every load change shouldn't be less than the 80 iterations (16 sec.) to let the control algorithm be able to converge to optimum control gains.

The above timings are affected by many factors as network scale and loading pattern applied. For instance, our network scale was based on a simplified three bus network with two generators, two loads and two transmission lines. Accordingly, the state space and algebraic representations were quite simple and small. However, if network complexity is directly proportional to the scale of the network. If the network scale increases, the complexity of the problem increases due to the numerous and various parameters to be introduced leading to a more complicated problem to be solved and computational time might increase.

On the other hand, due to the simplicity of the utilized three bus model, and since the system condition of load and generation is observable, a pre-determined control gains table might be set at different loading and generation conditions. In that context, at any loading and generation condition, the control gains might be easily chosen from the table by DSO. Table 5.6 shows the control gains pre-set at different levels of load and generation. Since we have two loads, two generators and four control gains, the table size might be big enough to be introduced in the thesis. Though, we fixed two out of the four parameters which are P_{L1} and P_{G2} and tried to portray our idea with just having only two parameters. In that case, with changing the values of P_{L3} and P_{G1} we can easily determine the required control gains for optimization.

Table 5.6. Load generation table with pre-set control gains

		Load range (P_{L3}) kW															
		0~50				51~100				101~150				151~200			
		kp1	kd1	kp2	kd2	kp1	kd1	kp2	kd2	kp1	kd1	kp2	kd2	kp1	kd1	kp2	kd2
Generation range (P_{G1}) kW	-17.6	0.0181	0.1184	0.1375	0.1725												
	-7.4	0.0161	0.1349	0.1814	0.1750												
	3.0	0.0143	0.1056	0.1281	0.1580												
	13.5	0.0116	0.0754	0.1508	0.1708												
	24.2	0.0107	0.0728	0.0899	0.1344												
	35					0.0095	0.0769	0.1569	0.1735								
	46.1					0.0084	0.0863	0.1885	0.1774								
	57.3					0.1816	0.1799	0.1695	0.1730								
	68.7					0.1816	0.1799	0.1695	0.1730								
	80.4					0.1816	0.1799	0.1696	0.1730								
	92.3									0.1816	0.1799	0.1696	0.1730				
	104.4									0.1723	0.1785	0.1745	0.1746				
	116.8									0.0434	0.1618	0.1238	0.1700				
	129.4									0.0218	0.1501	0.1284	0.1713				
	142.3									0.0016	0.0462	0.1106	0.1616				
	155.6													0.0023	0.0440	0.0091	0.0245
	169.1													0.0008	0.0376	0.0222	0.0347
	183.1													0.0010	0.0581	0.0960	0.1483
	197.4													0.0006	0.0404	0.0022	0.0076
	212.1													0.0006	0.0394	0.0018	0.0076

The previous table could be utilized in small scale networks. However, if the scale of the network increases, it would be very difficult to obtain that kind of table due to the enormous complexity of the problem that emerges die to the increase of the number of parameters in the network. For instance, the number of generators, distribution lines and loads lead to an increase in the state space and algebraic representations of the network and the computation times rises drastically. To cope with that problem, the proposed online voltage control method using the suggested PSO method would be a perfect fit as a solution to enhance the dynamic response and reduce the computation time instead of having a pre-set gains table. To demonstrate the sufficiency of the proposed method in such large-scale networks, an eigenvalue analysis is conducted on a larger scale model of eight bus network as shown in Fig. 5.15. This model comprises of three generators sets, nine distribution lines and five loads dispersed all over the network. The flowing currents were suggested through the distribution lines and the S matrix is calculated. The formulation of the distribution line currents is shown as follows:

$$i_{21}(t) + i_{51}(t) + i_{41}(t) = i_{L1}(t) + i_{C1}(t)$$

$$i_{21}(t) + i_{23}(t) + i_{C2}(t) = i_{52}(t) + i_{S2}(t)$$

$$i_{23}(t) = i_{C3}(t) + i_{L3}(t)$$

$$i_{S4}(t) + i_{54}(t) = i_{C4}(t) + i_{41}(t) + i_{47}(t)$$

$$i_{S5}(t) = i_{C5}(t) + i_{51}(t) + i_{52}(t) + i_{54}(t) + i_{56}(t) + i_{58}(t)$$

$$i_{56}(t) = i_{C6}(t) + i_{L6}\ (t)$$

$$i_{47}(t) = i_{C7}(t) + i_{L7}(t)$$

$$i_{58}(t) = i_{C8}(t) + i_{L8}(t)$$

Terminal voltages are shown as follows:

$$V_{B1}(t) = \frac{1}{C}\int (i_{21}(t) + i_{51}(t) + i_{41}(t) - i_{L1}(t))dt$$

$$V_{B2}(t) = \frac{1}{C}\int (i_{S2}(t) + i_{52}(t) - i_{21}(t) - i_{23}(t))dt$$

$$V_{B3}(t) = \frac{1}{C}\int (i_{23}(t) - i_{L3}(t))dt$$

$$V_{B4}(t) = \frac{1}{C}\int (i_{S4}(t) + i_{54}(t) - i_{41}(t) - i_{47}(t))dt$$

$$V_{B5}(t) = \frac{1}{C}\int (i_{S5}(t) - i_{51}(t) - i_{52}(t) - i_{54}(t) - i_{56}(t) - i_{58}(t))dt$$

$$V_{B6}(t) = \frac{1}{C}\int (i_{56}(t) - i_{L6}(t))dt$$

$$V_{B7}(t) = \frac{1}{C}\int (i_{47}(t) - i_{L7}(t))dt$$

$$V_{B8}(t) = \frac{1}{C}\int (i_{58}(t) - i_{L8}(t))dt$$

Finally, load currents can be shown as follows:

$$i_{Ln}(t) = \frac{P_{Ln}}{V_{Bn}(t)}$$, Where n =1, 3,6,7 & 8.

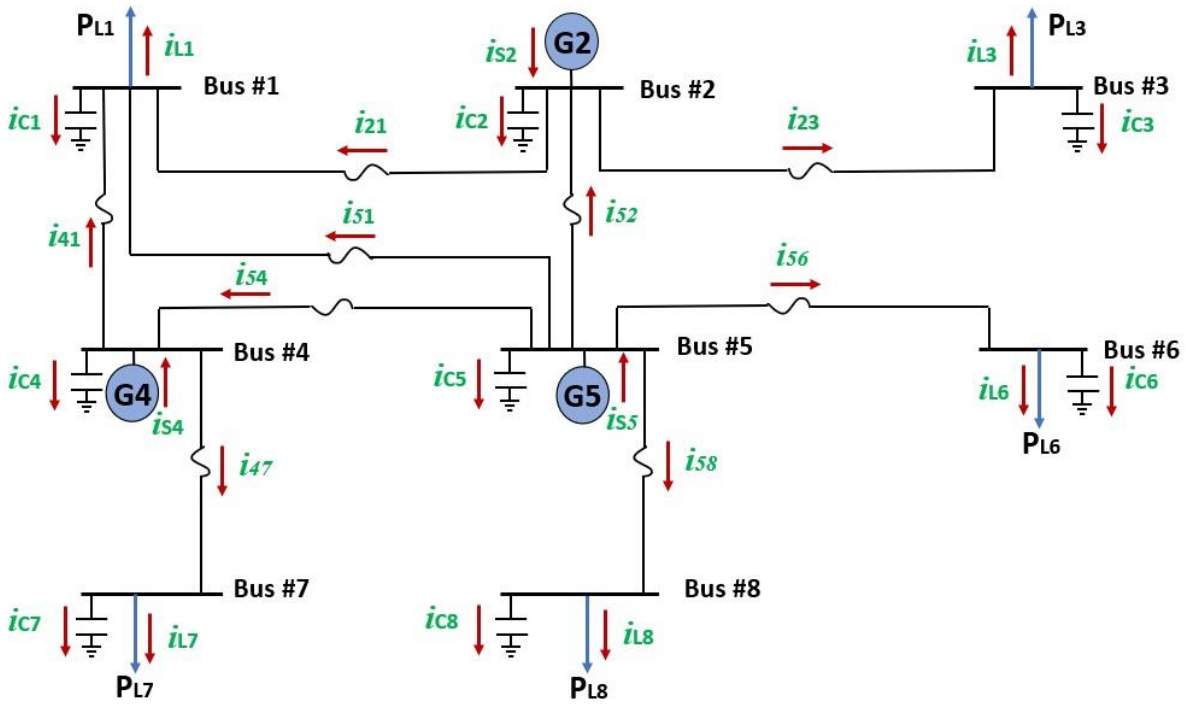

Fig. 5.15. 8-bus DC microgrid model

Accordingly, A and B matrices can be illustrated as follows:

$$\frac{d}{dx}\begin{bmatrix} i_{S2} \\ i_{S4} \\ i_{S5} \\ V_{B1} \\ V_{B2} \\ V_{B3} \\ V_{B4} \\ V_{B5} \\ V_{B6} \\ V_{B7} \\ V_{B8} \\ i_{21} \\ i_{23} \\ i_{41} \\ i_{47} \\ i_{51} \\ i_{52} \\ i_{54} \\ i_{56} \\ i_{58} \\ a_2 \\ a_4 \\ a_5 \end{bmatrix} = \begin{bmatrix} A_{15} = {}^{-1}/_{L}\,(kp_2 * E_2 + 1),\ A_{1,21} = {}^{-1}/_{L}\,(kd_2 * E_2) \\ A_{27} = {}^{-1}/_{L}\,(kp_4 * E_4 + 1),\ A_{2,22} = {}^{-1}/_{L}\,(kd_4 * E_4) \\ A_{38} = {}^{-1}/_{L}\,(kp_5 * E_5 + 1),\ A_{3,23} = {}^{-1}/_{L}\,(kd_5 * E_5) \\ A_{4,12} = A_{4,14} = A_{4,16} = {}^{1}/_{C} \\ A_{51} = -A_{5,12} = -A_{5,13} = A_{5,17} = {}^{1}/_{C} \\ A_{6,13} = {}^{1}/_{C} \\ A_{72} = -A_{7,14} = -A_{7,15} = A_{7,18} = {}^{1}/_{C} \\ A_{83} = -A_{8,16} = -A_{8,17} = -A_{8,18} = -A_{8,19} = -A_{8,20} = {}^{1}/_{C} \\ A_{9,19} = {}^{1}/_{C} \\ A_{10,15} = {}^{1}/_{C} \\ A_{11,20} = {}^{1}/_{C} \\ A_{12,4} = -A_{12,5} = {}^{-1}/_{L_{Line}}\ , A_{12,12} = {}^{-R_{Line}}/_{L_{Line}} \\ A_{13,5} = -A_{13,6} = {}^{1}/_{L_{Line}}\ , A_{13,13} = {}^{-R_{Line}}/_{L_{Line}} \\ A_{14,4} = -A_{14,7} = {}^{-1}/_{L_{Line}}\ , A_{14,14} = {}^{-R_{Line}}/_{L_{Line}} \\ A_{15,7} = -A_{15,10} = {}^{1}/_{L_{Line}}\ , A_{15,15} = {}^{-R_{Line}}/_{L_{Line}} \\ A_{16,4} = -A_{16,8} = {}^{-1}/_{L_{Line}}\ , A_{16,16} = {}^{-R_{Line}}/_{L_{Line}} \\ A_{17,5} = -A_{17,8} = {}^{-1}/_{L_{Line}}\ , A_{17,17} = {}^{-R_{Line}}/_{L_{Line}} \\ A_{18,7} = -A_{18,8} = {}^{-1}/_{L_{Line}}\ , A_{18,18} = {}^{-R_{Line}}/_{L_{Line}} \\ A_{19,8} = -A_{19,9} = {}^{1}/_{L_{Line}}\ , A_{19,19} = {}^{-R_{Line}}/_{L_{Line}} \\ A_{20,8} = -A_{20,11} = {}^{1}/_{L_{Line}}\ , A_{20,20} = {}^{-R_{Line}}/_{L_{Line}} \\ A_{21,1} = -A_{21,12} = -A_{21,13} = A_{21,17} = {}^{1}/_{\eta * C}\ , A_{21,21} = {}^{-1}/_{\eta * T_D} \\ A_{22,2} = -A_{22,14} = -A_{22,15} = A_{22,18} = {}^{1}/_{\eta * C}\ , A_{22,22} = {}^{-1}/_{\eta * T_D} \\ A_{23,3} = -A_{23,16} = -A_{23,17} = -A_{23,18} = -A_{23,19} = -A_{23,20} = {}^{1}/_{\eta * C}\ , A_{23,23} = {}^{-1}/_{\eta * T_D} \\ Others\ \ A_{i,j} = 0 \end{bmatrix} x + \begin{bmatrix} 0 \\ 0 \\ 0 \\ {}^{-1}/_{C} \\ 0 \\ {}^{-1}/_{C} \\ 0 \\ 0 \\ {}^{-1}/_{C} \\ {}^{-1}/_{C} \\ {}^{-1}/_{C} \\ 0 \\ 0 \\ 0 \\ 0 \\ 0 \\ 0 \\ 0 \\ 0 \\ 0 \end{bmatrix} y + \begin{bmatrix} d_2(t)E_2/L \\ d_4(t)E_4/L \\ d_5(t)E_5/L \\ 0 \\ 0 \\ 0 \\ 0 \\ 0 \\ 0 \\ 0 \\ 0 \\ 0 \\ 0 \\ 0 \\ 0 \\ 0 \\ 0 \\ 0 \\ 0 \\ 0 \\ 0 \end{bmatrix}$$

A matrix

B matrix

Constants matrix

Accordingly, *C* and *D* matrices are shown as follows:

$$0 = \begin{bmatrix} C_{44} = \frac{P_{L1}}{V_{B1}^2} \\ C_{66} = \frac{P_{L3}}{V_{B3}^2} \\ C_{99} = \frac{P_{L6}}{V_{B6}^2} \\ C_{10,10} = \frac{P_{L7}}{V_{B7}^2} \\ C_{11,11} = \frac{P_{L8}}{V_{B8}^2} \\ Others \;\; C_{i,j} = 0 \end{bmatrix} x + \begin{bmatrix} 0 \\ 0 \\ 0 \\ 1 \\ 0 \\ 1 \\ 0 \\ 0 \\ 1 \\ 1 \\ 1 \\ 0 \\ 0 \\ 0 \\ 0 \\ 0 \\ 0 \\ 0 \\ 0 \\ 0 \\ 0 \\ 0 \\ 0 \end{bmatrix} y$$

C matrix D matrix

Ultimately, S matrix has the same size of A matrix, where $S = (A - BD^{-1}C)$

To demonstrate the effectiveness of the proposed method on the new model, the same control sequence is applied. Firstly, whenever a load changes, the configuration of S matrix changes consequently. Afterwards, the eigenvalues are obtained and organized in a descending order taken into consideration their signs. Consequently, the objective fn. of each particle is obtained, compared with the previous local best one and the new local and global best objective functions' values in addition to the particles' local and global best positions are decided. Finally, particles' positions and speeds are updated based on the new control gains. Fig. 5.16 shows the comparison between the global best objective function when the conventional method of fixed control gains is applied and when the idea of allocating some of the particles to do a random search is applied. From both figures we can confirm that with the proposed method of random particles, better value of objective function can be shown. Thanks to the random particles, gains cannot be trapped in a local-minima and a continuous search for optimum solution is held. As a result, the normal particles followed the random ones to search for optimum solution in various search fields reaching more optimum solution. That is reflected in Fig. 5.17(a) and (b) which depict particles' global best positions with the conventional and proposed methods respectively.

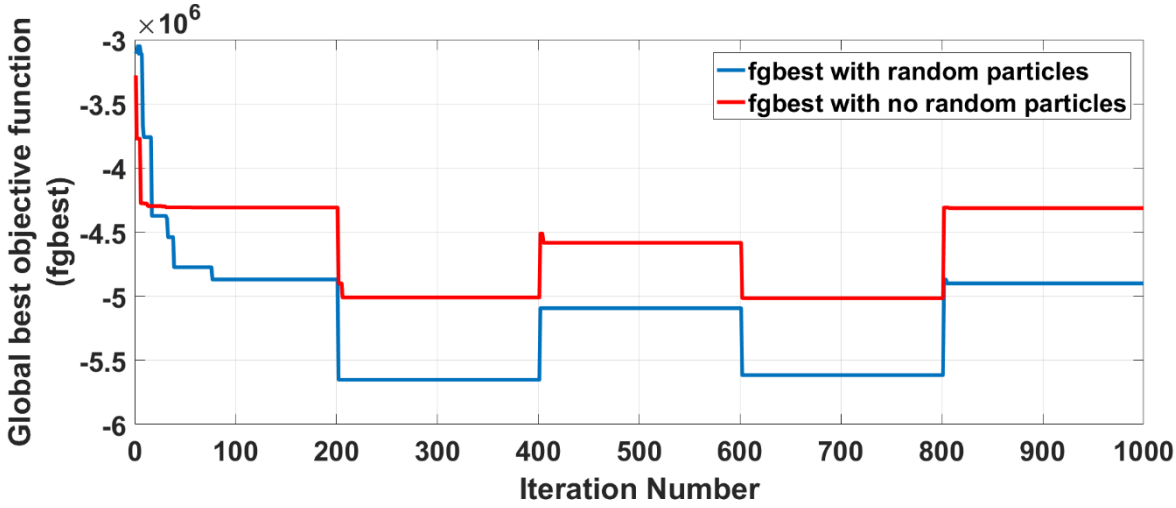

Fig. 5.16. Comparison between global best objective fn. with and without the proposed method

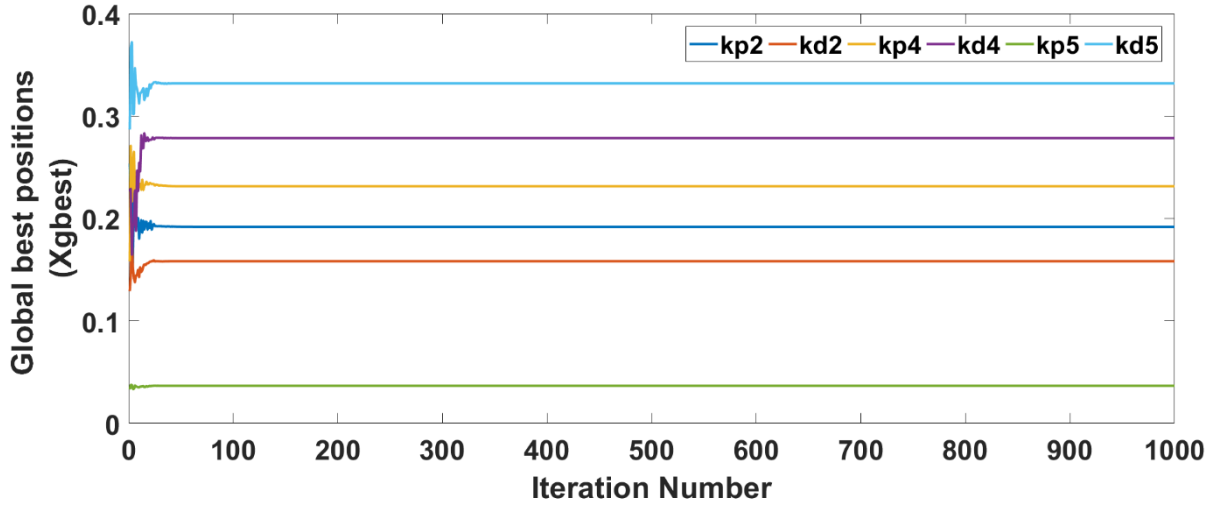

(a)

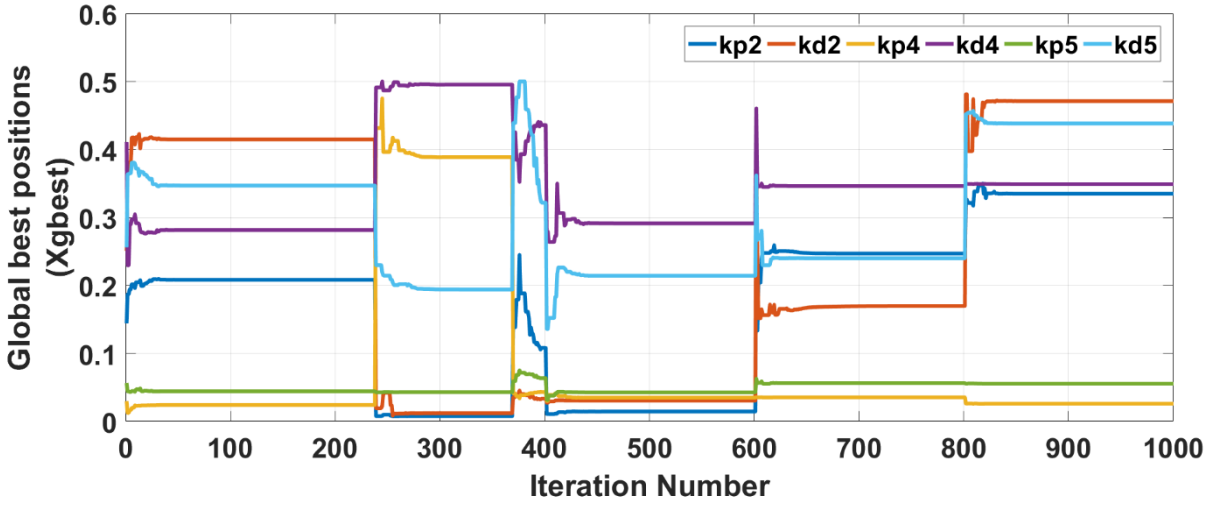

(b)

Fig. 5.17. Particles' global best positions (X_{gbest}) with the:
(a) Conventional method at fixed control gains (b) Proposed method with random particles

Same as the previous discussion about the simplified 3-bus model, in the 8-bus model and as shown in Fig. 5.17 (a) and (b), there are some observations.

- For the proposed method, it is shown that, the control gains are updated in just 30 to 40 iterations that require only 6 to 8 sec. in an actual time frame.

- Since we don't have the actual data to determine the optimum time interval, in our simulation case, the time interval for every load condition was applied for 200 iterations like for 40 sec. In that context, around 15 to 20 % of the time interval is used for calculation.

- Based on observations from the simulation results, the time interval could be shortened to reach about 30 to 40 iterations only so the load could be changed every 6 to 8 sec.

- In that case, especially for continuous load pattern, the time step for every load change shouldn't be less than the 30 to 40 iterations (6 to 8 sec.) to let the control algorithm be able to converge to optimum control gains.

- For the conventional method, and since the gains are trapped in a local minimum, it is quite difficult to focus on the optimization time or the time interval. However, with the restarting technique, we can clarify that the algorithm takes nearly 30 iterations as of 6 sec. to calculate the optimum control gains.

- In that context, the time interval for load change should be around 30 to 40 iterations (6 to 8 sec).

- It is also illustrated that when the scale and the complexity of the grid is enlarged, the time taken for optimization is increased as we compare the results of Fig. 5.17 with that of Fig. 5.7. When the scale of the model is enlarged from simplified 3-bus model to be an 8-bus model, the optimization time calculation increases from 10 iterations (2 sec) to 30-40 iterations (6-8 sec). Similarly, the gains update time interval increases from 10-20 iterations (2-4 sec) in the simplified model to 30-40 iterations (6-8 sec) in the 8-bus model.

On the other hand, Fig. 5.18 (a) and (b) depict the comparison of the time series voltage control in both conventional and proposed method cases respectively. As shown in Fig. 5.18, it is confirmed that applying the control gains resulted from the proposed method could improve network stability more that the conventional method does. With the proposed method the time constant needed to stabilize the voltage at terminal 6 is reduced from about 150 ms with the conventional method to almost 50 ms only by using the proposed method. That can be also demonstrated in Table 5.7 that shows the eigenvalues obtained in both cases.

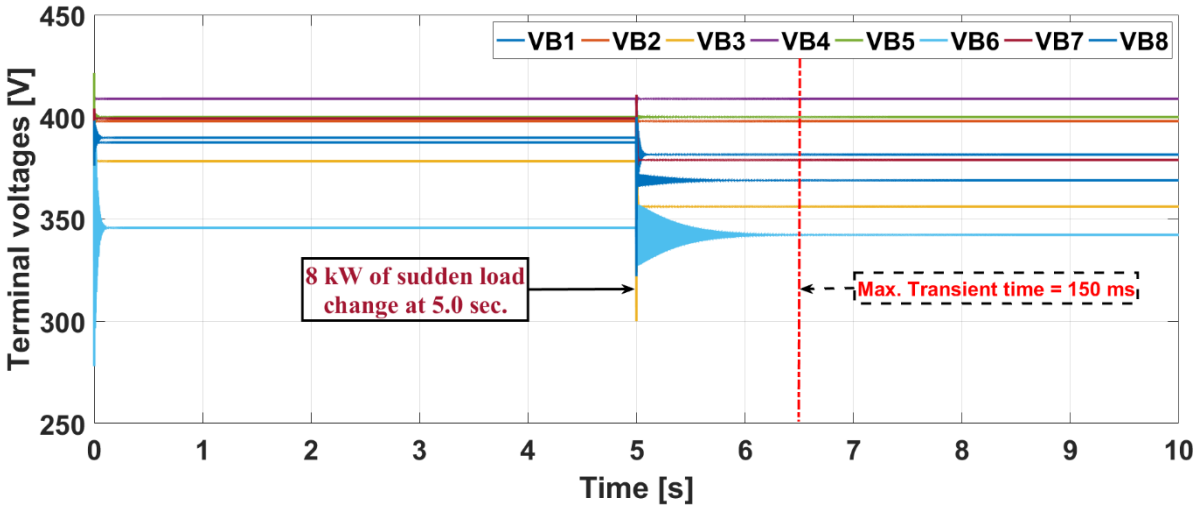

(a)

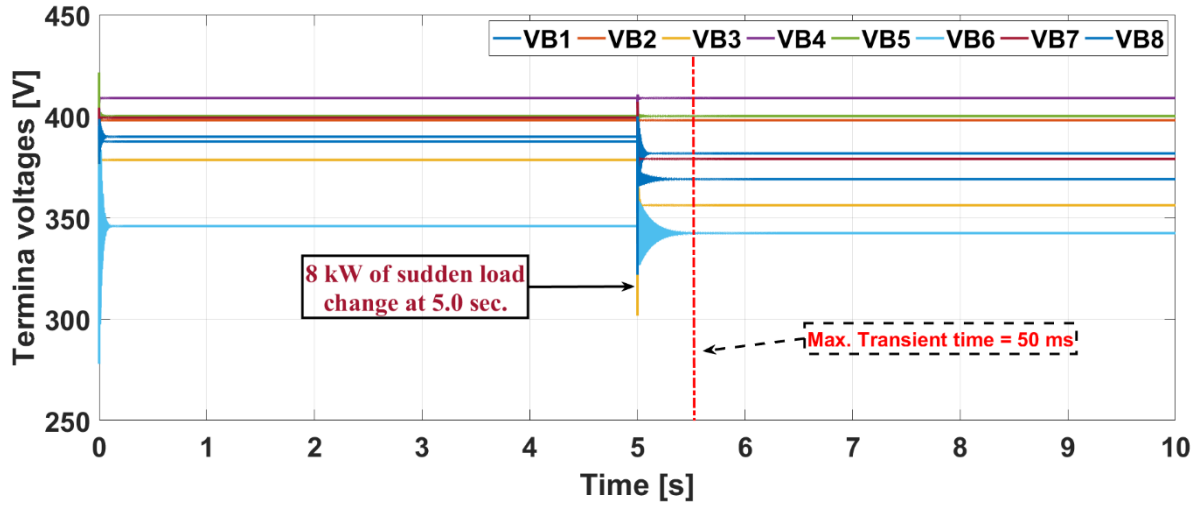

(b)

Fig. 5.18. 8- bus model terminal voltages with the:
(b) Conventional method at fixed control gains (b) Proposed method with random particles

Table 5.7. Comparison of eigenvalues in all cases

	Eigenvalues $*10^4$	
	High loading condition	Low loading condition
High load gains	-0.0714 + 0.0000i	-0.0185 ± 1.0389i
	-0.0759 + 0.0000i	-0.0221 ± 0.9735i
	-0.0769 ± 0.3039i	-0.0267 ± 1.1802i
	-0.0887 ± 0.3132i	-0.0518 ± 0.2812i
	-0.0944 ± 0.2974i	-0.0569 ± 0.5090i
	-0.1010 ± 0.2854i	-0.0575 ± 0.2939i
	-0.1250 + 0.0000i	-0.0577 ± 0.2912i
	-0.1250 + 0.0000i	-0.0643 ± 0.3103i
	-0.1369 ± 0.3081i	-0.0832 + 0.0000i
	-0.1544 + 0.0000i	-0.0982 + 0.0000i
	-0.4296 + 0.0000i	-0.1250 + 0.0000i
	-0.9078 ± 0.5023i	-0.1250 + 0.0000i
	-4.8006 ± 3.5096i	-9.9993 + 0.0000i
	-4.9168 ± 5.3012i	-9.9995 + 0.0000i
	-8.1980 + 0.0000i	-9.9998 + 0.0000i
Low load gains	-0.0051 ± 2.0182i	
	-0.0242 ± 0.9641i	-0.0640 ± 0.0004i
	-0.0254 ± 1.1912i	-0.0640 ± 0.3107i
	-0.0708 ± 0.3079i	-0.0641 ± 0.3098i
	-0.0728 ± 0.2925i	-0.0656 ± 0.2865i
	-0.0739 ± 0.2961i	-0.0712 ± 0.3044i
	-0.0855 + 0.0000i	-0.0938 ± 0.3049i
	-0.1013 ± 0.5221i	-0.1161 + 0.0000i
	-0.1095 + 0.0000i	-0.1250 + 0.0000i
	-0.1177 ± 0.3058i	-0.1250 + 0.0000i
	-0.1250 + 0.0000i	-0.2368 + 0.0000i
	-0.1250 + 0.0000i	-0.5218 + 0.0000i
	-9.9992 + 0.0000i	-4.7675 ± 1.1401i
	-9.9992 + 0.0000i	-4.8858 ± 3.7609i
	-9.9996 + 0.0000i	-4.9321 ± 6.1144i

From Table 5.7 it is found that, similar to the simplified model, the high load gains give better stability performance compared to low load gains at high loading conditions. Likely, at low loading conditions, low load gains are better than high load gains. For instance, Fig. 5.19 shows the terminal voltages after a sudden load change when the low load gains are used at high loading condition in comparison with Fig. 5.18 when the high load gains are used. It is illustrated that a better performance is obtained when high load gains are used. We can show that at using low load gains to stabilize the grid with high loading conditions might lead to instability if there is any sudden load change.

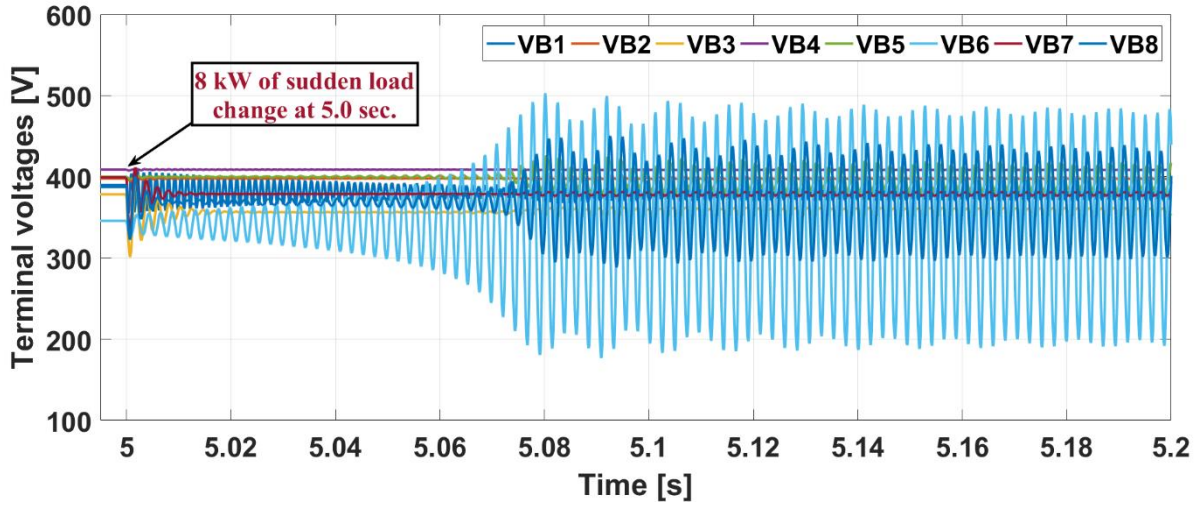

Fig. 5.19. Terminal voltages at high loading condition with low load gains

In this section, we only introduced a step size load change. However, in real time applications, a continuous pattern of load change is applied. So, according to the load pattern, the algorithm will act to get the optimum control gains. In our research we applied the step size change of load pattern to easily show how the algorithm works efficiently in a few seconds to get the optimized solutions. However, with a continuously pattern of load change the algorithm will always change the gains until the load stabilizes. Fig. 5.20 (a) and (b) illustrate the continuous load patterns applied at the two busses. This loading pattern conforms with the actual residential load pattern in most of our houses where there are peak values during rush hours and times where the load is at its minimum. Accordingly, when this continuous load pattern is applied instead of the step change scheme, the algorithm showed sufficiency in searching the search space for optimum solutions in a rapid pace with fast computation time. Fig. 5.21 (a) and (b) illustrate the obtained objective function and the optimized control gains respectively. These figures prove the importance and the ability of the proposed method to solve the problem and determine the optimum solution even in different network circumstances. As shown, we can observe that the algorithm proposed different solutions whenever load changes all over the simulation.

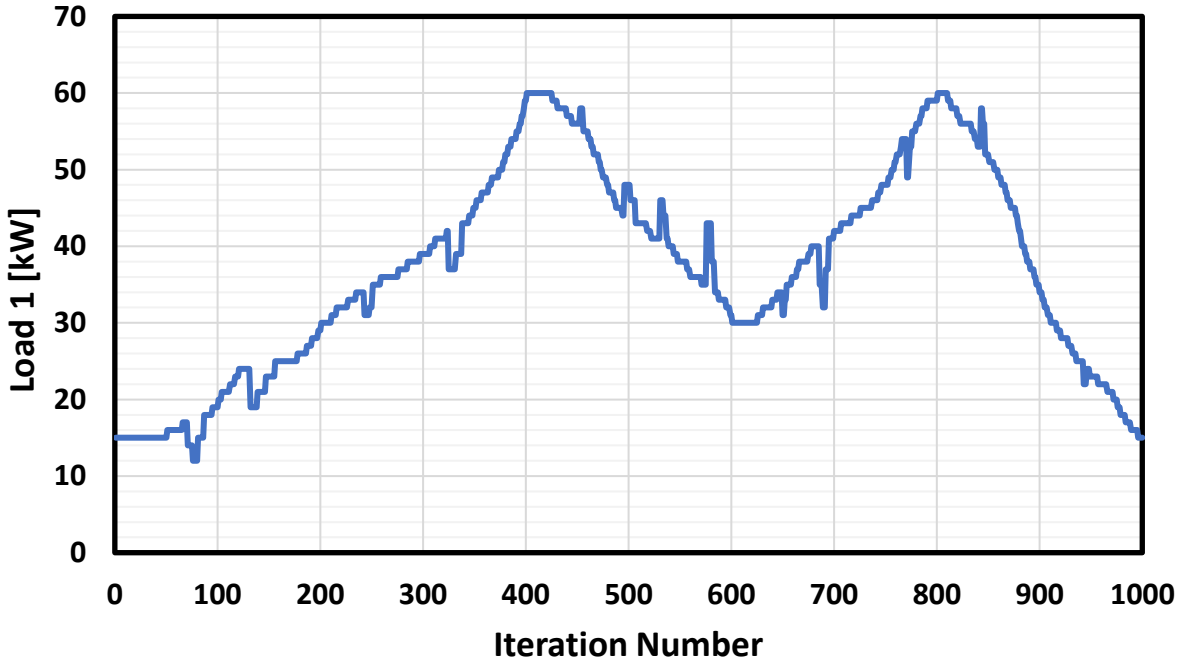

(a)

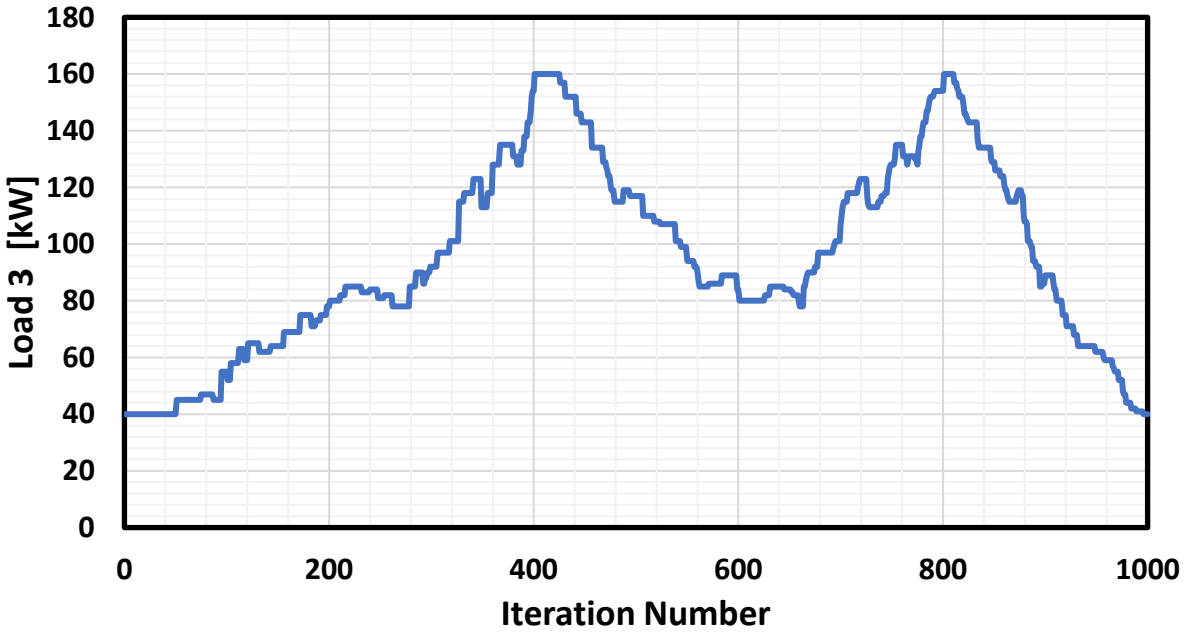

(b)

Fig. 5.20. Loading powers with continuous load patterns:
(a) Load 1 at bus #1 (b) Load 3 at bus #3

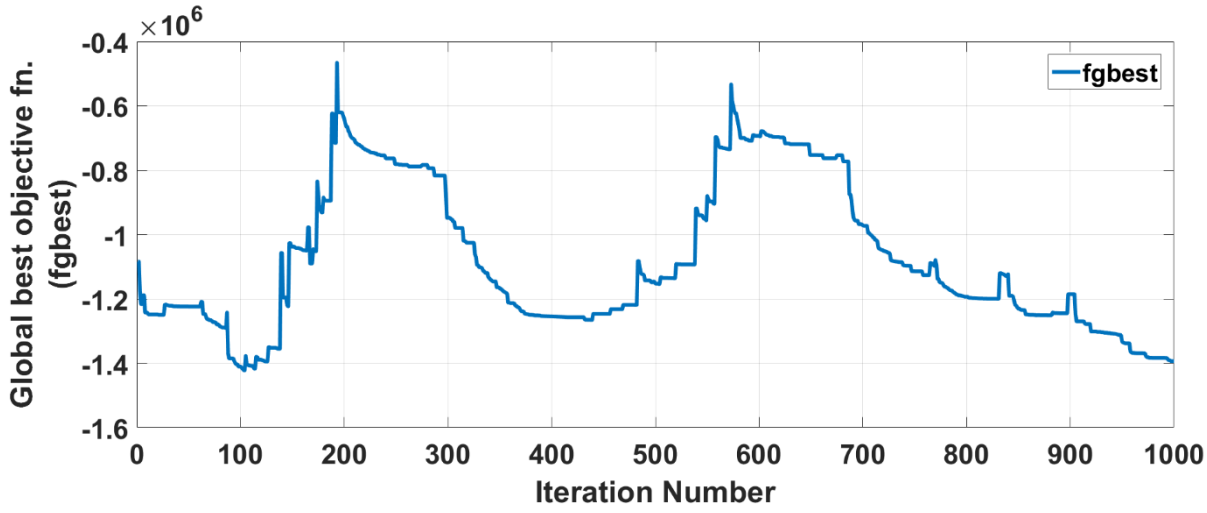

(a)

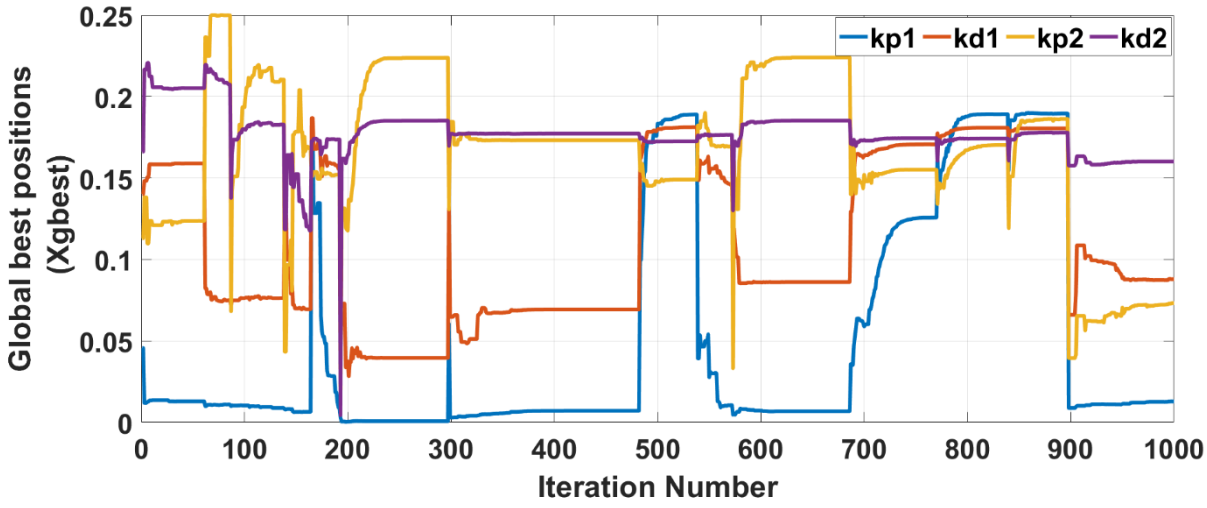

(b)

Fig. 5.21. PSO performance with continuous load pattern:
(a) Global best objective fn. and (b) Global best positions of control gains

On the other hand, if a time delay is added and considered in the switching model of the primary control as shown in Fig. 5.22, a short perturbation with higher frequency will occur after load change until a steady state is approached. Switching delay is added in the primary control circuit that represents the actual delay taken by the converter from the instant it receives the control signal to the instant it sends the control output. Fig. 5.23 (a) and (b) illustrate the obtained terminal voltages in case of a time delay for low and high loading conditions respectively. Since the carrier frequency was about 100 kHz, as the simulation step size was 1/(10^5), though, we set the time delay to 5*10^(-5).

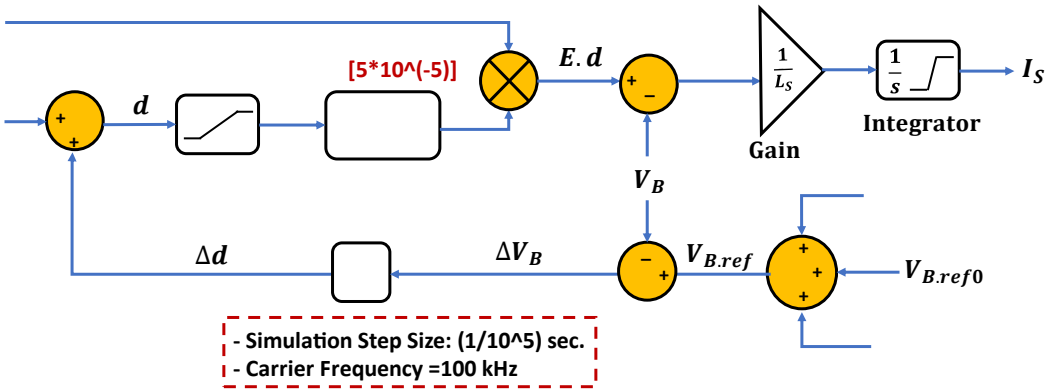

Fig. 5.22. Primary control model with switching time delay

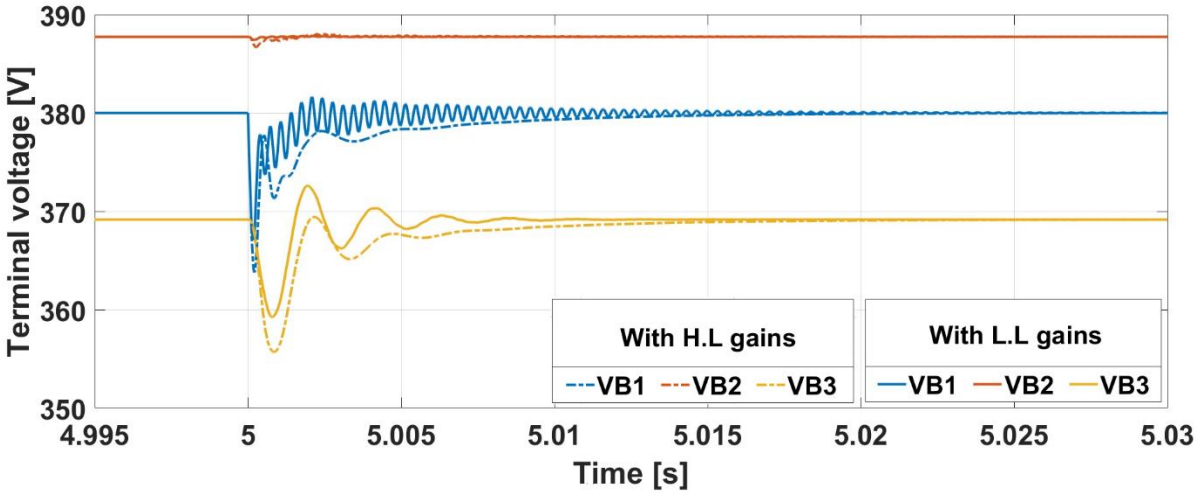

(a)

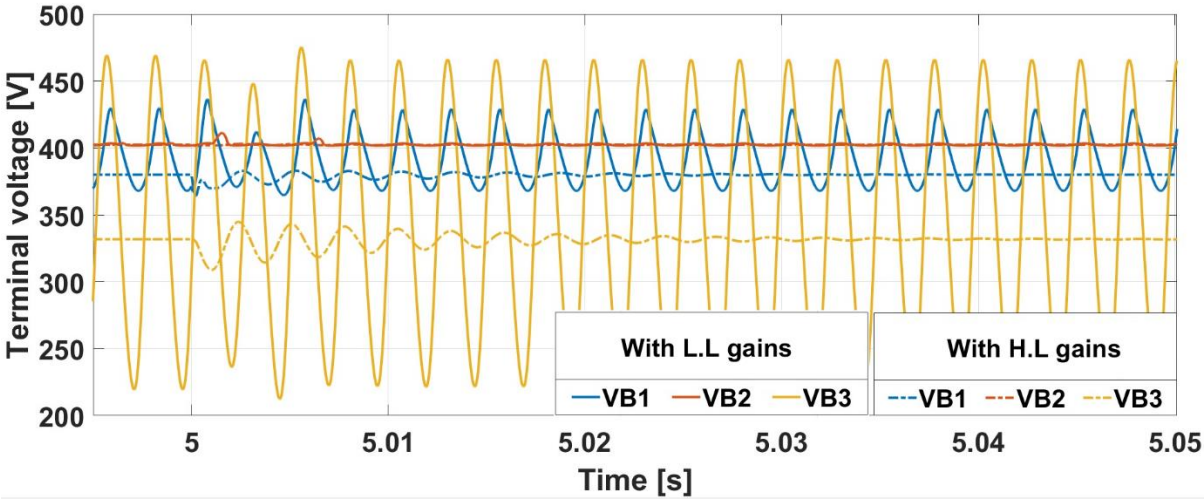

(b)

Fig. 5.23. Terminal voltages with switching time delay:
(a) At low load condition, and (b) At high load condition

If we compare Fig. 5.23 (a) and (b) with Fig. 5.13 and 5.14, we can observe that adding switching time delay add some perturbations especially at busses 1 and 3. In addition, it took longer time to stabilize the voltage compared to with no time delay inserted case. From the above figures, it is also shown that, with time delay it took about 25 ms, while with no delay it took 7 ms as transient time to stabilize the voltage after sudden load change at low load condition. However, for high load condition, it took 30 ms with delay, while it was 10 ms with no delay inserted.

From another perspective, the number of trials needed to be conducted to find the best objective function is discussed. Table 5.8 shows the average value of all trials in all loading conditions and how they are close in value to that of the full search technique. Eleven trials are used to obtain the optimum solution and the best value of objective function.

Table 5.8. Average values of objective fn. after several trials at different loading conditions

Trial	1	2	3	4	5	6	7	8	9	10	11	Avg.
L.L Obj. fn.*10^6	-1.424732	-1.419395	-1.487679	-1.483115	-1.448621	-1.482902	-1.451135	-1.414968	-1.426405	-1.444695	-1.498455	**-1.452958**
M.L Obj. fn.* 10^6	-1.214851	-1.294176	-1.258008	-1.276997	-1.233661	-1.273899	-1.179340	-1.238238	-1.191630	-1.233862	-1.301020	**-1.245062**
H.L Obj. fn.*10^5	-6.48000	-7.18955	-6.86494	-7.19103	-6.78520	-6.72454	-6.44369	-6.64635	-6.81504	-6.72254	-7.20728	**-6.68256**

Fig. 5.24 and 5.25 show the obtained fitness function values at low and high loading conditions respectively. It is shown that the error or the difference between the average and best values are not so large, and that gives a better indication that even in some cases one or even few trials might be enough.

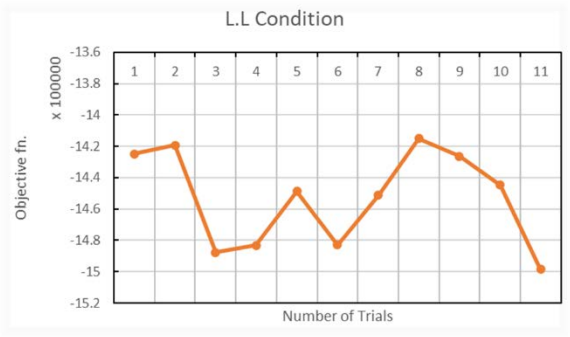

Fig. 5.24. Average values of objective fn. After several trials at low loading condition

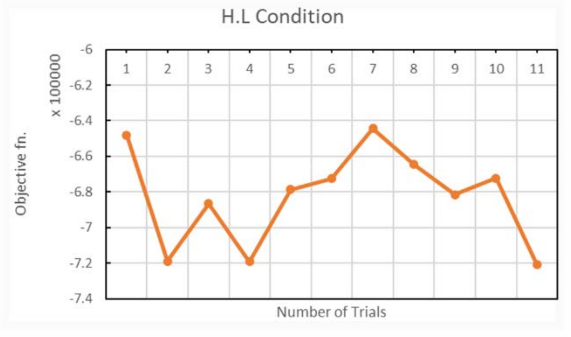

Fig. 5.25. Average values of objective fn. After several trials at high loading condition

5.3 Summary

This chapter discussed the simulation using 3-bus DC microgrid model by applying a comparison between conventional and proposed method of PSO. A conventional method applying only normal particles without any random search techniques against a suggested method of a combination of normal and random particles to enhance control performance. Control performance is improved with the suggested techniques as it gives better objective functions' values. In addition, optimum control gains were obtained in contrary with the conventional method, where the control gains were trapped in local minimums close to extreme values and lacking global search when it was needed. Contour figures were also depicted, showing that the obtained control gains from online PSO using the proposed method were very close to that obtained from the full search technique to show how precise the suggested method is, as a contradiction with the conventional method. On the other hand, the conventional method was even showing instability during high load conditions, where the eigenvalues were positive and gave positive fitness function value due to usage of the penalty factor term.

CHAPTER 6

HIERARCHICAL CONTROL STRUCTURE

6.1 Introduction to hierarchical control system

This chapter discusses about the hierarchical control approach for voltage control of DC microgrids. The control pattern is divided into three main control systems: primary, secondary and tertiary control levels. Each control level is applied on a defined timescale to mitigate bus terminal voltage by setting new reference values according to various factors ranging between loading conditions and generation cost.

In previous chapters, we illustrated deeply the primary controller and how to efficiently determine PD control gains in real time consequent to sudden load changes. However, primary control just regulates terminal voltages in a centralized mode, while reference value of the voltage is kept fixed. Though, using only primary controller might not be enough. Voltage offset appeared between required voltage values and obtained ones. In that context, a new decentralized methodology is suggested to eliminate that offset through updating voltage reference values based on a secondary controller perspective and eliminate voltage fluctuations exceeding the stability limits. In addition, an upper level of control mainly named tertiary controller is proposed for optimal dispatch of DG and controlling transmission line current. Cost effective equations formulation is developed to determine the optimal voltage value with the lowest generation cost. Though, if any load change occurs, the whole PID logic is applied on different time intervals to regulate terminal voltages.

6.2 Necessity of hierarchical control System

Despite all the advantages that could be provided by simply using DC systems especially small scale microgrids, still there is a crucial need to implement a sufficient control system to enhance network performance. The main theme of such control system has to be power flow control and terminal voltages regulation.

In this study, a hierarchical control mechanism based on primary, secondary and tertiary controllers is proposed and applied on different time scales. Primary control is an adaptive droop control which is applied to adjust local terminal voltage by adjusting the duty ratio of each generator. This could be done by adjusting the optimum PD control parameters using PSO described previously in Chapter 4. However, there must be an offset bus voltage measured and set values. Consequently, secondary controller is introduced to eliminate that offset by re-adjusting the terminal voltage set point, suppressing voltage fluctuations and restore voltage back to its desired value. Secondary controller comprises of two main parts: voltage and current regulators each of which work successively to regulate terminal voltages and adjust SDC output current [11], [12].

The main goal of voltage regulator is to regulate local terminal voltages by comparing its value with the average voltage collected from the neighbouring agents across the microgrid. The offset resulted from primary control is processed firstly by supressing voltage fluctuations exceeding stability and thermal limits of the converters following the ± 5% of DC voltage span. Once the fluctuations are supressed, a correction term is produced. Consequently, current regulator is applied to regulate local voltages by regulating its output current. The current regulator compares the per-unit value of converter output current by the average of the output currents collected from the neighbouring agents. Another correction term is produced. Both correction terms are used to re-adjust local terminal voltages by re-calculating a new voltage set point. Both regulators require an important communication pattern to achieve their task. Both regulators require an important communication pattern to achieve their task. Finally, tertiary controller is applied for optimal dispatch of generation based on fuel cost. Loading ratio has been taken as an objective factor for proper load sharing amongst sources and proper synchronization of incremental costs [13]-[16].

This study also introduces transmission line current control. In previous studies, tertiary controller is only aiming at cost control. However, in this research another responsibility is added to it. Adjusting terminal voltages based on controlling transmission line currents beyond thermal capacity limits of transmission lines. A third correction term is produced to adjust terminal voltage based on a tertiary control perspective. In addition, for power conversion systems, there is a crucial need to achieve different voltage levels and for control services

they offer in DC microgrids [51]. SDC is considered a fast-switching converter with overall operating efficiency of about 96%. One of the factors that has a great influence on DC microgrid stability is the point of load (POL) converters that act as a constant power load for SDC. That's why SDC is very important to solve stability issues that may result in case of constant power loads. On the other hand, there are several constraints that have to be taken into consideration. Thermal and stability limits of terminal voltages, thermal capacity of distribution lines and communication delay between several agents or converters.

6.3 Proposed cooperative control mechanism

DC networks have many merits over their AC counterparts. For instance, they have better power quality, voltage stability, less cost, less losses and higher efficiency. In addition, DC microgrids are small in scale and easy to be controlled. However, a sufficient control system is required to harvest all the fruits of these advantages. In this research a hierarchical scheme control is proposed and considered to be efficient enough to control local terminal voltages. As mentioned in previous sections, the control pattern comprises of primary, secondary and tertiary controllers. A cooperative performance between primary and secondary controllers occurs to regulate terminal voltage, eliminate voltage offset between measured and desired values and suppress voltage fluctuations. Nevertheless, tertiary controller is needed for economic dispatch control (EDC) and to reduce generating cost based on pre-defined generation cost equations. In addition, maintaining thermal capacity limits of transmission lines is needed to avoid any overloading and maintain terminal voltage stability. Fig. 1.1 depicts the whole layers of proposed hierarchical control scheme.

Primary controller as described in previous section is an adaptive droop control that is regulating bus voltages by adjusting the duty ratio of power supplies. That could be achieved by using PSO to optimize control gains that could reduce power fluctuations and balance power generation between several power sources. However, regardless its fast response in a short time scale, primary control doesn't give a high performance as it suffers from poor voltage regulations, particularly when we can't neglect line impedances. Consequently, secondary control is applied to restore voltage back to its desired value. Secondary control is divided into two parts as follow:

6.3.1 Voltage regulator

Fig. 6.1 shows how voltage regulator is used to adjust local terminal voltage suppress voltage fluctuations beyond stability limits and producing a correction term to set a new value of desired terminal voltage. According to IEEE Standards, for DC voltage regulation, a voltage span of ± 5% of microgrid reference voltage value which is about ± 20 volts is allowed. To demonstrate how voltage regulator works, lets suggest a voltage instability leading to fluctuations exceeding the stability limits. Firstly, the dead zone will suppress and eliminate voltage fluctuations. Afterwards, a correction term is then produced with the help of PI control to restore voltage back to its setpoint.

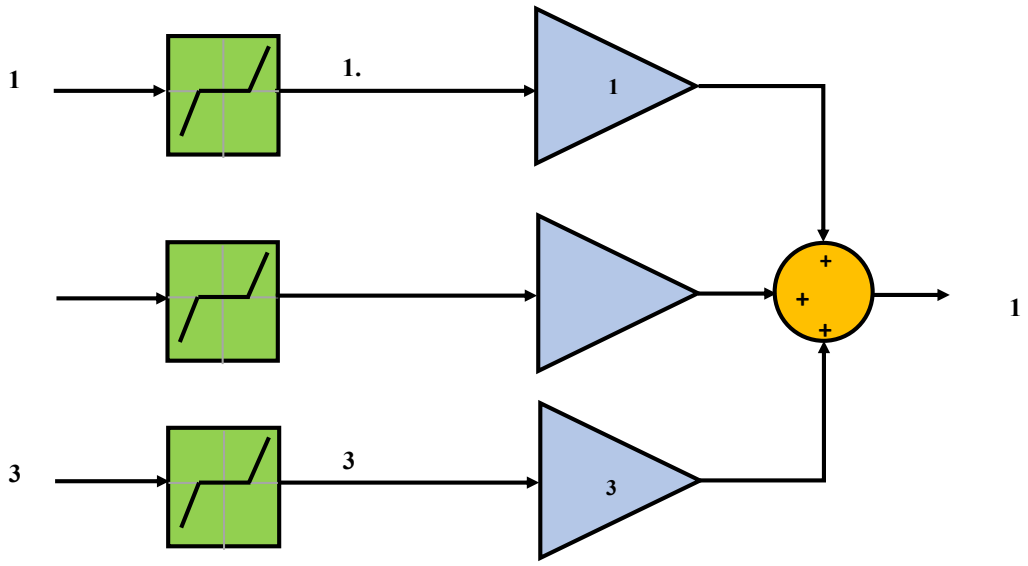

Fig. 6.1. Voltage regulator for secondary controller [18] © 2020 IEEE

Referring to the above figure, after adjusting terminal voltage within the boundaries, we multiply the resulted voltage value with a weight coefficient depending on the terminal we are controlling the voltage at. For instance, if the controlled voltage is at terminal 1, in that case its weight coefficient is set to a higher value compared to other terminals that are affecting terminal 1 voltage, in which we adjust their weight coefficient to be smaller. Likely for terminals 2 and 3, as we adjust weight coefficient of their voltage to be higher than the other neighbouring terminals. Accordingly, as shown in Fig. 6.1, since we adjust

terminal 1 voltage, C_{VB1} is set to a higher value, while C_{VB2} and C_{VB3} are set to smaller values. Same applies for terminals 2 and 3.

6.3.2 Current regulator

Current regulator is applied directly after voltage regulator. When voltage regulator finishes suppressing fluctuations, current regulator starts to regulate terminal voltage by adjusting SDC output current. That is achieved regarding the ratio of connected power source capacity to the total power generation capacity in the grid as shown in Fig. 6.2. In that context, if the generator connected to any terminal has a higher share of power, the current regulator adjusts the current output of SDC to be higher than that of the terminal that has a lower share generation output.

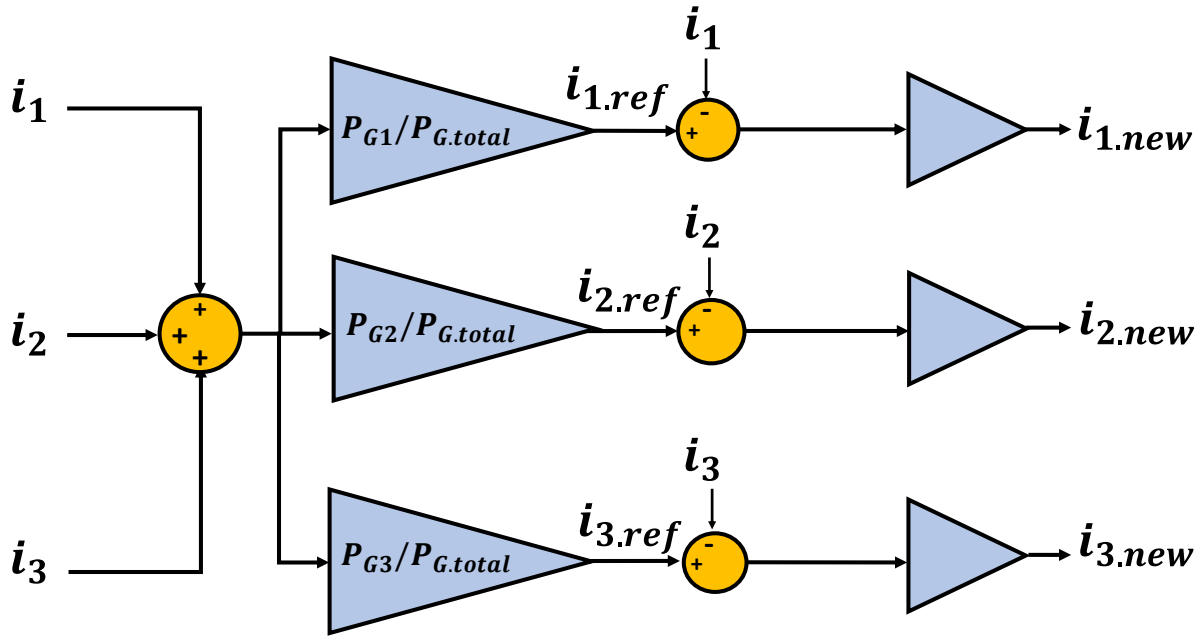

Fig. 6.2. Current regulator for secondary controller [18] © 2020 IEEE

A new reference output current value is produced per each converter. This set point is compared with the actual output, and the error is adjusted by PI controller and a correction term is produced by current regulator. The final correction term by secondary controller for terminal voltage regulation can be shown in Fig. 6.3. If voltage dead band of all terminals did not exceed pre-set accuracy, then voltage is within the limits and in such case, only maintaining converter's output current

is the main goal. However, if each of the dead band voltages exceeds the accuracy, then continuing the process of the supressing voltage fluctuations is needed.

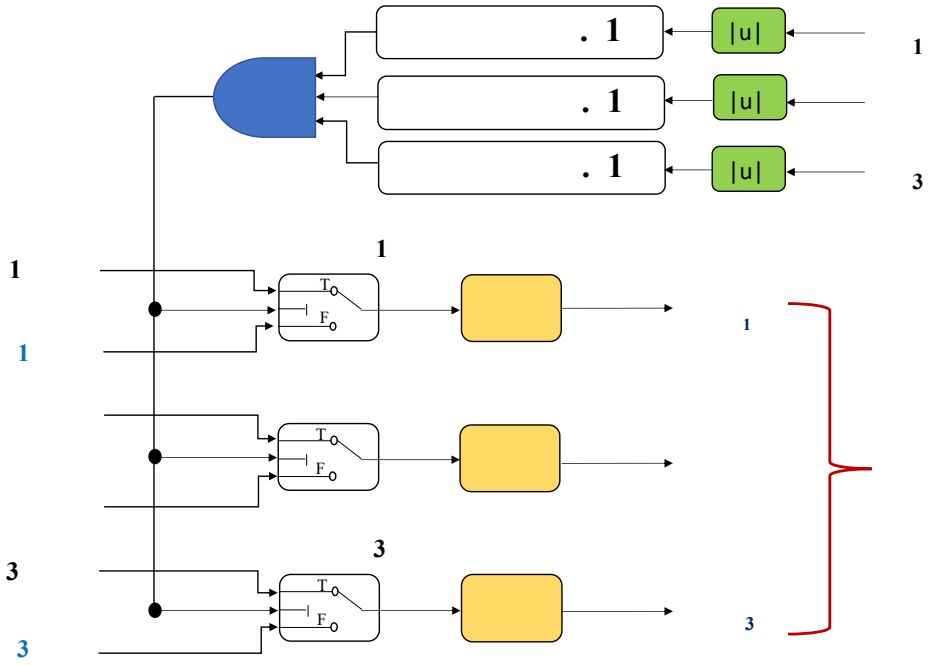

Fig. 6.3. Converter voltages secondary control correction terms [18] © 2020 IEEE

6.4 Tertiary based control mechanism

Tertiary controller is the upper control level in the hierarchy. The main goal of tertiary control is to regulate local terminal voltages and control power flow within grid terminals in an islanded mode or between different grids in a cluster form based upon optimal dispatch control and reducing generation cost. As shown in Fig. 6.4 and as demonstrated in [14], tertiary controller is used to update the reference value of local voltage according to the incremental cost of each generator. Where incremental cost is the rate of change of generation cost per power capacity of each generator. This is achieved by updating loading ratio of each converter (r_i). Generation costs are represented with 2nd order polynomials in terms of converter output current as can be shown in (59).

$$C_i(P_i) = \alpha_i + \beta_i i_i + \gamma_i i_i^2 \tag{59}$$

Incremental costs (λ_i) are then calculated accordingly. λ_i is mathematically shown in (60).

$$\lambda_i \triangleq \frac{dC_i}{dP}(P_i) = \beta_i + 2\gamma_i i_i \tag{60}$$

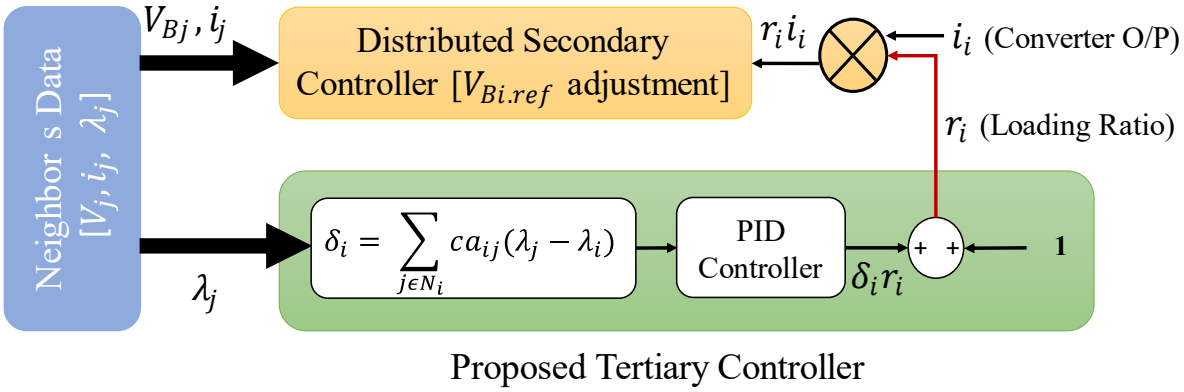

Fig. 6.4. Functionality of proposed tertiary controller [18] © 2020 IEEE

Before activating the controller, the initial value of loading ratio of each generator is considered as 1 ($r_i = 1$). However, when the controller is activated, the controller calculates the incremental cost of each generator and compare it with the average neighbouring data. Accordingly, the loading ratio of every converter is calculated according to (61):

$$\delta_i = \sum_{j \epsilon N_i} ca_{ij}(\lambda_j - \lambda_i) \tag{61}$$

Any mismatch would be processed through PI controller to produce a correction term based on tertiary controller and generation cost rate of change to reduce the offset. The coefficient c is a design parameter that adjusts the convergence speed, while a_{ij} represents the communication weight from node j to node i. Fig. 6.5 shows the tertiary controller model and the correction term according to updated loading ratio respectively. On the other hand, another task is added to tertiary controller, which is to maintain transmission line currents within thermal capacity and overcome overloading conditions. For instance, in the simplified 3 bus DC microgrid model, if we have an overloading in one transmission line, while the other transmission line is in normal case with no overloading. In such case, we reduce voltage at the sending end and increase voltage at the receiving end to absorb the overload. However, in case of high severity where both lines are

overloaded. In such case, we have to check the priorities and which line situation is more prone to danger situation as shown in Fig. 6.5. For instance, if none of distribution lines is overloaded, just tertiary control signal is based on adjusting generation cost. If each of line *i* or *j* is overloaded, then tertiary control signal is adjusted to reduce voltage at sending end and increase voltage at receiving end to absorb that overload. However, if both lines are overloaded, then priorities would be checked to work on the most severe case.

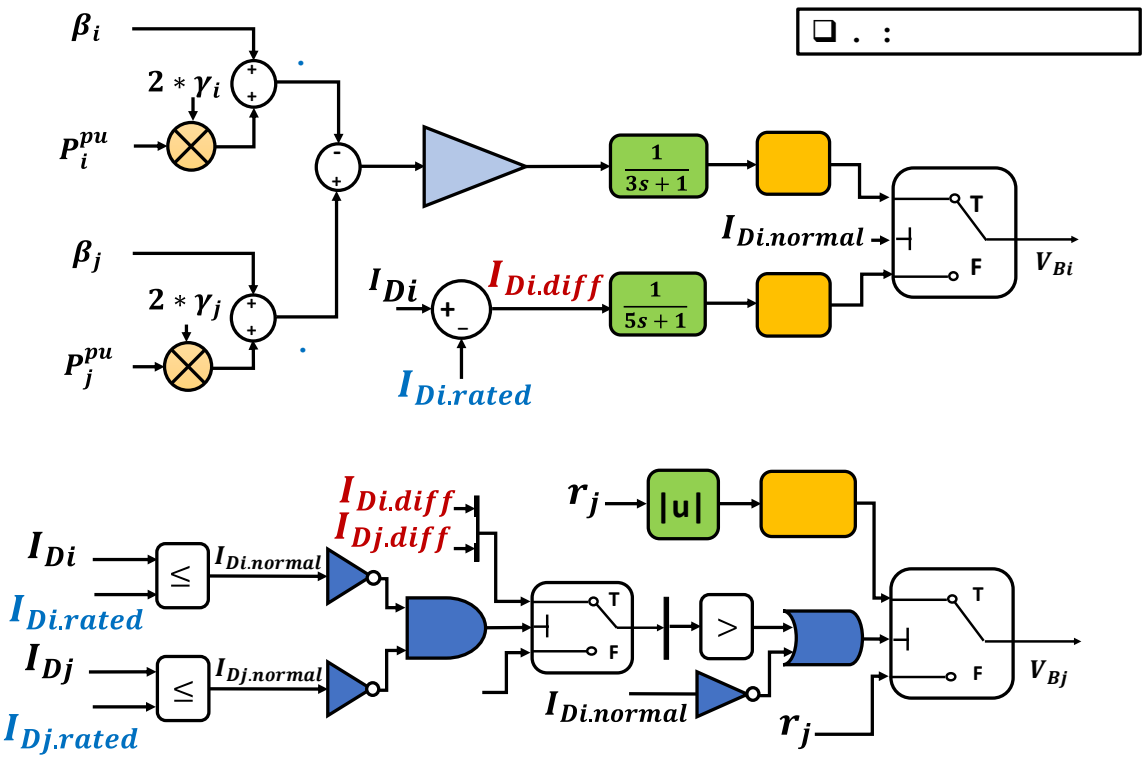

Fig. 6.5. Tertiary controller [18] © 2020 IEEE

Ultimately, the local voltage has been updated based on the hierarchical control method. Three correction terms have been added to determine the new set point to regulate power flow between converters as shown in (62). The new set point will be compared with the local measured value of terminal voltage again and go through the same process.

$$V_{Bi.\,ref} = V_{Bi.\,ref_0} - r_i\, i_i + \delta_{VBi} \qquad (62)$$

Fig. 6.6 illustrate the new reference voltage value. It is calculated by considering both secondary and tertiary controllers' correction terms.

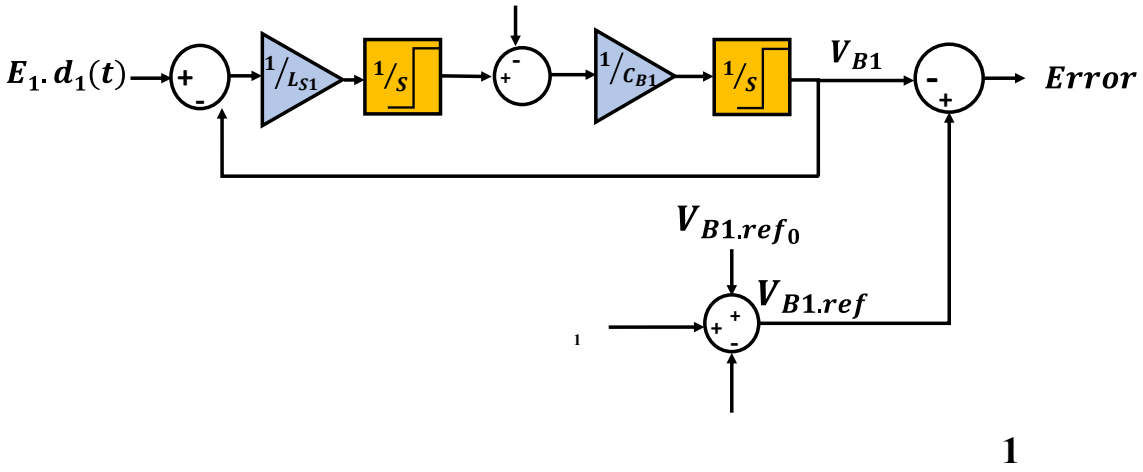

Fig. 6.6. Modified correction term [18] © 2020 IEEE

Where $V_{Bi.\ ref}$ is the new local voltage setpoint, $V_{Bi.\ ref_0}$ is the global voltage setpoint all over the microgrid, δ_{VBi} is the secondary control correction term and finally, $r_i\ i_i$ is the loading ratio correction term based on tertiary controller.

6.5 Simulation results and discussion

Simulations were carried out using simplified 3-bus DC microgrid model shown in Fig. 3.3. This model mainly comprises of two distributed generators and two load systems connected at different terminals as described in chapter 3. Generation and incremental costs are given as follows in (63) and (64) respectively.

$$\begin{aligned} C_1 i_1 &= 0.2 + 0.1\ i_1 + 0.08\ i_1^2 \\ C_2 i_2 &= 0.4 + 0.25\ i_2 + 0.19\ i_2^2 \\ C_3 i_3 &= 0.2 + 0.12\ i_3 + 0.1\ i_3^2 \end{aligned} \tag{63}$$

$$\lambda_{i1} = 0.1 + 0.16\ i_1$$

$$\lambda_{i2} = 0.25 + 0.38\, i_2 \tag{64}$$

$$\lambda_{i3} = 0.12 + 0.2\, i_3$$

When the controllers are activated, primary and secondary controllers are implemented to regulate terminal voltages, control power flow and balance power generation. At 35 sec. load increases at bus 3 to assess how the hierarchical control mechanism would act with voltage fluctuations. From Fig. 6.7, it seems that both secondary and tertiary controllers tried to suppress voltage fluctuations by changing voltage operating point. The figure shows that both secondary and tertiary controllers tried to raise bus 1 voltage by increasing its generation output, to maintain voltage drop level at bus 3 and to follow thermal upper and lower limits. However, at bus 2, secondary controller decreased local voltage to stick to the boundaries of thermal limits.

On the other hand, tertiary controller's priority is to reduce generation cost. In that context, at bus 2 we can see how voltage exceeds thermal and stability limits, showing an obvious change in setting local voltage values based on generation cost. For that reason, the rate of change of tertiary controller voltage values was a bit slow to follow as it prioritized the rate of change in marginal or incremental cost of generation than thermal limits focused by secondary controller.

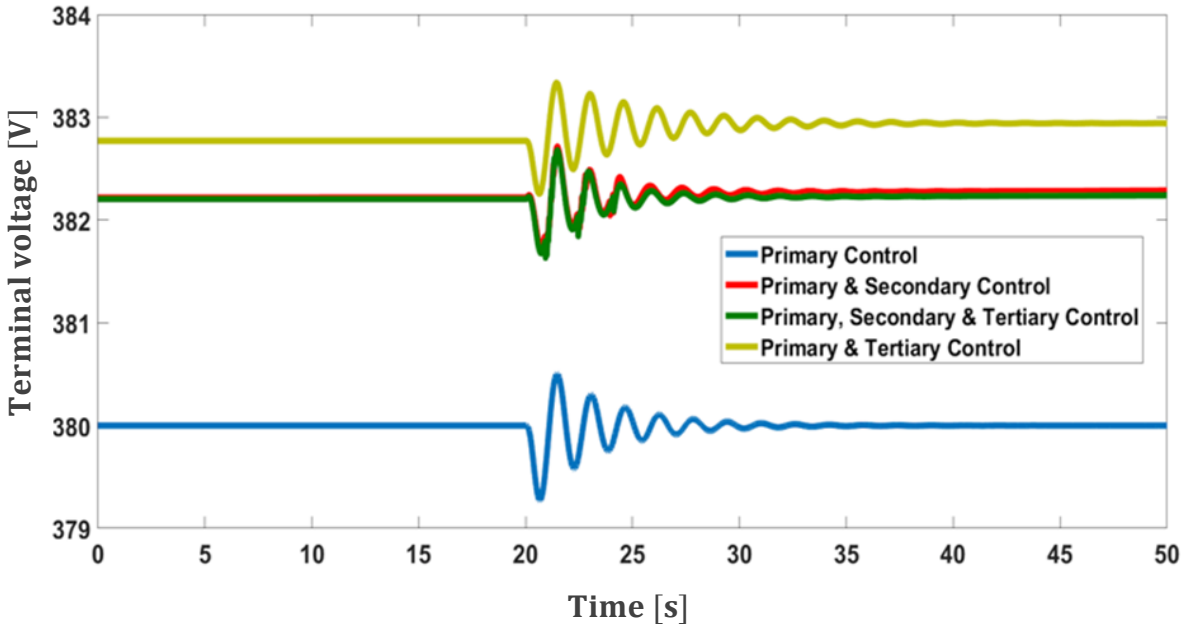

(a)

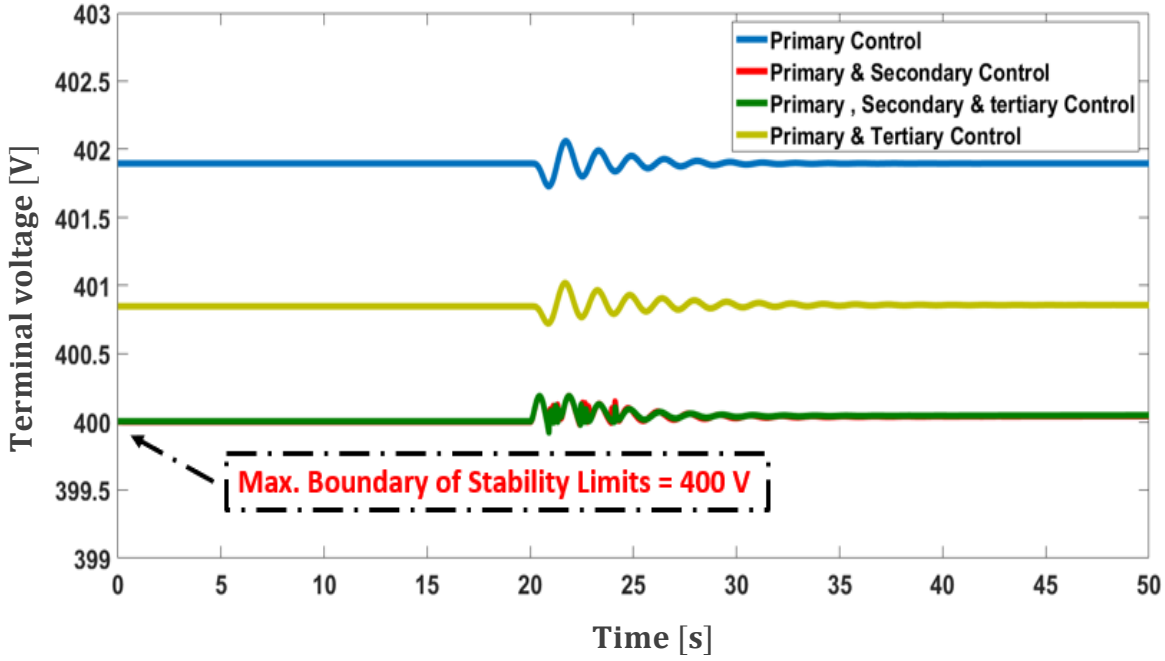

(b)

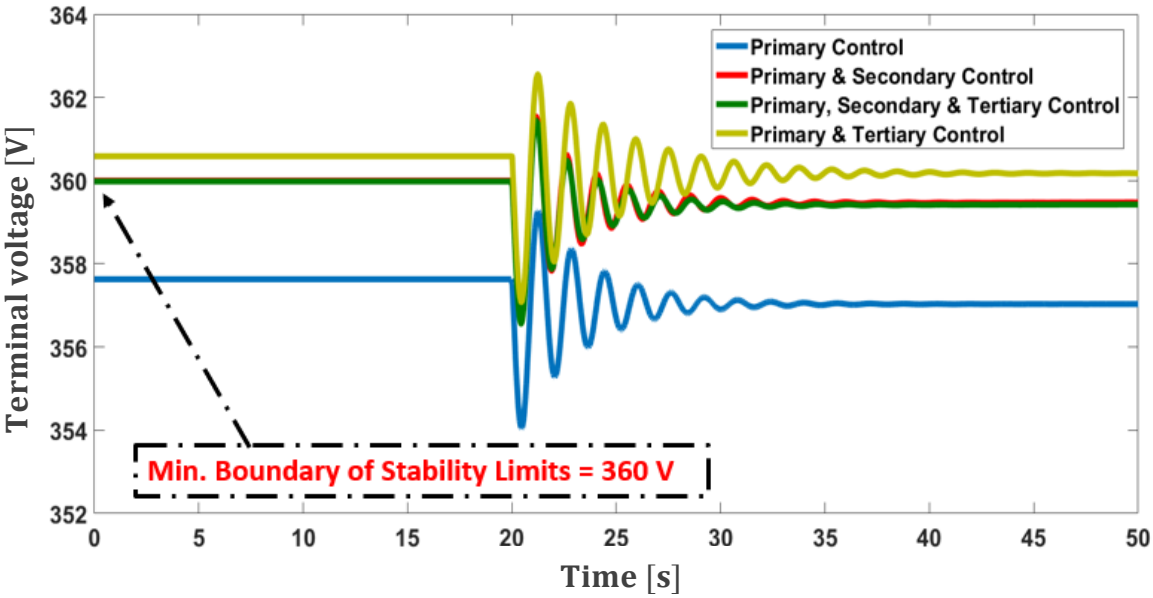

(c)

Fig. 6.7 (a) V_{B1}, (b) V_{B2} and (c) V_{B3} with proposed hierarchical control [18] © 2020 IEEE

Consequently, Fig. 6.8 shows the results if only tertiary controller is applied. It is found that, in such case, to obtain and equal share of minimum generation cost, voltage violation of upper and lower thermal limits occurs in VB_2 that exceeds upper thermal limit and VB_3 that falls below lower thermal limit.

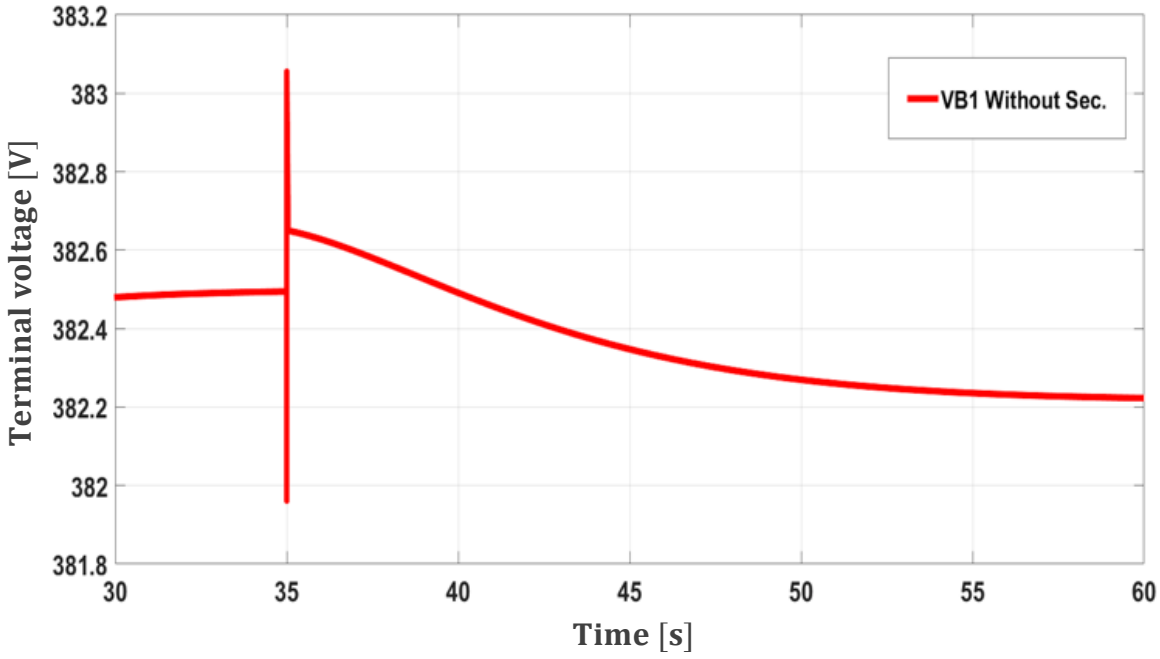
VB1 Without Sec.
Terminal voltage [V]
Time [s]
383.2
383
382.8
382.6
382.4
382.2
382
381.8
30
35
40
45
50
55
60

(a)

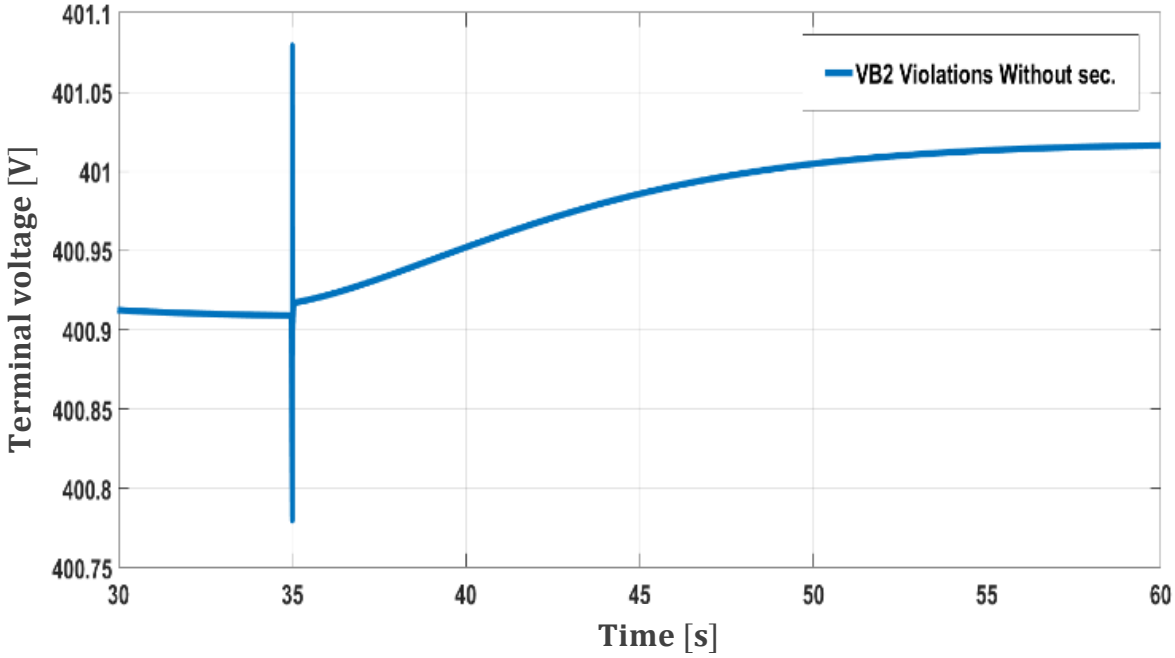
VB2 Violations Without sec.
Terminal voltage [V]
Time [s]
401.1
401.05
401
400.95
400.9
400.85
400.8
400.75
30
35
40
45
50
55
60

(b)

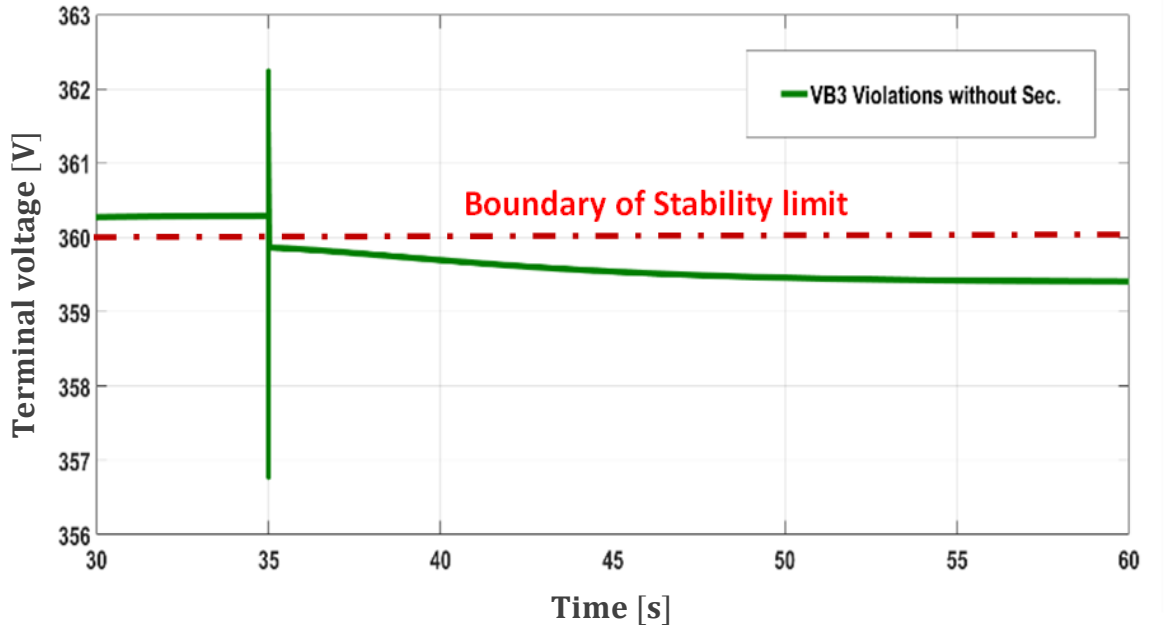

(c)

Fig. 6.8 (a) V_{B1}, (b) V_{B2} and (c) V_{B3} without applying secondary controller [18] © 2020 IEEE

Fig. 6.9. shows the ability of tertiary controller to reduce generation cost when compared with primary control only case. Moreover, Fig. 6.10 show how if secondary controller is applied, the incremental costs of both generators did not meet as secondary controller prioritizes abiding by voltage stability limits than generation cost. However, if secondary controller is eliminated, minimum generation cost is achieved.

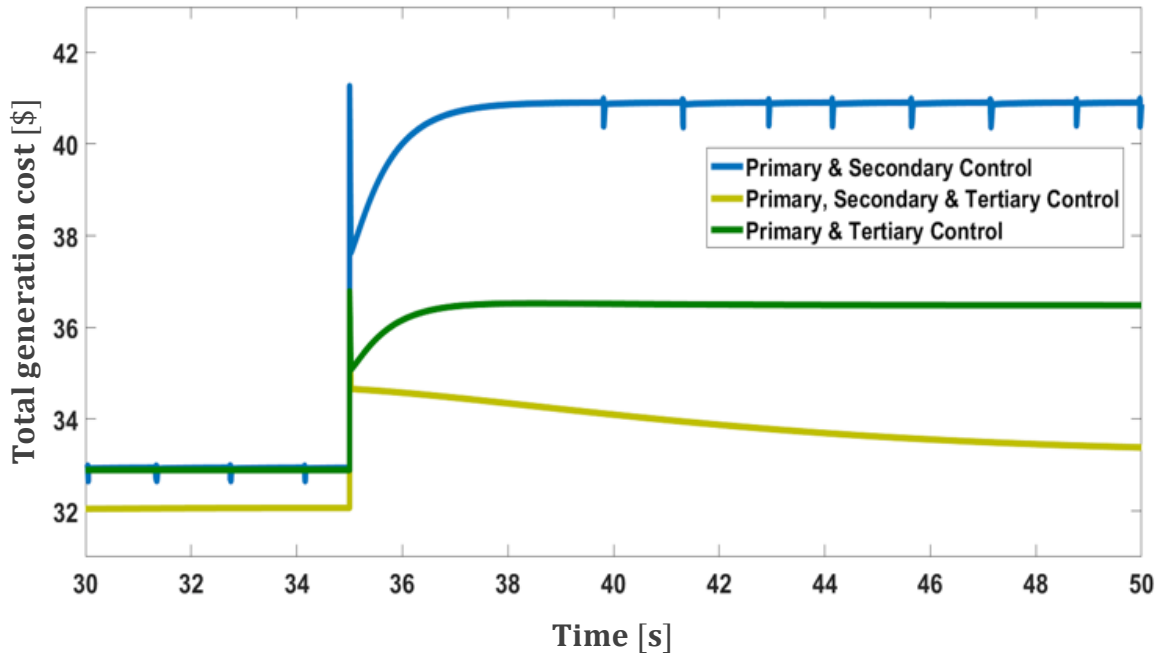

Fig. 6.9. Total generation cost [18] © 2020 IEEE

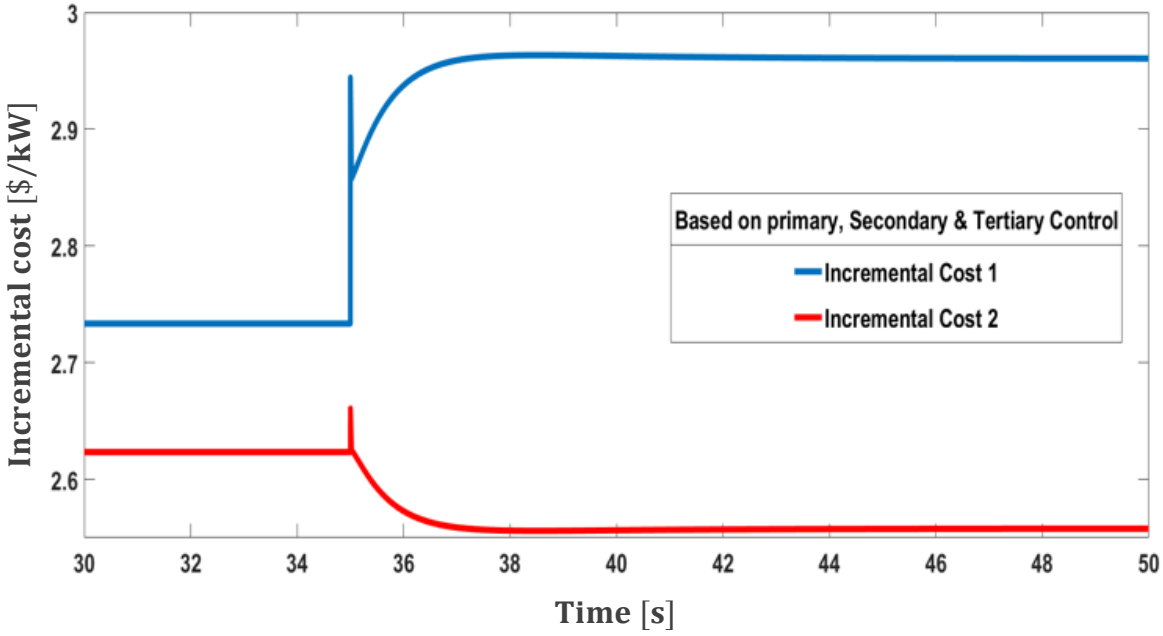

(a)

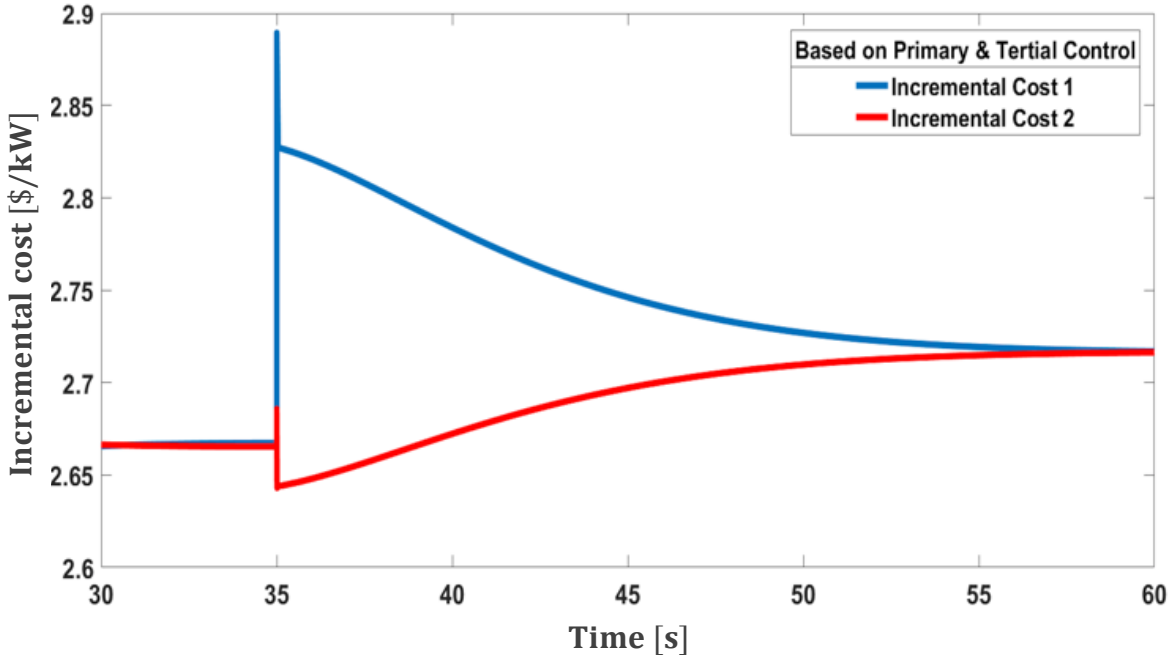

(b)

Fig. 6.10 Incremental cost of both generators (a) with secondary controller and (b) without secondary controller [18] © 2020 IEEE

Ultimately, the transmission line currents with and without applying tertiary overloading control mechanism are shown in Fig. 6.11(a) and (b). We can easily recognize that, in case of primary controller only, transmission line 2 is overloaded. However, after applying tertiary controller, new set points were set for terminal voltages to eliminate overloading and maintain normal condition.

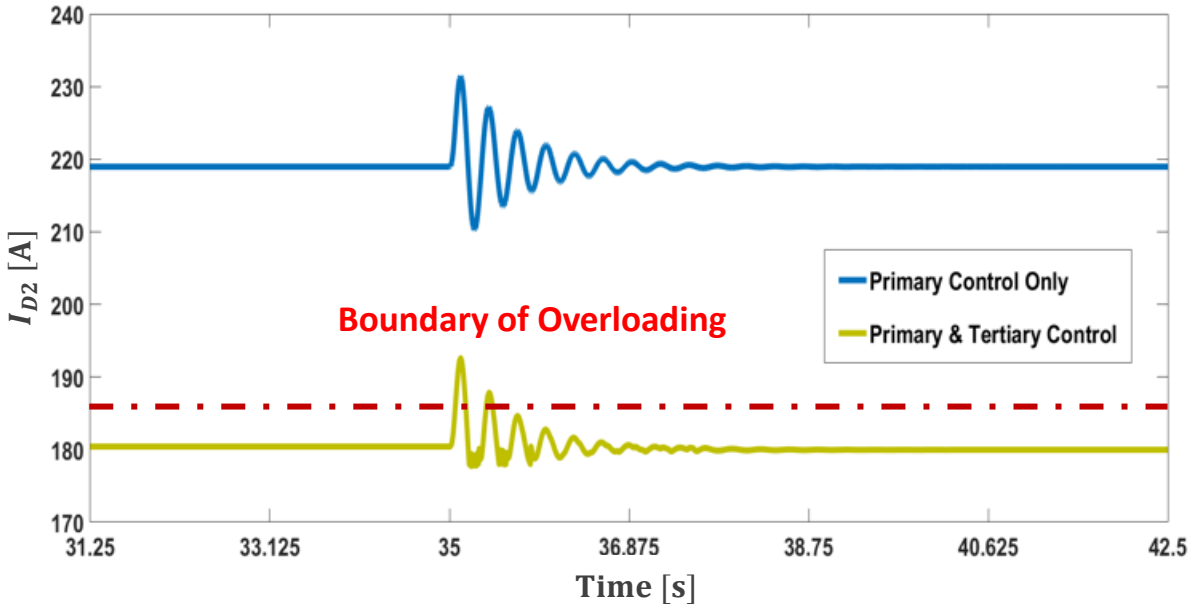

(a)

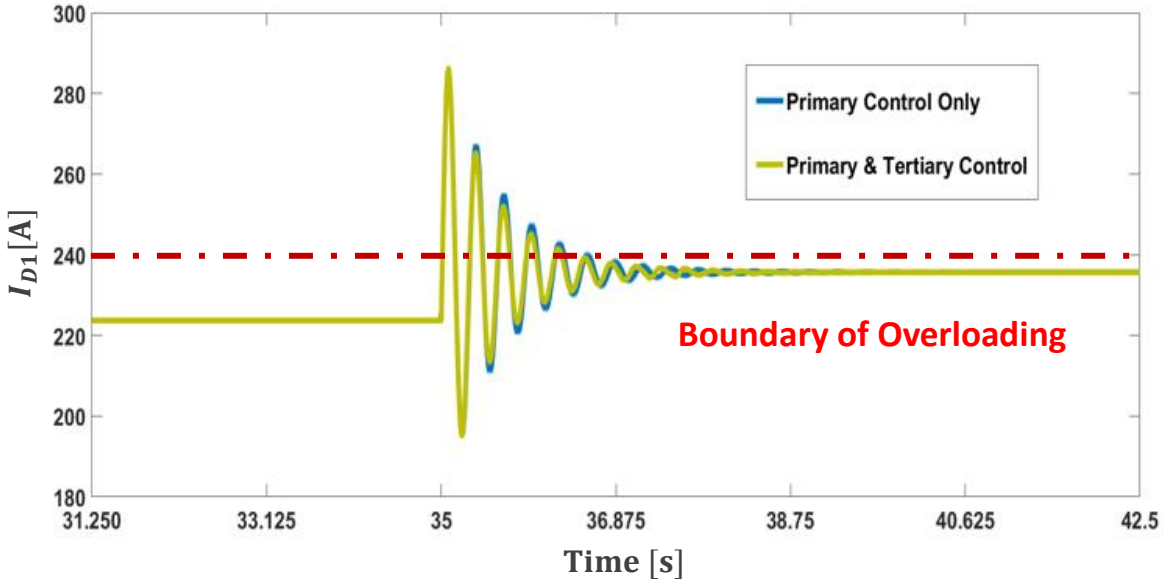

(b)

Nevertheless, Incremental cost as shown in Fig. 6.11(c) still a disadvantage as incremental cost is not improved and must be enhanced in the future even without applying secondary controller.

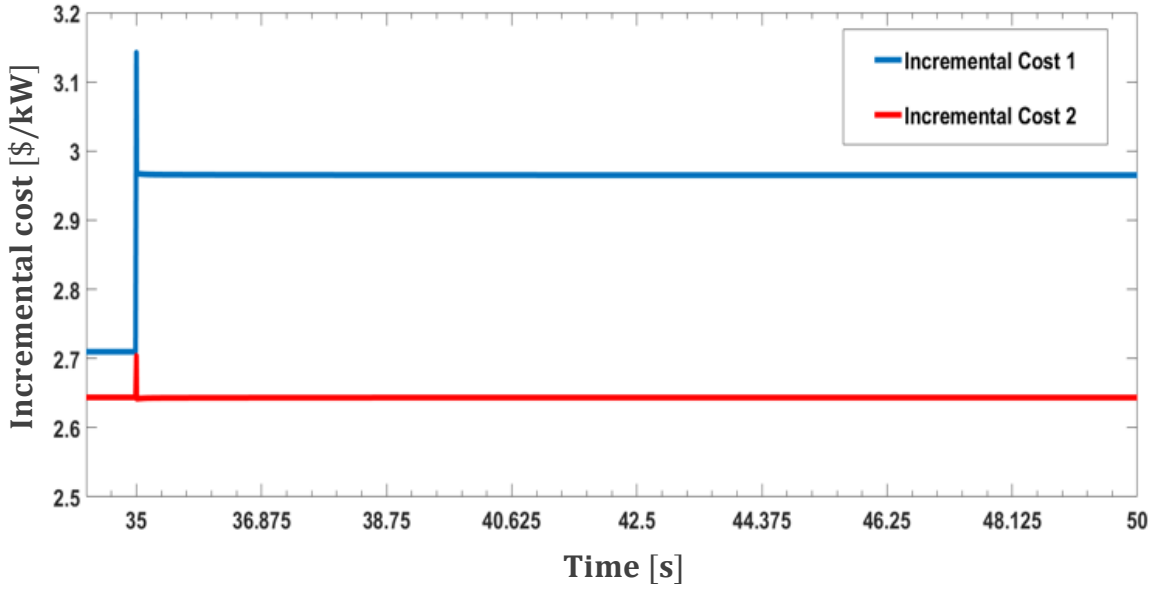

(c)

Fig. 6.11 (a) Transmission line 2 current , (b) Transmission line 1 current and (c) Incremental Cost [18] © 2020 IEEE

On the other hand, terminal voltages can be shown in Fig. 6.12.

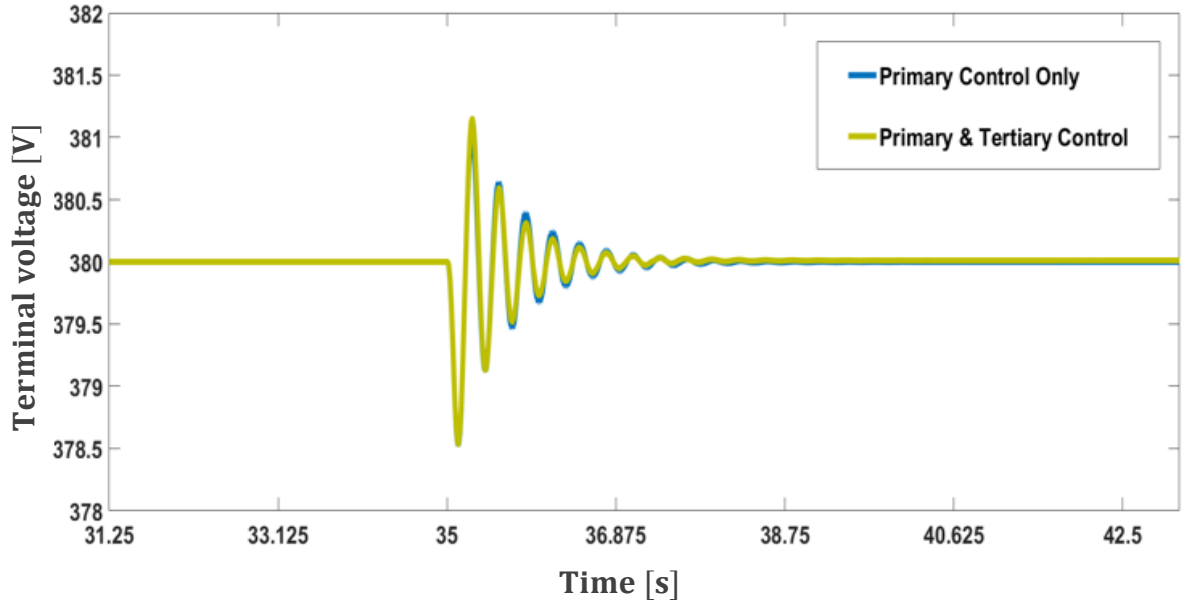

(a)

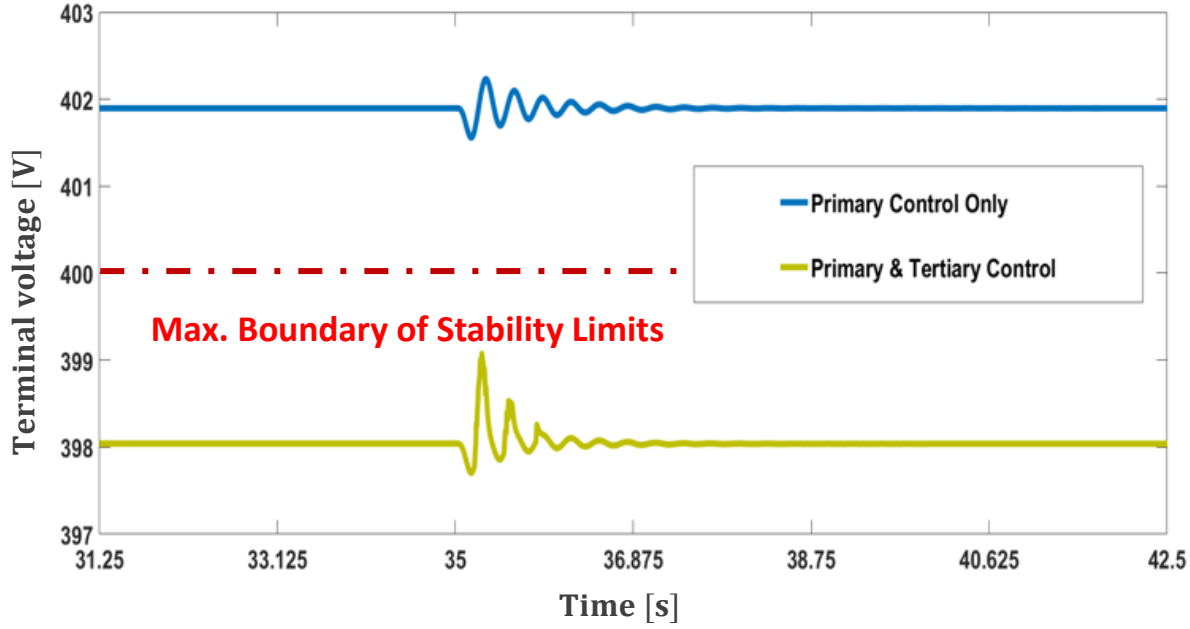

(b)

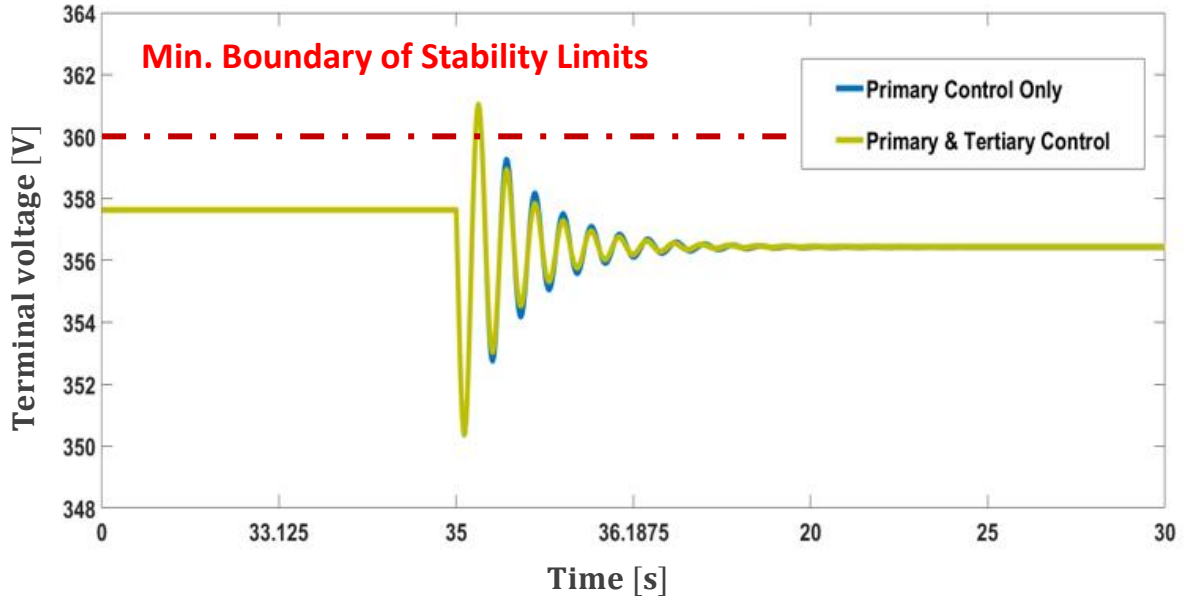

(c)

Fig. 6.12 (a) V_{B1}, (b) V_{B2} and (c) V_{B3} with transmission lines' currents control strategy [18]

In Fig. 6.12, we can recognize that even after applying transmission line current control, and even with no secondary controller, max. and min. voltage boundaries are not violated or exceeded except at terminal 3.

6.6 Summary

This chapter discussed the proposed hierarchical control strategy and its effect on regulating terminal voltages. Since the primary control level is not enough to restore the voltage back within the stability boundary, secondary and tertiary controllers are applied to eliminate voltage fluctuations beyond the stability limits and reduce generation cost respectively. That is done by adjusting the reference values for local terminal voltages based on correction terms obtained from secondary and tertiary controllers. Both control levels require strong decentralized communication between neighbouring agents to exchange data such as terminal voltages, converters output currents and incremental costs. This chapter also discussed how secondary controller prioritizes voltage stability limits, while tertiary controller has a great tension in reducing generation cost, sometimes as a trade-off voltage stability. Ultimately, the impact of transmission line current tertiary-based control is discussed and its effect on both line currents and terminal voltages in all cases with and without secondary controller. As a further step, an effort would be exerted to enlarge network scale and build a cluster form of several grids to assess the control effectiveness on factual basis.

CHAPTER 7

CONCLUSION AND FUTURE WORK

7.1 Conclusion

In this work, the utmost importance is to present a new methodology for DC microgrid online voltage control using PSO with random particles search. Eigenvalue analysis was performed to precisely describe grid characteristics. The performance was validated and improved using parallel global and local searches seeking optimum solutions when compared with the control technique applying only normal search conditions. The validation of the control scheme was achieved by simulating the model in different loading conditions. Control gains are updated based on those load variations. Even with one particle conducting normal search, control performance was improved. A comparison has been also made on how optimum load gains promote network stability in various loading conditions and how that is reflected on local terminal voltages. Ultimately, this work presents a simplified 3-bus dc microgrid model. However, in future studies, larger scale dc microgrid model with taking a chopper for load side into consideration would be utilized to represent a factual and more realistic control scheme. Moreover, this study is mainly designated to primary controller only.

On the other hand, secondary and tertiary controllers are spotted on in the second section of this thesis. Cooperative decentralized control is introduced as secondary control level. It is mainly divided into two main parts. Firstly, voltage regulator that is applied to sufficiently suppress voltage fluctuation and offsets - caused by primary controller - within the stability limits using dead band zone to eliminate any superseding voltage fluctuation. Successively, current regulator is used to maintain converters output currents based on share of generators output power connected to it. Ultimately, the utmost control level called tertiary controller is implemented for optimal dispatch of power generators to combine between both voltage stability and the lowest possible generation costs. As a result, we can notice, how tertiary controllers produce correction terms to re-set

new values of voltage references based on the cheapest way to generate power.

7.2 Future Work

Although the research objectives have been met by the proposed strategy, yet more work has to be done to improve system dynamic performance in the future work even under severe loading conditions. That can be achieved as follows:

1. A bigger model of DC microgrid with multiple terminals has to be considered to verify the validity of the control model on a real case of study.

2. Inserting renewables as solar and wind and energy storage systems as batteries in the model to add more non-linear items in the model to emulate a real case of study and how these items might affect grid stability.

3. Variable and continuously changing loads must be taken into consideration, which refers more to reality and adding more factual verification to network.

LIST OF PUBLICATIONS

M ’

Journal papers

[Ref. 1] Salim N.B., **Aboelsoud H.,** Tsuji T., Oyama T., Uchida K. “Load frequency control of Two-area network using renewable energy resources and battery energy storage system” (2017), *Journal of Electrical Systems*, 13 (2), pp. 348-365.

Proceedings

[Ref. 2] **Hossam Aboelsoud**. Takao Tsuji, “Transient Stability Control Using HVDC in Egyptian Power Grid”, *ICEE 2016*, 3-7 July 2016, Okinawa, Japan.

[Ref. 3] **Hossam Aboelsoud**. Takao Tsuji, “Transient Stability Analysis with Wind Power Integrated HVDC Transmission System in the Egyptian Grid”, *ICEE 2017,* 3-7 July 2017, Weihai, China.

[Ref. 4] **Hossam Aboelsoud**. Takao Tsuji, “Transient Stability Enhancement by Active/Reactive Power Control of Hybrid HVDC in the Egyptian Power Grid with Wind Power Integration”, *Solar and Wind Integration Workshop,* 22-27 October 2017, Berlin, Germany.

[Ref. 5] **Hossam Aboelsoud**. Takao Tsuji, “Transient Stability Management Using Current Source Based HVDC Transmission Systems for Active/Reactive Power Control”, *ICEE 2018*, 24-28 June, 2018, Seoul, South Korea.

PhD Degree

Journal papers

[Ref. 7] **Hossam Aboelsoud**. Naoya Ikeda, Takao Tsuji, Masahide Hojo, Naotaka Okada, "Online Voltage Control of DC Microgrids with Different Loading Conditions Using Particle Swarm Optimization," *IEEJ Transactions on Electrical and Electronic Engineering,* https://doi.org/10.1002/tee.23567, 07 March 2022.

Proceedings

[Ref. 7] **Hossam Aboelsoud**. Takao Tsuji, "Cooperative Decentralized Tertiary Based Control of DC Microgrid with Renewable Distributed Generation," *2019 IEEE Third International Conference on DC Microgrids (ICDCM)*, 2019, pp. 1-6, doi: 10.1109/ICDCM45535.2019.9232871.

[Ref. 8] **Hossam Aboelsoud**. Takao Tsuji, "Cooperative Decentralized Hierarchical Based Voltage Control of DC Microgrids," *2019, 29th Australasian Universities Power Engineering Conference (AUPEC)*, 2019, pp. 1-8, doi: 10.1109/AUPEC48547.2019.211839.

REFERENCES

[1] M. Kalantar and S. M. Mousavi G.: "Dynamic behavior of a stand-alone hybrid power generation system of wind turbine, microturbine, solar array and battery storage", Elsevier, Applied Energy, vol. 87, issue 10, pp.3051- 3064 (pub. 2010).

[2] H. Li and Z. Chen: "Overview of different wind generator systems and their comparisons", IET Renewable Power Generation, vol. 2, no. 2, pp. 123-138, doi: 10.1049/iet-rpg:20070044 (pub. 2008).

[3] D. Chen and L. Xu: "DC microgrid with variable generations and energy storage", IET Conference on Renewable Power Generation, Edinburgh, pp. 1-6, doi: 10.1049/cp.2011.0167 (pub. 2011).

[4] X. Li, D. Hui and X. Lai: "Battery Energy Storage Station (BESS)-Based Smoothing Control of Photovoltaic (PV) and Wind Power Generation Fluctuations", IEEE Transactions on Sustainable Energy, vol. 4, no. 2, pp. 464-473, doi: 10.1109/TSTE.2013.2247428 (pub. 2013).

[5] J.Mitra and M. Vallem: "Determination of storage required to meet reliability guarantees on island-capable microgrids with intermittent sources", IEEE PES T&D Conference and Exposition, Chicago, IL, pp. 1-1, doi: 10.1109/TDC.2014.6863410 (pub.2014).

[6] N. Hatziargyriou, H. Asano, R. Iravani and C. Marnay: "Microgrids", in IEEE Power and Energy Magazine, vol. 5, no. 4, pp. 78-94, doi: 10.1109/MPAE.2007.376583 (pub.2007).

[7] S. Moayedi and A. Davoudi: "Distributed cooperative load sharing in parallel DC-DC converters", Proc. 29th IEEE Appl. Power Electron. Conf. Expo., pp. 2907–2912 (pub. 2014).

[8] D. Chen and L. Xu: "Autonomous DC Voltage Control of a DC Microgrid with Multiple Slack Terminals", IEEE Transactions on Power Systems, vol. 27, no. 4, pp. 1897-1905, doi: 10.1109/TPWRS.2012.2189441 (pub. 2012).

[9] Yunjie Gu, Xin Xiang, Wuhua Li and Xiangning He: "Mode Adaptive Decentralized Control for Renewable DC Microgrid with Enhanced Reliability and Flexibility", IEEE Transactions on Power Electronics, vol. 29, No. 9, DOI: 10.1109/TPEL.2013.2294204 (pub. 2014).

[10] V. Nasirian, A. Davoudi, and F. L. Lewis: “Distributed adaptive droop control for DC Microgrids”, Proc. 29th IEEE Appl. Power Electron. Conf. Expo., pp. 1147– 1152 (pub. 2014).

[11] Vahidreza Nasirian, Seyedali Moayedi, Ali Davoudi and Frank L. Lewis: “Distributed Cooperative Control of DC Microgrids”, IEEE Transactions on Power Electronics, Vol. 30, No. 4, DOI 10.1109/TPEL.2014.2324579 (pub. 2015).

[12] V. Nasirian, Y. Karimi, A. Davoudi, M. R. Zolghadri, M. Ahmadian, and S. Moayedi: “Dynamic model development and variable switching- frequency control for DCVM Cu’k converters in PFC applications”, IEEE Transactions, Ind. Appl., vol. 49, no. 6, pp. 2636– 2650 (pub. 2013).

[13] Tomislav Dragicevic, Dan Wu, Qobad Shafiee, and Lexuan Meng: “Distributed and Decentralized Control Architectures for Converter-Interfaced Microgrids”, Chinese Journal of Electrical Engineering, Vol.3, No.2, pp. 41- 52, DOI: 10.23919/CJEE.2017.8048411 (pub. 2017).

[14] Vahidreza Nasirian, Frank L. Lewis and Ali Davoudi: “Distributed Optimal Dispatch for DC Distribution Networks”, IEEE First International Conference on DC Microgrids (ICDCM), Atlanta, GA, USA, DOI: 10.1109/ICDCM.2015.7152017 (pub. 2015).

[15] Lexuan Meng, Tomislav Dragicevic, Juan Vasquez, Josep Guerrero and Eleonora Riva Sanseverino: “Hierarchical Control with Virtual Resistance Optimization for Efficiency Enhancement and State- of Charge Balancing in DC Microgrids”, IEEE First International Conference on DC Microgrids (ICDCM), Atlanta, GA, USA, DOI:10.1109/ICDCM.2015.7152000 (pub. 2015).

[16] Seyedali Moayedi and Ali Davoudi: “Distributed Tertiary Control of DC Microgrid Clusters”, IEEE Transactions on Power Electronics, Vol. 31, Issue: 2, pp. 1717 – 1733, DOI: 10.1109/TPEL.2015.2424672 (pub. 2016).

[17] H. A. E. Elhassaneen and T. Tsuji: “Cooperative Decentralized Tertiary Based Control of DC Microgrid with Renewable Distributed Generation”, IEEE Third International Conference on DC Microgrids (ICDCM), Matsue, Japan, pp. 1-6, doi: 10.1109/ICDCM45535.2019.9232871 (pub. 2020) © 2011 IEEE.

[18] H. Aboelsoud and T. Tsuji: “Cooperative Decentralized Hierarchical Based Voltage Control of DC Microgrids”, 29th Australasian Universities Power Engineering Conference (AUPEC), Nadi, Fiji, pp. 1-8, doi: 10.1109/AUPEC48547.2019.211839 (pub. 2020) © 2011 IEEE.

[19] Y. Han, X. Ning, P. Yang and L. Xu: “Review of Power Sharing, Voltage Restoration and Stabilization Techniques in Hierarchical Controlled DC Microgrids”, IEEE Access, vol. 7, pp. 149202-149223, doi: 10.1109/ACCESS.2019.2946706 (pub. 2019).

[20] M. Juneja and S. K. Nagar: “Particle swarm optimization algorithm and its parameters: A review”, International Conference on Control, Computing, Communication and Materials (ICCCCM), Allahbad, pp. 1-5, doi: 10.1109/ICCCCM.2016.7918233 (pub. 2016).

[21] M. A. Awadallah and B. Venkatesh: “Bacterial Foraging Algorithm Guided by Particle Swarm Optimization for Parameter Identification of Photovoltaic Modules”, Canadian Journal of Electrical and Computer Engineering, vol. 39, no. 2, pp. 150-157, doi: 10.1109/CJECE.2016.2519763, (pub. 2016).

[22] T. S. Babu, J. P. Ram, T. Dragičević, M. Miyatake, F. Blaabjerg and N. Rajasekar: “Particle Swarm Optimization Based Solar PV Array Reconfiguration of the Maximum Power Extraction Under Partial Shading Conditions”, IEEE Transactions on Sustainable Energy, vol. 9, no. 1, pp. 74-85, doi: 10.1109/TSTE.2017.2714905, (pub. 2018).

[23] H. Li, D. Yang, W. Su, J. Lü and X. Yu: “An Overall Distribution Particle Swarm Optimization MPPT Algorithm for Photovoltaic System Under Partial Shading”, IEEE Transactions on Industrial Electronics, vol. 66, no. 1, pp. 265-275, doi: 10.1109/TIE.2018.2829668 (pub. 2019).

[24] M. Kermadi, Z. Salam, J. Ahmed and E. M. Berkouk: “An Effective Hybrid Maximum Power Point Tracker of Photovoltaic Arrays for Complex Partial Shading Conditions”, IEEE Transactions on Industrial Electronics, vol. 66, no. 9, pp. 6990-7000, doi: 10.1109/TIE.2018.2877202 (pub. 2019).

[25] K. Hu, S. Cao, W. Li and F. Zhu: “An Improved Particle Swarm Optimization Algorithm Suitable for Photovoltaic Power Tracking Under Partial Shading Conditions”, in IEEE Access, vol. 7, pp. 143217-143232, doi: 10.1109/ACCESS.2019.2944964 (pub. 2019).

[26] F. Cingoz, A. Elrayyah and Y. Sozer: “Optimized Settings of Droop Parameters Using Stochastic Load Modeling for Effective DC Microgrids Operation”, IEEE Transactions on Industry Applications, vol. 53, no. 2, pp. 1358-1371, doi: 10.1109/TIA.2016.2633538 (pub. 2017).

[27] M. N. Hussain and V. Agarwal: “Optimal Placement of Constant Power Loads at Different Buses of a DC Microgrid Ensuring Maximum Stability Margins”, IEEE Journal of Emerging and Selected Topics in Power Electronics, doi: 10.1109/JESTPE.2019.2960882 (pub. 2019).

[28] D. Dabhi and K. Pandya: “Enhanced Velocity Differential Evolutionary Particle Swarm Optimization for Optimal Scheduling of a Distributed Energy Resources with Uncertain Scenarios”, IEEE Access, vol. 8, pp. 27001-27017, doi: 10.1109/ACCESS.2020.2970236 (pub. 2020).

[29] C. D. Rodríguez-Gallegos et al.: “A Siting and Sizing Optimization Approach for PV–Battery–Diesel Hybrid Systems”, IEEE Transactions on Industry Applications, vol. 54, no. 3, pp. 2637-2645, doi: 10.1109/TIA.2017.2787680 (pub. 2018).

[30] P. Wang, W. Wang and D. Xu: “Optimal Sizing of Distributed Generations in DC Microgrids with Comprehensive Consideration of System Operation Modes and Operation Targets”, IEEE Access, vol. 6, pp. 31129-31140, doi: 10.1109/ACCESS.2018.2842119 (pub. 2018).

[31] K. Dezelak, P. Bracinik, M. Höger and A. Otcenasova: “Comparison between the particle swarm optimisation and differential evolution approaches for the optimal proportional–integral controllers design during photovoltaic power plants modelling”, IET Renewable Power Generation, vol. 10, no. 4, pp. 522-530, doi: 10.1049/iet-rpg.2015.0108 (pub. 2016).

[32] N. A. Khan, G. A. S. Sidhu and F. Gao: “Optimizing Combined Emission Economic Dispatch for Solar Integrated Power Systems”, IEEE Access, vol. 4, pp. 3340-3348, doi: 10.1109/ACCESS.2016.2587665 (pub. 2016).

[33] https://www.solar.com/learn/what-is-net-energy-metering

[34] https://vethon-solar-pvt-ltd.business.site

[35] https://energytracker.asia/potential-of-renewable-energy-in-japan/

[36] https://www.isep.or.jp/en/1075/

[37] Alexis Kwasinski and Chimaobi N. Onwuchekwa: “Dynamic Behavior and Stabilization of DC Microgrids with Instantaneous Constant Power Loads”, IEEE Transactions on Power Electronics, vol. 26, No. 3, DOI:10.1109/TPEL.2010.2091285 (pub. 2011).

[38] A. Emadi, A. Khaligh, C. H. Rivetta and G. A. Williamson: “Constant power loads and negative impedance instability in automotive systems: definition, modeling, stability, and control of power electronic converters and motor drives”, IEEE Transactions on Vehicular Technology, vol. 55, no. 4, pp. 1112-1125, doi: 10.1109/TVT.2006.877483 (pub. 2006).

[39] AL-Nussairi, M.K.; Bayindir, R.; Padmanaban, S.; Mihet-Popa, L.; Siano, P.: “Constant Power Loads (CPL) with Microgrids: Problem Definition, Stability Analysis and

Compensation Techniques", in Energies, 10, 1656; https://doi.org/10.3390/en10101656 1656 (pub. 2017).

[40] https://en.wikipedia.org/wiki/Artificial_intelligence

[41] https://en.wikipedia.org/wiki?curid=349771

[42] Esfe, M.H., Eftekhari, S.A., Hekmatifar, M. et al. "A well-trained artificial neural network for predicting the rheological behavior of MWCNT–Al2O3 (30–70%)/oil SAE40 hybrid nanofluid". Sci Rep 11, 17696 (2021). https://doi.org/10.1038/s41598-021-96808-4

[43] https://en.wikipedia.org/wiki?curid=40254

[44] https://en.wikipedia.org/wiki?curid=10136

[45] https://en.wikipedia.org/wiki?curid=49180

[46] S. F. M. Khedr, M. E. Ammar and M. A. M. Hassan, "Multi objective genetic algorithm controller's tuning for non-linear automatic voltage regulator," 2013 International Conference on Control, Decision and Information Technologies (CoDIT), 2013, pp. 857-863, doi: 10.1109/CoDIT.2013.6689655.

[47] https://en.wikipedia.org/wiki?curid=2932246

[48] Kachitvichyanukul, V. (2012) "Comparison of Three Evolutionary Algorithms: GA, PSO, and DE," Industrial Engineering and Management Systems. Korean Institute of Industrial Engineers. doi: 10.7232/iems.2012.11.3.215.

[49] Ozcan H., "Comparison of particle swarm and differential evolution optimization algorithms considering various benchmark functions", Politeknik Dergisi, 20(4): 899-905, (2017)

[50] Klemen Dezelak, Peter Bracinik, Marek Höger, Alena Otcenasova, "Comparison between the particle swarm optimisation and differential evolution approaches for the optimal proportional–integral controllers design during photovoltaic power plants modelling", IET Renewable Power Generation, https://doi.org/10.1049/iet-rpg.2015.0108, (2016)

[51] S. Moayedi, V. Nasirian, F. L. Lewis, and A. Davoudi, "Team-oriented load sharing in parallel DC-DC converters," IEEE Transactions, Ind. Appl., vol. 51, no. 1, pp. 479–490, Jan./Feb. 2015.

Contact E-mail Address: hossamsoudy_2007@hotmail.com